AN ABSTRACT OF THE THESIS OF

John T. Shay for the degree of Master of Science in Geology presented on March 30, 1990.

Title: Structure of the Crust Beneath Lake Superior from Forward Modeling of Large Aperture Seismic Data.

Abstract approved: Redacted for Privacy
Dr. Anne Trehu

Both travel times and amplitudes of large offset refracted and reflected arrivals observed during GLIMPCE (Great Lakes International Multidisciplinary Program on Crustal Evolution) along line A in Lake Superior have been modeled using two-dimensional ray tracing techniques. Forward modeling was used to iteratively refine an initial velocity model that was constructed from results of tau-sum analysis of the travel time data at each station combined with information from the coincident common depth point (CDP) reflection profile. When converted to time the resulting model agrees quite well with the CDP reflection profile. A 50-100 ms time advance anomaly associated with the Isle Royal Fault is observed at every station. This anomaly has been modeled as shallow, high velocity blocks located directly beneath the fault. The blocks correlate well with the walls of a steep-sided bathymetric trough and are believed to represent highly indurated upper Keweenawan sediments which may have resulted from hydrothermal alteration. Approximately 2 km of sedimentary rock (2.8-4.6 km/sec) overlie an 8 km thick sequence of volcanics and interflow sediments (5.0-6.5 km/sec) within the rift graben observed on the reflection data. Beneath this sequence is a 6-8 km thick sequence

of 6.6-7.0 km/sec material that is interpreted to represent metamorphosed volcanics. The velocity of the material at the base of the rift graben is not well constrained (approximately 7.0 -7.2 km/sec), but probably comprises an additional 10-12 kilometers of meta-volcanic rocks and intrusions that extend to the base of the graben as imaged on the CDP reflection profile. Boundaries between these sequences are indicated by reflections observed at several of the wide-aperture stations. A marked decrease in the apparent velocity and amplitude of the first arrivals is observed on reversed sections at ranges exceeding 100 km. This decrease in apparent velocity has been modeled as lower velocity continental crustal rocks (approximately 6.5 km/sec) at a depth of about 15-20 km adjacent to the 7.0 km/sec material in the graben. Calculation of the gravity response of the seismic model demonstrates that the gravity high centered over the rift can be entirely attributed to high density rocks occupying the central half-graben imaged on the CDP profile. Wide angle reflections from about 15-30 km depth beneath the flanks of the graben indicate the presence of velocity discontinuities that may represent rift related detachment surfaces and/or pre-rift structures. Modeling of wide angle reflections indicate a high degree of structural relief preserved within the lower crust. The high velocities modeled for this region, coupled with information from the CDP profile, suggest that the lower crust represents Archean crust that has been either heavily intruded or underplated by mafic magma. The style and volume of volcanic emplacement is similar to that of Phanerozoic rifted continental margins and flood basalt provinces. By analogy, the volcanism within the midcontinent rift appears to have resulted from decompression melting during lithospheric extension above a broad, asthenospheric thermal anomaly recently referred to in the literature as the "Keweenawan hot spot".

Structure of the Crust Beneath Lake Superior from Forward Modeling of Large Aperture Seismic Data

by

John T. Shay

A THESIS

submitted to

Oregon State University

in partial fulfillment of

the requirements for the

degree of

Masters of Science

Completed March 30, 1990

Commencement June 1991

APPROVED:

Redacted for Privacy

Professor of Oceanography in charge of major

Redacted for Privacy

Chair of department of Geosciences

Redacted for Privacy

Dean of the Graduate School

Date thesis is presented March 30, 1990

Typed by researcher for John T. Shay

ACKNOWLEDGEMENTS

I would first like to express my sincere appreciation to the members of my committee, Drs. Anne Tréhu, Robert Lillie, John Dilles, and James Ayres for their helpful suggestions, criticisms, and discussions during the course of this research. I am very grateful to the staff and students of both the Department of Geology and the College of Oceanography for their support and friendship. In particular, I wish to thank Marcia Turnbull and Theresa Belden for their time and effort. I would also like to thank Sierra Geophysics of Kirkland, Washington for their support in producing the library copies of this thesis. I am also grateful to ARCO oil company and the United States Geological Survey Branch of Atlantic and Gulf of Mexico Marine Geology for providing critical financial assistance. Partial support for this research came from NSF grant EAR-8904413 awarded to Dr. A. M. Tréhu.

With completion of this work in sight, I finally get to treat myself to the long awaited pleasure of thanking the many people who helped (more than they will ever know) make this thesis a reality. At the top of my thank you list sits the name of my wife, Joan. After all those coffee breaks and coffee put-back-togethers, a simple thank you would sound rather hallow... so, it is with great affection and admiration that I dedicate this work to you. To either side of Joan rest my children, Dana and David, who could always be counted on to provide rainbows on the darkest days. I wish to thank all of my family members residing in New Mexico, California (Shays and Oltmans), Colorado, West Germany, Louisianna and New Jersey for their unwavering love and support. I am also deeply grateful to Cathy Hettleman, Michael Levy, Ann and Tom Hanson, Steve Bourgeois, Hugh Ryan, John and Ruth Stewart, Geoff Quinn, Emmy

Sokoloff, the Axelrod family , and the Lyman-Holt family for helping me keep my priorities straight when everything seemed so crooked.

I want to offer a special word of thanks to: my parents who, by their daily actions, taught me the importance of perseverance, integrity, ... and love, Sharon, Mike, Pat, Rick, Ray and Joe who were always there when I needed them, Eunice Hoyland and Kathyrn Nemes for sharing with me their humor and wisdom, Don Marsee for being a kindred spirit in a seemingly spiritless age, Chuck Sears for the loan of his Macintosh computer and for sharing with me his wonderous visions of the future, Ken Werner, Eric Gravens and Gary Huftile for their friendship and sizable coffee allowances, Kathryn and Peter Howd for being such dear friends and for their delightful southwestern hospitality (especially during those final maddening days... ugh, weeks?), Tom Lippmann for his unbridled approach to life and for playing the role of the "perfect" graduate student (somebody has to be it), Dr. Anne Tréhu for giving me the opportunity to work on such a remarkable data set and for not telling me the horrors of forward modeling before I got started, and Dr. Jill Whitman for showing me that the horrors of graduate school can be overcome. Again, to each and every one of you I give my most heartfelt thanks.

TABLE OF CONTENTS

Introduction 1

Regional Geology 8

Pre-volcanic rocks 13

Syn-vocanic rocks 13

Post-volcanic rocks 15

Review of the Common Depth Point Reflection Profile 17

The Northern Flank 20

The Central Basin 20

The Southern Flank 22

Data Acquisition and Processing 24

Seismic Model: Introduction 28

Constraints 28

Modeling approach 29

Overview of the model 31

Seismic Model: Layer-by-layer Validation and Interpretation 38

Layer 1 38

The Keweenaw Fault 45

The Isle Royale Fault Zone (IRFZ) 46

Layer 2 49

Layer 3 67

Layers 4 and 5 71

RMS fits 73

Comparison of Forward and Inverse Models 75

Gravity Response of the Seismic Model 79

Discussion 84

The Northern Flank 84

The Central Basin 87

The Southern Flank 89

The Archean Crust 89

The Lower Crust and Moho 90

References 96

Appendix A: Uninterpreted Record Sections 110

Appendix B: Synthetic Record Sections 117

Appendix C: Instrument Location Plots 124

LIST OF FIGURES

Figure		Page
1	Index map of the Midcontinent Rift System	2
2	Location map of the GLIMPCE seismic survey	5
3	Wide aperture site locations along line A of GLIMPCE	7
4	Interpreted reflection profile along line A of GLIMPCE	18
5	a) Record section from OBS-C4 prior to deconvolution	27
	b) Record section from OBS-C4 following deconvolution	
6	Comparison plots of velocity depth functions	30
7	a) Velocity-depth model along line A of GLIMPCE	32
	b) Detailed view of upper 5km of the velocity-depth model	
8	Comparison of velocity-time model and the migrated CDP profile	35
9	a) Near surface (0-6 km) ray diagram for OBS-A2	39
	b) Record section from OBS-A2 with travel time curves overlaid	
10	a) Near surface (0-5 km) ray diagram for OBS-C4	40
	b) Record section from OBS-C4 with travel time curves overlaid	
11	a) Near surface (0-5 km) ray diagram for OBS-C9	41
	b) Record section from OBS-C9 with travel time curves overlaid	
12	a) Near surface (0-5 km) ray diagram for OBS-C3	42
	b) Record section from OBS-C3 with travel time curves overlaid	
13	Detailed comparison of velocity-time model and the migrated CDP profile in the vicinity of the Isle Royale Fault Zone	47

14	a) Full model ray diagram for site SUP4	52
	b) Record section from station SUP4 with travel time curves overlaid	
	c) Synthetic record section for site SUP4	
15	a) Full model ray diagram for OBS-A2	54
	b) Record section from OBS-A2 with travel time curves overlaid	
	c) Synthetic record section for OBS-A2	
16	a) Full model ray diagram for OBS-C4	56
	b) Record section from OBS-C4 with travel time curves overlaid	
	c) Synthetic record section for OBS-C4	
17	a) Full model ray diagram for OBS-C9	58
	b) Record section from OBS-C9 with travel time curves overlaid	
	c) Synthetic record section for OBS-C9	
18	a) Full model ray diagram for OBS-C3	60
	b) Record section from OBS-C3 with travel time curves overlaid	
	c) Synthetic record section for OBS-C3	
19	a) Full model ray diagram for site C1	62
	b) Record section from station C1with travel time curves overlaid	
	c) Synthetic record section for site C1	
20	a) Comparison of forward model and 63 node inverse model	77
	b) Comparison of forward model and 250 node inverse model	78
21	a) Gravity model along line A of GLIMPCE	80
	b) Bouguer gravity anomaly response of the model	
22	Geological/seismic model along line A of GLIMPCE	85
23	Conceptual model of the development of the MRS	92
24	Conceptual model of continental breakup and formation of first oceanic crust.	94

25	Record section from instrument SUP4	111
26	Record section from OBS-A2	112
27	Record section from OBS-C4	113
28	Record section from OBS-C9	114
29	Record section from OBS-C3	115
30	Record section from instrument C1	116
31	Synthetic section calculated for instrument SUP4	118
32	Synthetic section calculated for OBS-A2	119
33	Synthetic section calculated for OBS-C4	120
34	Synthetic section calculated for OBS-C9	121
35	Synthetic section calculated for OBS-C3	122
36	Synthetic section calculated for instrument C1	123
37	Instrument location plot for OBS-A2	125
38	Instrument location plot for OBS-C4	126
39	Instrument location plot for OBS-C9	127
40	Instrument location plot for OBS-C3	128

LIST OF TABLES

Table		Page
1	Stratigraphic and seismic velocity correlation diagram for rocks in the vicinity of Lake Superior.	10
2	Estimated locations of the ocean bottom seismometers.	25
3	Summary of RMS fits.	74
4	Densities of rocks from the vicinity of the midcontinent rift.	81

The legend lives on from the Chippewa on down of the big lake they call Gitchygoomie.

Superior they said never gives up her dead when the gales of November come early.

The wreck of the Edmund Fitzgerald
by Gordon Lightfoot

Structure of the Crust Beneath Lake Superior from Forward Modeling of Large Aperture Seismic Data

Introduction

Lake Superior lies at the northern end of the Midcontinent Gravity Anomaly (MGA, Figure 1). The MGA exceeds 2000 kilometers in length and extends northeasterly from Kansas through Iowa, Minnesota, and Wisconsin. The distinctive arcuate shape of Lake Superior follows the trend of the MGA as it swings southeastly into south-central Michigan (Chase and Gilmer, 1973; Wold and Hinze, 1982; Van Schmus and Hinze, 1985). Although first described as a gravity anomaly (Woolard,1943), the MGA is also associated with a large amplitude magnetic anomaly (King and Zietz, 1971).

The source of these potential field anomalies has been the object of numerous investigations (Steinhart and Smith, 1966; Wold and Hinze, 1982; Van Schmus and Hinze, 1985). Models of gravity anomaly profiles crossing the MGA consistently suggest that there is a large body of dense material (2.9-3.0 gm/cc) at a depth of a few kilometers beneath the MGA (Ocola and Meyer, 1973; Hinze and Wold, 1982; Green, 1982; McSwiggen et al., 1987; Fadaie et al., 1988; Chandler et al., 1989; Hutchinson and White, 1989; Hutchinson et al., submitted). Surface exposures around Lake Superior and drillhole data from throughout the MGA indicate that the potential field anomalies are related to a thick sequence of Keeweenawan age (1100 ± 10 Ma) basaltic lavas (Thiel, 1956; King and Zietz, 1971; Van Schmus et al., 1982). On the basis of these geophysical observations and exposed geology (Davidson, 1982) it is generally agreed that the MGA is due to a failed Precambrian rift of mid-Keweenawan age.

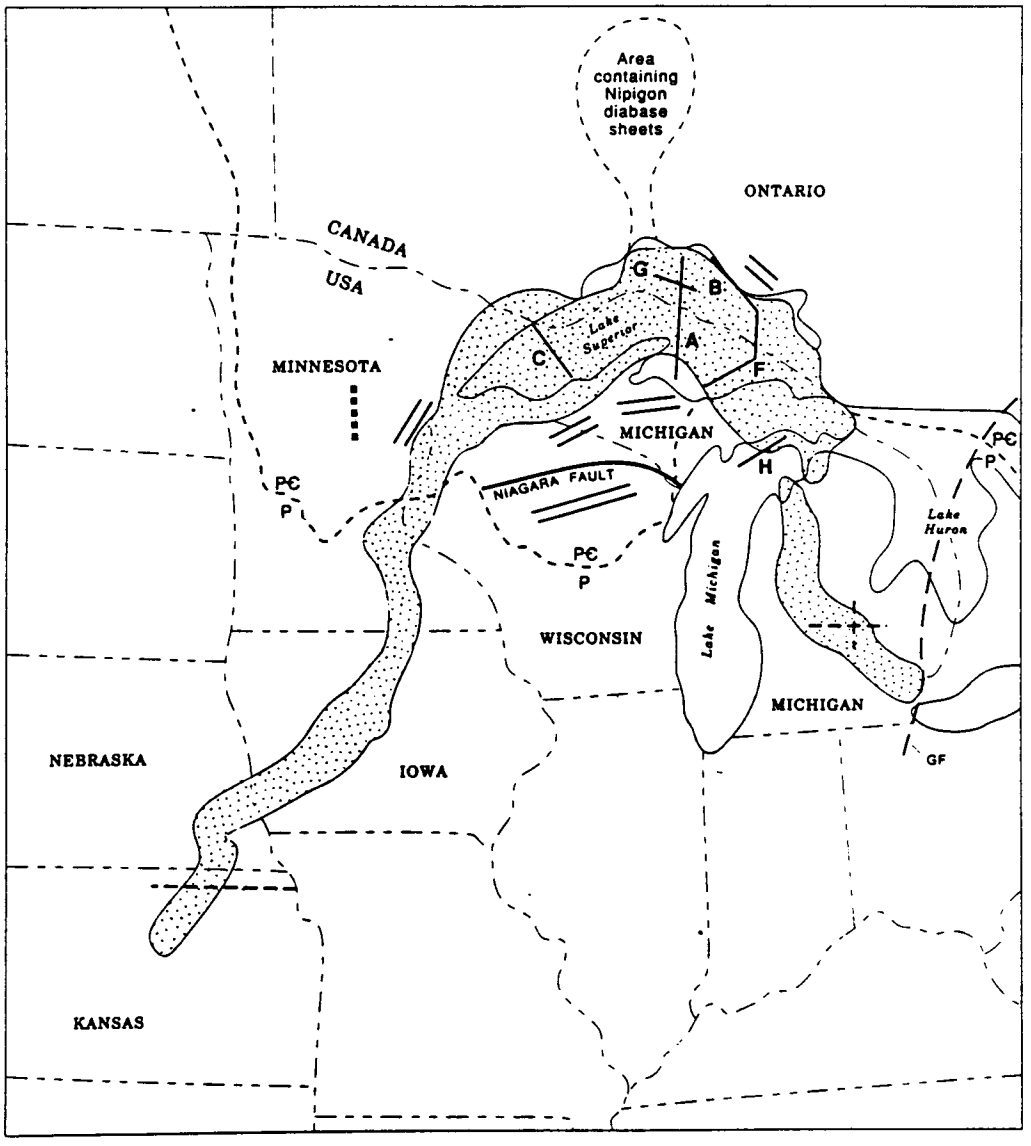

Figure 1. Index map showing location of the positive Bouguer gravity anomaly (shaded) produced by rocks of the midcontinent rift system (MRS) and some major geologic features of the region. Heavy solid lines are seismic reflection profiles from the GLIMPCE experiment. Heavy dashed lines in Kansas, Minnesota and southern Michigan are locations of reflection profiles collected by COCORP (Serpa et al., 1984; Gibbs et al., 1984; Brown et al., 1982). Short dashed line is contact of Phanerozoic (P) strata with Precambrian (PC). Location and trend of Keweenawan diabase dike swarms shown schematically by heavy double lines. GF, Grenville Front. (Modified after Cannon et al., 1982)

The idea that the MGA is associated with a midcontinent rift dates back to Black (1955) , Lyons (1959), and Smith et al. (1966). The geological and geophysical evidence for a rift is so compelling that the feature is commonly refered to as the Midcontinent Rift System (MRS; Wold and Hinze, 1982). Although recent seismic experiments in this region have revealed variable crustal structures associated with the MRS (Serpa et al., 1984; Brown et al., 1982; Brown et al., 1983; Zhu and Brown, 1986; Dickas, 1986; Behrendt et al., 1988; McGinnis et al., 1989; Cannon et al., 1989) , the observed structures consistently support the concept of a midcontinent rift.

Previous seismic refraction surveys conducted in this region have provided only a first-order understanding of the velocity structure of the MRS. Shallow seismic refraction profiles (up to 120 km offset) indicate the presence of a 2-3 km thick Proterozoic sedimentary basin (2.8-4.6 km/s) underlain by high velocity material (5.2-7.1 km/s). The high velocity material has generally been interpreted to represent volcanic material associated with the axial region of the MRS (Steinhart and Meyer, 1961; Smith et al., 1966; Mooney et al., 1970; Halls and West, 1971; Ocola and Meyer, 1973; Luetgert and Meyer, 1982; Luetgert, unpublished manuscript). The continental basement rocks which form the flanks of the rift in the vicinity of Lake Superior display near surface velocities of about 5.9-6.3 km/s (Steinhart et al., 1961). Very large offset data were collected in this region during the 1963 Upper Mantle Project and the 1966 Project Early Rise (Steinhart, 1964; Cohen and Meyer, 1966; Smith et al., 1966; Berry and West, 1966). Both of these experiments were primarily designed to look at the upper mantle beneath the MRS and the neighboring Canadian Shield using large explosive sources and recording at offsets of up to 2500 km. Halls (1982) compiled crustal time-terms to create an apparent crustal thickness map for the Lake Superior region. The map indicates that the crust beneath the central part of Lake Superior is anomalously thick (> 50 km) compared to the surrounding crust (approx. 35-40 km). Unfortunately, the resolution of

the time-term map was insufficient to show the detailed structural relationship between the MRS and the thickened crust.

In 1986, the U.S. Geological Survey, the Geologic Survey of Canada, and several academic institutions[1], collected deep crustal seismic data in the Great Lakes region (Figure 2) under the auspices of GLIMPCE (Great Lakes International Multidisciplinary Program on Crustal Evolution). Wishing to avoid the infamous November gales of Lake Superior (Lightfoot, 1972), the experiment was carried out in early October. Prior to GLIMPCE, only two non-commercial multi-channel seismic reflection profiles had been shot across the MRS. Both of these lines, collected by COCORP (Consortium for Continental Reflection Profiling), were located near the ends of the MRS (Figure 1); one in northeastern Kansas (Serpa et al., 1984) and the other in central Michigan (Brown et al., 1982; Zhu and Brown, 1986). Both of these profiles reveal asymmetric rift basins with maximum twtt (two-way travel time) through the basins of about 3 s (8 km) and 6 s (18 km) in Kansas and Michigan, respectively. The seismic reflection profiles collected by GLIMPCE extended the view of the MRS to its central region beneath the waters of Lake Superior (Behrendt et al., 1988, 1989; Green et al., 1988; Cannon et al., 1989). The GLIMPCE common depth point reflection profiles (Milkereit et al., 1988) show rift basins with up to 10 s twtt (about 35 km). The basins were clearly formed in an extensional environment and were later disrupted by minor reverse faulting. It was also observed that the asymmetry of the rift changes polarity along the length of the MRS; suggesting a segmentation length along the axis of the rift of less than 100 km. A detailed discussion of the structure and stratigraphy of the rift basins imaged within Lake Superior during GLIMPCE is given in Cannon et al., (1989).

---

[1]University of Wisconsin, Madison, WI; University of Wisconsin, Oshkosh, WI; Northern Illinois University, Dekalb, IL; Southern Illinois University, Carbondale, IL; University of Saskatchewan, Saskatoon, Saskatchewan; University of Western Ontario, London, Ontario.

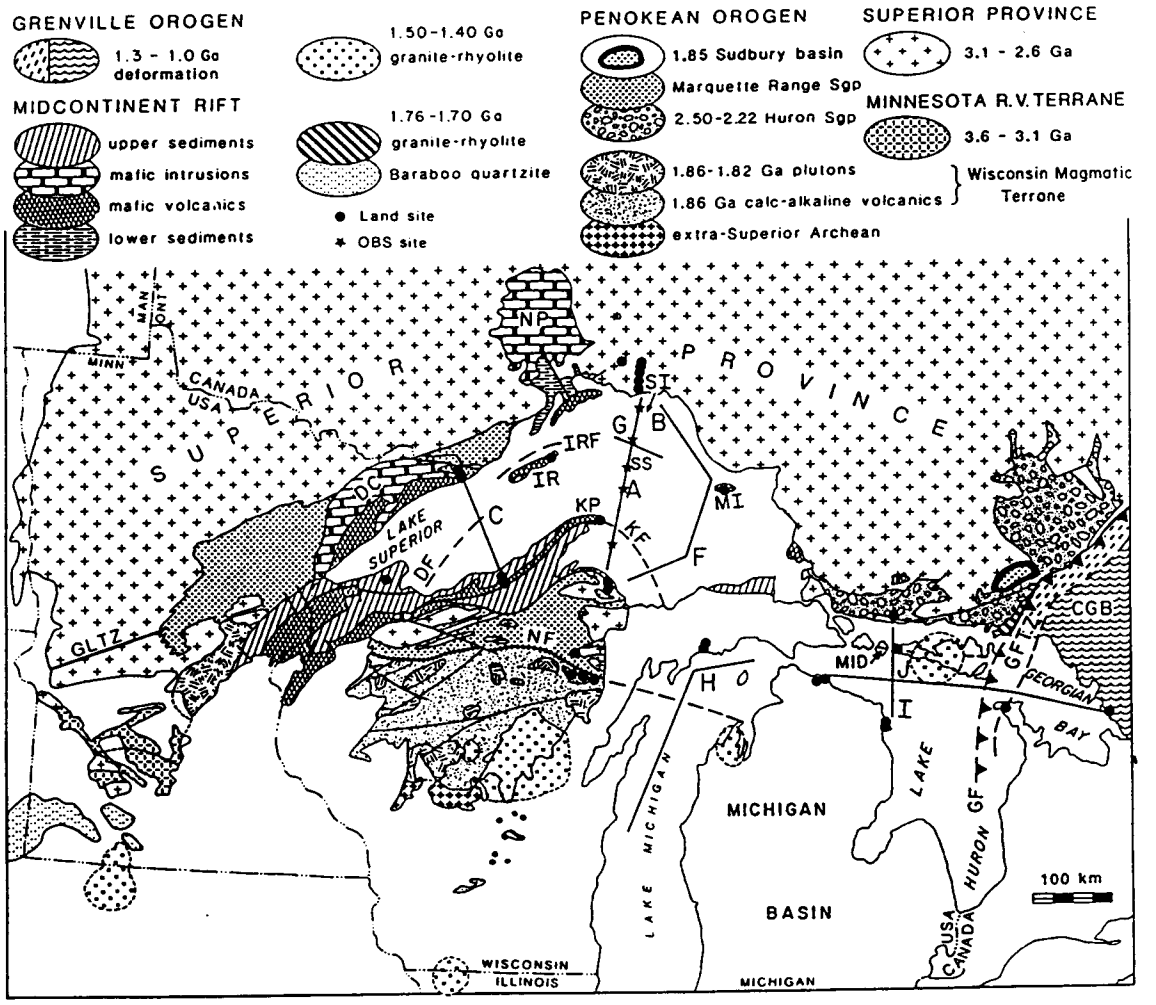

Figure 2. Location map of the GLIMPCE 1986 seismic survey on geological background modified from Hoffman (1988). CGB, Central gneiss belt; DC, Duluth complex; DF, Douglas fault; GF Grenville front; GFTZ, Grenville front tectonic zone; GLTZ, Great Lakes tectonic zone; IR, Isle Royale; IRF, Isle Royale fault; KF, Keweenaw fault; KP, Keweenaw Peninsula; MI, Michipocoten Island; MID, Manitoulin Island discontinuity; NF, Niagara fault; NP, Nipigon plate; Sgp, Supergroup; SI, Slate Islands; SS Superior Shoals; A, coincident reflection/refraction line; B-C, E-J, seismic reflection lines. (Taken from Green et al.,1988).

As part of the GLIMPCE experiment, a coincident set of reflection and refraction seismic profiles were shot across the central part of Lake Superior. The wide-aperture data were collected using seismometers deployed on shore and on the lake bottom (Line A, Figures. 2 and 3). Although this thesis specifically addresses the analysis and interpretation of the large aperture data, the constraints and insights provided by the common depth point (CDP) profile have been fully incorporated. The advantages afforded by having both reflection and refraction seismic profiles permitted a much clearer and more comprehensive model of the MRS beneath central Lake Superior to be developed.

The first part of this thesis presents a brief review of the regional and local geology. The local geology, in the immediate vicinity of line A of GLIMPCE, will be covered as part of an overview of the CDP profile and its recent interpretation by Cannon et al. (1989). The second part of the thesis will cover the analysis of the wide-aperture data and present a two-dimensional (2-D) seismic model for the crust beneath Lake Superior along line A. The seismic model is the result of forward modeling of the wide-aperture data using 2-D raytracing techniques. To evaluate the Bouguer gravity anomaly response of the seismic model, the third part of the thesis presents a 2-D gravity model which is geometrically identical to the seismic model. The remainder of the thesis will be used to discuss and summarize the modeling results.

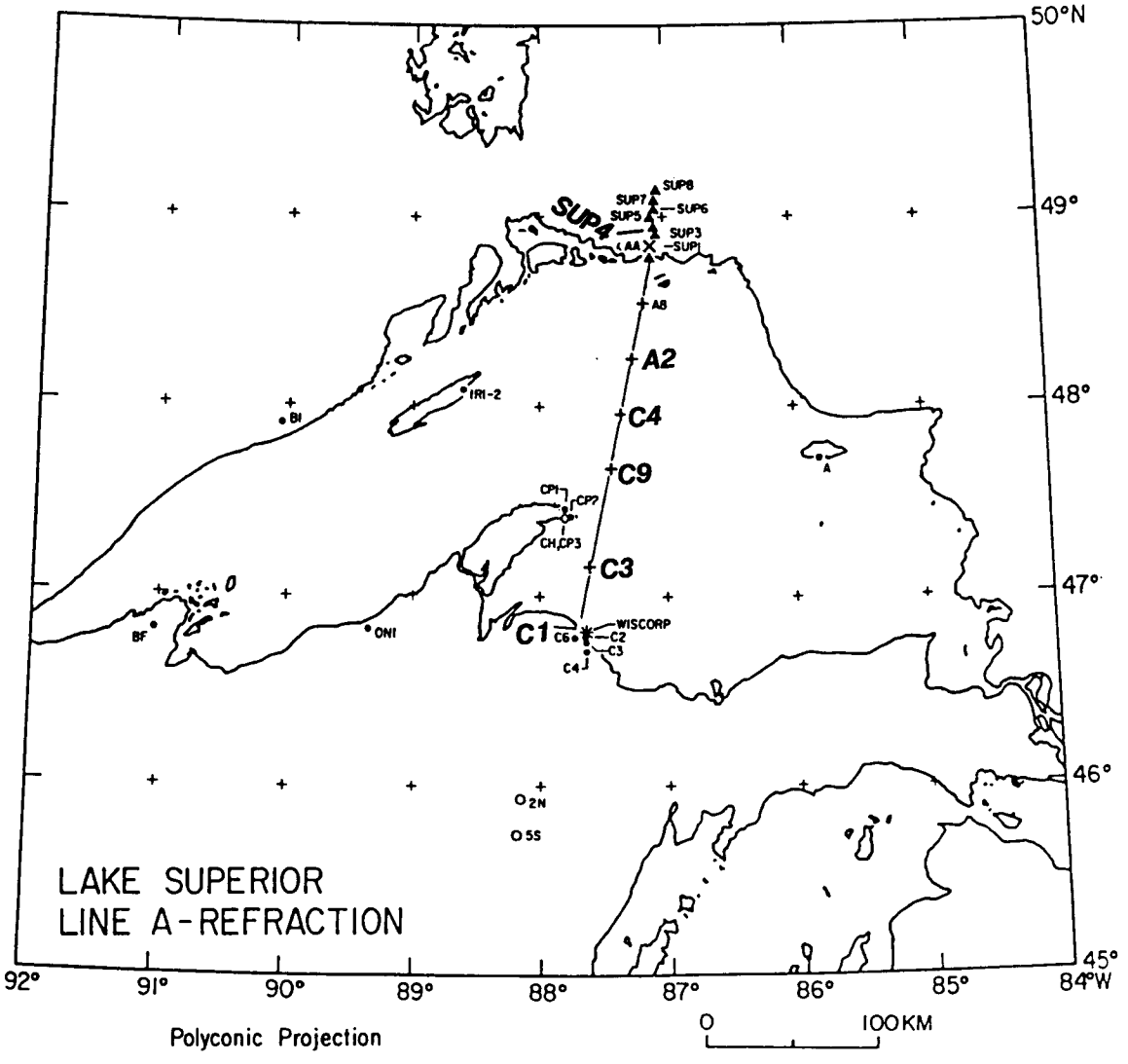

Figure 3. Wide aperture site locations along GLIMPCE line A. Wide-aperture data from stations in bold print were used in this study.

Regional Geology

The Midcontinent Rift System (MRS) cuts across several Precambrian basement terranes which together comprise a portion of the North American craton which existed prior to 1200 my ago. The Archean basement in the region of the Lake Superior basin is generally divided into a northern granite-greenstone belt and a southern gneiss-migmatite belt (Figure 2). In the vicinity of line A, the Lake Superior basin lies entirely within the northern granite-greenstone belt. The boundary between the two terranes, which is commonly refered to as the Great Lakes Tectonic Zone (GLTZ) (Sims et al., 1980; Gibbs et al., 1984; Hinze et al., 1988), lies approximately 120 km south of the southern end of line A (Niagara fault on Figure 2). From the COCORP profiles collected in central Minnesota (Figure 1), Gibbs et al. (1984) have interpreted the GLTZ as a northward dipping thrust fault, possibly representing a suture zone between the two Archean terranes. The northern granite-greenstone terrane formed 2.6-3.1 Ga and remained relatively stable until Keweenawan time. In contrast, the southern gneiss-migmatite terrane formed 2.6-3.6 Ga but was subjected to extensive Early Proterozoic (1.8-1.9 Ga, Penokean) orogenic deformation (Morey and Sims, 1976). Apparent offsets of the GLTZ have been used by Klasner et al. (1982) to estimate that there has been approximately 50 km of crustal extension across the MRS in the vicinity of Lake Superior. Chandler (1983) suggested a similar degree of extension (~ 60 km) along the north segment of the rift based on the observed offsets in magnetic anomalies.

Exposure of lithologic units related to the rift are confined to areas in the immediate vicinity of Lake Superior and together comprise the Keweenawan Supergroup. Problems in identifying, correlating and dating the rocks associated with rifting have created a situation in which there is no accepted definition for either the lithostratigraphic or chronostratigraphic boundaries of the Keweenawan (Van Schmus and Hinze, 1985).

The scarcity of good geologic control has led many investigations, including this one, to rely heavily upon geophysical properties to identify and correlate strata. The stratigraphic scheme used in this study (Table 1) is modified after Davidson (1982) to include absolute age dates, and the seismic velocity observations of Smith et al. (1966), Halls (1969), Mooney et al. (1970), Halls and West (1971), Anzoleaga (1971), Ocola and Meyer (1973), Luetgert and Meyer (1982). The overlap of seismic velocities across formation boundaries and the gradational character of many of the contacts makes it impossible to set discrete velocity boundaries to each formation. The velocity-stratigraphy correlations used in this study (Table 1) are based upon a review of previous investigations and available geologic controls in the vicinity of line A. The stratigraphic thicknesses and velocities presented in the velocity model below are generally consistent with those reported in these earlier studies. It should be noted that Table 1 is intended only to facilitate comparison to previous work and is in no way intended to set definitive velocity boundaries on the stratigraphy.

Above the Archean basement and underlying the Keweenawan Supergroup are the basinal clastic rocks of the Sibley Group and its equivalents. The Sibley Group consists of more than 400 meters of strata comprising primarily quartzose sandstone, mudstone, and dolomite. Whereas the sandstones appear to be fluvial, the finer clastics and dolomite appear to be lacustrine or possibly marine deposits (Ojakangas and Morey, 1982a). Paleocurrent indicators within the Sibley Group suggest that it may have been deposited in a failed rift basin whose boundaries encompass the northern end of line A (Ojakangas and Morey, 1982a). Although these rocks are considerably older than the early stage Keweenawan rocks (1340 Ma versus 1100 Ma), their basal position and possible rift origin has generated considerable debate as to whether the Sibley Group should be included within the pre-volcanic unit of the lower Keweenawan (Van Schmus and Hinze, 1985). This study retains the designation of Davidson (1982) which places the Sibley Group within the pre-Keweenawan.

Table 1. Stratigraphic and seismic velocity correlation diagram for rocks in the vicinity of Lake Superior. The table is intended to facilitate comparison with previous seismic investigations and not to set definitive p-wave velocities to individual stratigraphic units. The stratigraphic diagram was modified after Davidson (1982).

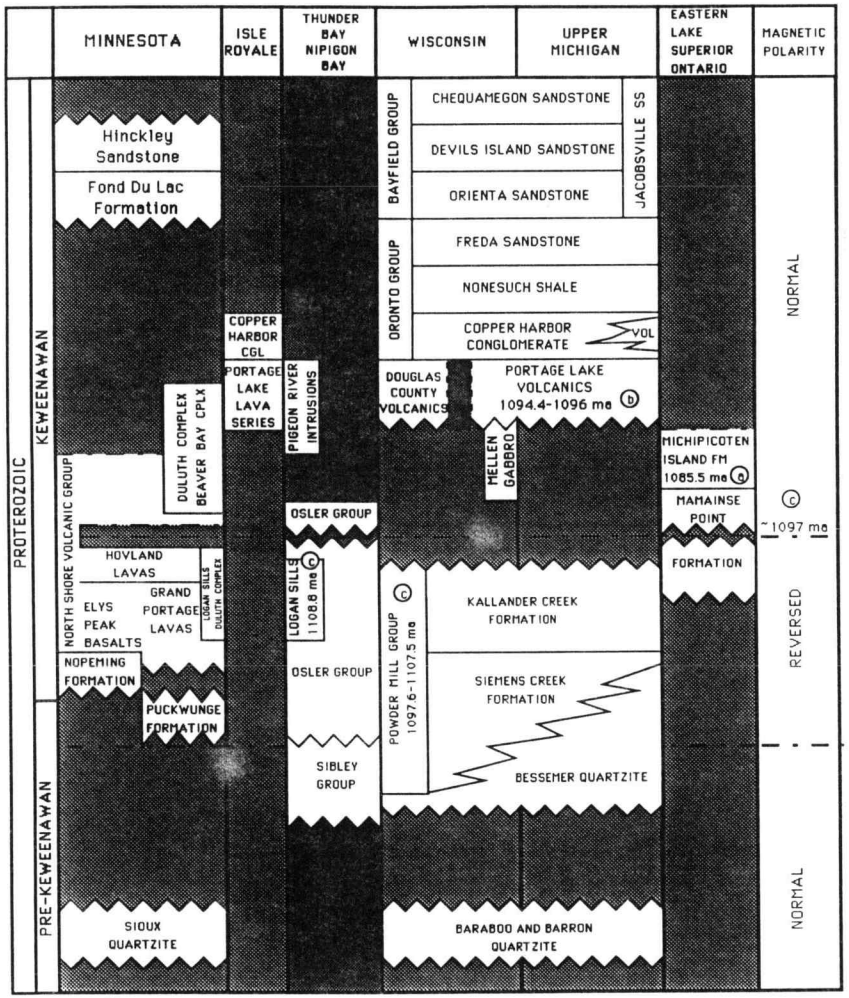

(a) Radiometric ages from Palmer and Davis (1987)
(b) Radiometric ages from Paces and Davis (1988)
(c) Radiometric ages from Davis and Sutcliffe (1985)

Table 1

AGE	LITHO	P-WAVE VELOCITIES (km/s) OF ROCKS NEAR THE MRS							
		THIS STUDY	SMITH ET AL., 1966	HALLS, 1969	MOONEY ET AL., 1970	HALLS AND WEST, 1971	ANZOLEAGA, 1971	OCOLA AND MEYER, 1973	LUETGERT AND MEYER, 1982
UPPER KEWEENAWAN	BAYFIELD/JACOB. SS	1a 2.5 - 2.8 1b 3.5 - 4.0		3.70-4.65	2.8-3.6	3.66	3.4-4.6	3.4-3.5	2.92-3.77
	ORONTO GROUP	1c 4.4 - 4.6		3.69-5.96	4.5	4.06-4.93	4.5-4.7	4.5-4.7	4.7-5.2
MIDDLE KEWEENAWAN	SYN-RIFT VOLCANICS AND SEDIMENTS	2a 5.2 - 5.6 2b 5.9 - 6.3 2c 5.2 - 6.6 2d 5.2 - 7.0 2e 6.3 - 7.2	6.6-6.7	4.91-6.77 6.31-6.72 Amphibole-bearing metabasalts	5.0-5.5	5.5-6.47	5.4-5.6	5.4-5.6	5.2-6.0 6.4 Upper Refractor North Shore 6.85 Upper Refractor Central Regior
LOWER KEWEENAWAN									
PRE-KEWEENAWAN	CONT. CRUST AND PRE-RIFT SEDIMENTS	3a 6.0 - 6.5 3b 6.6 - 6.7 3c 5.8 - 5.95 3d 6.0 - 6.1 3e 6.2 - 6.6 3f 6.6 - 6.7	5.6	6.65-7.02 Mafic Intrusions	5.7-6.2 Felsic Intrusions 6.6-7.1 Mafic Intrusions		6.5 Duluth Gabbro	6.5-6.9 Mafic Intrusions	
LOWER CRUST		Layer 4 7.2 - 7.3	6.95-7.2				6.9		
UPPER MANTLE		Layer 5 8.1	8.07					8.1	

Irrespective of the stratigraphic designation of the Sibley Group, this study was unable to distinguish a seismic unit corresponding unequivocally to any pre-volcanic clastic rocks. This is probably due both to the relative thinness of the pre-volcanic section (Ojakangas and Morey, 1982a) and similarity of the p-wave velocity of buried Archean basement material and basal pre-volcanic clastic sedimenatry rocks.

The Keweenawan Supergroup is divided into three groups: 1) Pre-volcanic clastic rocks which lie unconformably on the Archean basement, 2) syn-rift igneous rocks with intercalated clastic rocks, and 3) post-volcanic clastic rocks which were deposited either in a central rift trough that remained after cessation of igneous activity or in a broad sag basin that developed as a result of regional subsidence.

Details of the stratigraphic and structural relationships between the various units which comprise the Keweenawan Supergroup are exceedingly complex and well beyond the scope of this thesis. The enormous volume of literature dealing with the geology of the MRS in the region of Lake Superior is well summarized in Geological Society of America Memoir 156 (Wold and Hinze, 1982). In particular, Davidson (1982) provides a superb review of the geological evidence related to the interpretation of the Lake Superior Basin structure. Morey and Green (1982) provide a comprehensive review of the Keweenawan stratigraphy in the Lake Superior region. Green (1982) and Weiblen (1982) provide summaries of the geology and geochemistry of the igneous units, and good summaries of the sedimentary units are given by Merk and Jirsa (1982), Daniels (1982), Morey and Ojakangas (1982), Ojakangas and Morey (1982b), and Kalliolokoski (1982). Summaries covering the geochronology and paleomagnetism of Keweenawan rocks are given by Van Schmus et al. (1982) and Halls and Pesonen (1982) respectively.

Pre-volcanic rocks

The pre-volcanic unit of the lower Keweenawan includes rocks of the Bessemer Quartzite, the Nopeming Formation, the Puckwunge Formation, and the lower Osler Group (see Table 1). Although they may not have exact age equivalence, they are lithologically similar; all being relatively mature, quartzose sandstone units with mature basal conglomerates. They also occupy similar stratigraphic positions directly beneath the initial Keweenawan lava flows and above "Pre-Keweenawan" rocks in their respective parts of the rift basin (Ojakangas and Morey, 1982a). Because of their relative maturity, all of these rocks are believed to have been deposited in shallow basins (Ojakangas and Morey, 1982a). The shallowness of these pre-volcanic basins suggests that development of the rift was not very advanced and that volcanism began very early in the development of the MRS. Because this study was unable to distinguish between the pre-volcanic clastic rocks (including those of the Sibley Group) and rocks of the underlying Archean basement, a distinct seismic layer corresponding to these rocks does not appear in the seismic model presented below.

Syn-volcanic rocks

The entire syn-volcanic suite of rocks appears to have been deposited very rapidly over a time span of approximately 15 million years (see isotopic dates on Table 1). This is very surprising in light of the fact that there may be up to 32 km of vertical half graben fill beneath the central region of Lake Superior (Behrendt et al., 1988; Cannon et al., 1989). Based on cross-sectional areas revealed by seismic profiles across the MRS, Hutchinson et al. (submitted) estimate the total volume of extrusive basalt contained within the MRS to be approximately 1.3×10^6 km^3. Such enormous volumes and high rates of emplacement of basalt are consistent with what is known about other major flood basalt provinces (Richards et al., 1989; Hutchinson et al., submitted).

Two reversals in the paleomagnetic pole direction are recorded in the Keweenawan volcanic assemblage (Table 1). The magnetic reversal at 1097 Ma (date acquired by Davis and Sutcliffe (1985) for reversely magnetized Osler volcanics) is generally accepted as the boundary between lower and middle Keweenawan time. The older, magnetically reversed, suite of volcanics includes rocks of the Powder Mill Group, Osler Group, North Shore Volcanic Group, and the Mamainse Point Formation. The younger, magnetically normal, volcanics comprises rocks of the Osler Group, North Shore Volcanic Group, Mamainse Point Formation, Michipicoten Island Formation, Douglas County Volcanics, and the Portage Lake Volcanics.

The lavas are dominated by Al-rich olivine tholeiite, followed by transitional to weakly alkaline olivine basalt and a large proportion of high iron tholeiite that grades into basaltic andesite. Individual lava flows range in thickness from less than a meter to over 400 meters and have been traced along strike for distances of 30 to 145 km. Most of the flows lack any internal flow structure, which suggests that they represent ponded lava flows (Green, 1982). Down-dip thickening of the flows towards the axis of the Lake Superior syncline, as observed by Butler and Burbank (1929) and White (1966b), has long supported the concept of ponded flows deposited within a midcontinent rift. Recent rare-earth geochemical analysis of the North Shore Volcanic Group and Portage Lake Volcanics by Nicholson and Schulz (1989) indicate that as crustal extension and rifting progressed, the basaltic magmas experienced less amounts of crustal contamination. Nicholson and Shirey (submitted) present isotopic evidence from which they suggest rifting took place above an asthenospheric mantle plume. The concept of a mantle plume as the driving force behind the vulcanism associated with the MRS is supported by several kinematic and dynamic studies (Beaumont and Brown, 1989; Brown and Beaumont, 1989; Hutchinson et al., submitted).

The paleocurrent directions determined for the interflow sediments (Merk and Jirsa, 1982) are generally toward the rift axis and thus lend support to the general concept

of a rift basin. These sedimentary units are typically coarse, immature, polymictic, red-bed clastic rocks that were deposited by streams flowing over the surfaces of Keweenawan volcanic flows. Their outcrop is somewhat limited and their overall contribution to filling the rift graben is generally thought to be small (Green, 1982; Lippus, 1988; Cannon et al., 1989).

Post-volcanic rocks

The beginning of the late Keweenawan is marked by the deposition of post-volcanic sedimentary rocks that show close association with the main rift activity. These rocks consist primarily of immature clastic debris derived from the volcanic rocks of the lower and middle Keweenawan. These rocks are generally included in the Oronto Group (Daniels, 1982; Morey and Ojakangas, 1982). Overlying the Oronto Group and its equivalents are rocks containing detritus derived primarily from the surrounding Precambrian craton. These units are believed to have been deposited in broad basins formed by crustal subsidence due to increased density of the crust along the MRS. In contrast to the immaturity of the underlying Oronto Group, these rocks are relatively mature arenites (Morey and Ojakangas, 1982b). The principle units in this suite include the Bayfield Group, the Jacobsville Sandstone, the Fond du Lac Formation, and the Hinckley Sandstone. The Bayfield Group and Jacobsville Sandstone are generally considered to be equivalent formations (Hamblin, 1961; Davidson, 1982; Van Schmus and Hinze, 1985) and will be refered to in later discussion as the Bayfield-Jacobsville Group.

Although the term "Keweenawan" has largely become synonymous with continental rifting, the end of the Keweenawan was marked by a brief episode of compressional tectonics. It is generally agreed that this late stage compressional event produced the horst which follows the axis of the western branch of the MRS (Mooney et al., 1970; Cannon et al., 1989; Chandler et al., 1989). Within the western Lake Superior

basin, the horst is bounded on the north side by the Isle Royale Fault Zone (IRFZ) and on the south side by the Keweenaw fault. Both of these faults have been mapped as high angle reverse faults in the vicinity of line A (Figure 2).

Due to their proximity in time and space (see Figure 2), it has been suggested that the compressional event that generated the horst structure may be related to tectonic activity associated with the nearby Grenville orogeny (Van Schmus et al., 1982, Halls and Pesonen, 1982). However, it has also been suggested that the rift itself may have been induced by a Grenvillian collisional event (Donaldson and Irving, 1972; McWilliams and Dunlop, 1978; Gordon and Hempton, 1986). Such conflicting interpretations highlight the fact that the relationship between Grenvillian and Keweenawan tectonics remains largely unknown. Although the tectonic and structural relationship between these two provinces is not addressed in this thesis, seismic data collected during GLIMPCE has begun to shed new light on the problem (Green et al., 1988).

Review of the Common Depth Point Reflection Profile

The common depth point (CDP) profile shot along line A of GLIMPCE played a key role in the development of the velocity model by providing a normal incidence image of the crust. The position and attitude of any reflective interfaces within the seismic model should be consistent with reflectors observed on the CDP profile. To avoid repetitive citation it should be noted that the following review borrows heavily from the recent interpretation of the CDP profile put forth by Cannon et al. (1989). This review does not incorporate any information gained during the course of this study; those insights are given in the Seismic Model section of this thesis. For a more detailed discussion and comparison of all the Lake Superior reflection data collected during GLIMPCE, the reader is refered to the paper by Cannon et al. (1989).

The image of the rift revealed by the CDP data show a deep asymmetric central graben, bounded by gently dipping flanks (Figure 4). To facilitate discussion, Cannon et al. divided this general structure into three parts; the northern flank (SP 2800-3944, MR* 115-43), the central basin (SP 1500-2800, MR 186-115), and the southern flank (SP 101-1500, MR 256-186).

* *To facilitate comparison of the CDP profile with the seismic model (Figure 7a) and gravity model (Figure 21a) presented later, an equivalent model range (MR) has been included along with the CDP shot point (SP) numbers.*

Figure 4. Interpreted reflection profile along line A of GLIMPCE showing the subsurface geology beneath central Lake Superior. Bouguer gravity profile and magnetic profile from maps by O'Hara (1982). Velocity/depth profiles determined from refraction data (Halls and West, 1971; Luetgert and Meyer, 1982). M, approximate location of Moho; AG, Archean Gneiss; PLV, Portage Lake Volcanics; OG, Oronto Group; BS, Bayfield Group; JS, Jacobsville Sandstone. Vertical scale is seconds of two-way travel time. Vertical exaggeration is 1:1 for average velocity of 6 km/s. (Taken from Cannon et al., 1989).

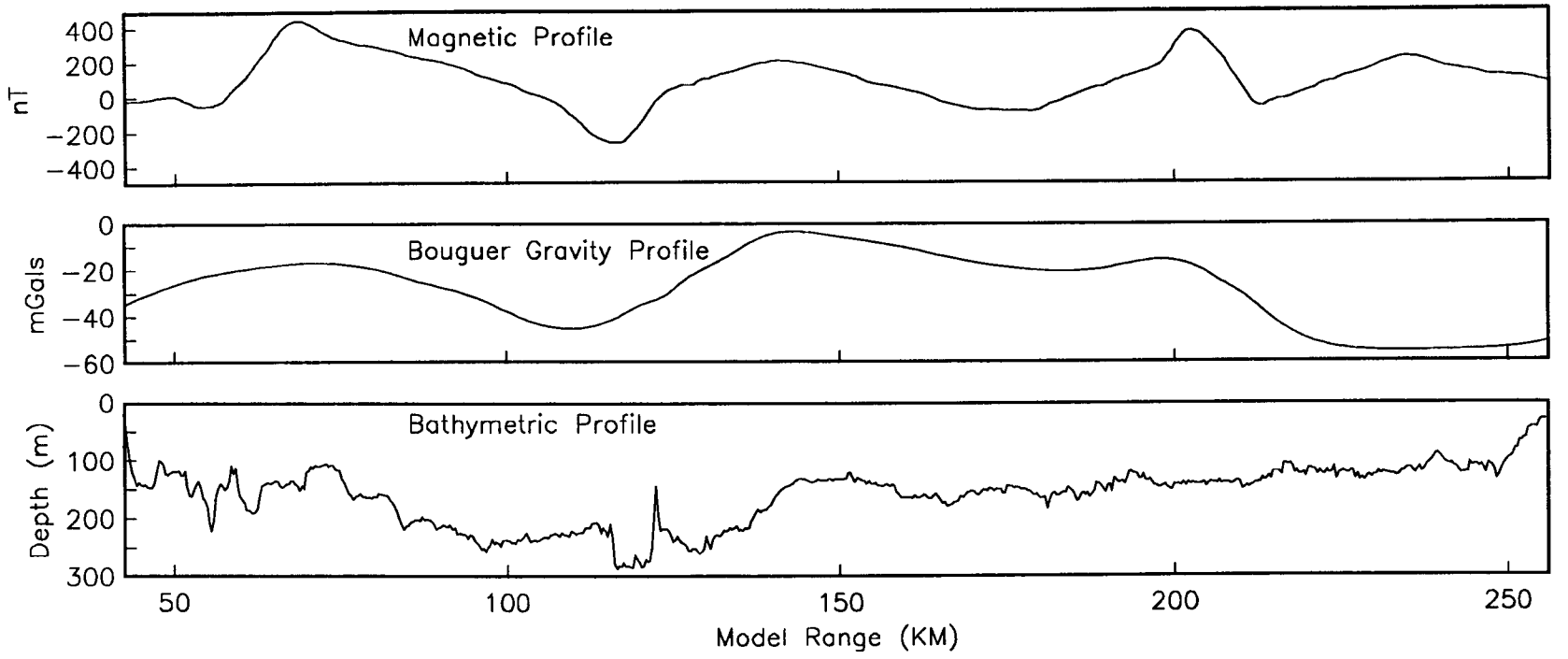

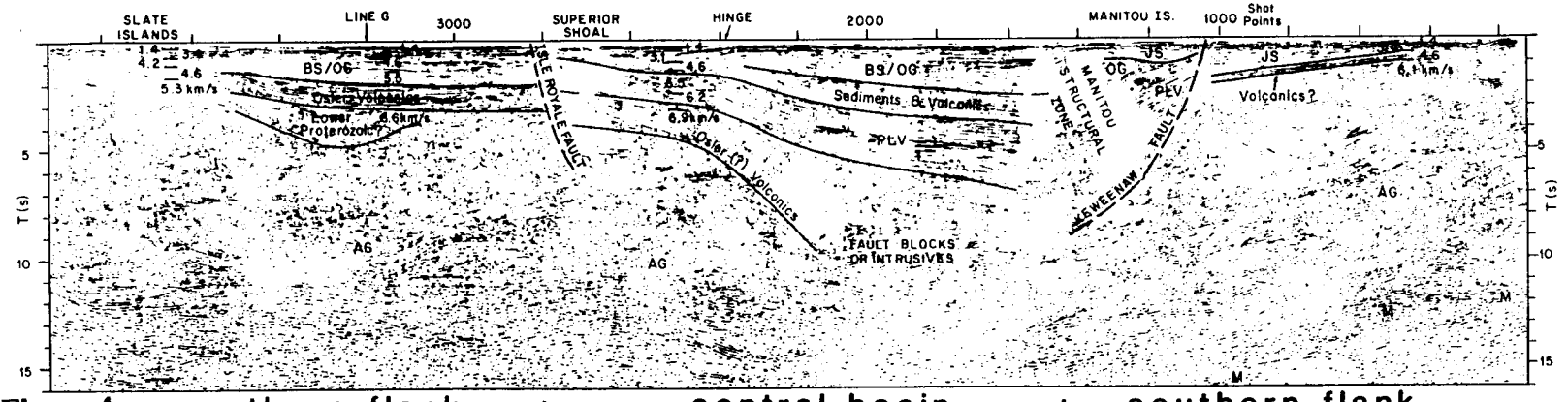

Figure 4 northern flank | central basin | southern flank

The Northern Flank

This portion of the reflection data reveals a simple basin structure with slightly dipping to horizontal Keweenawan strata overlying the Archean or Proterozoic basement. The shallowest band of reflectors (down to 2 s at SP 3200, MR 90) is believed to represent rocks equivalent to the Oronto and/or Bayfield Groups. Although this band of reflectors thins towards the north shore, poor seismic imaging north of SP 3700 (MR 58) obscures the details of how the strata terminates landward. The underlying sequence of strong reflectors (2-3 s at SP 3200, MR 90) is thought to represent volcanic rocks of the lower Keweenawan Osler Group. This correlation is supported by the fact that Osler Group rocks are exposed on islands northwest of line A. This unit thickens towards the south; reaching a maximum thickness of about 3.3 km (1s) at SP 3300 (MR 83). A 32 km wide buried syncline is imaged between SP 3000 and SP 3500 (MR 102-70). This basin appears to be a pre-Osler Group structure which unconformably underlies the inferred Osler Volcanics.

The complex reflections from the middle portions of the reflection profile along this northern flank are believed to originate from within the Archean basement. Basement rocks are exposed on the north shore and on the Slate Islands which sit approximately 15 km west of SP 3800 (MR 52).

The Central Basin

The central basin is bounded on the north by the IRFZ. The fault zone is characterized on the CDP profile as a 6 km wide zone of disrupted reflectors (SP 2725-2825, MP 114.5-120.5). Reverse movement on the fault has brought older volcanic rocks on the south side into contact with younger sedimentary rocks on the north side (Halls and West, 1971). Analysis of refracted arrivals from the multichannel data indicate that post-volcanic sediments (2.8-3.9 km/s) reside within the fault zone.

Intriguingly, the fault zone is associated with a steep-sided bathymetric trough whose southern wall coincides with a very narrow bathymetric high (Figure 4). Manson and Hall (1989) report that recent submersible dives reveal Jacobsville Sandstone outcropping along the Superior Shoal. The Shoal is located just north of GLIMPCE line A near the IRFZ.

There is significant thickening of the Keweenawan section south of the IRFZ; particularly across a hinge line near SP 2450 (MR 137). Within the central basin the Keweenawan section extends to a depth of more than 27 km (9 s) and displays a prominent fanning, or thickening, of seismic units to the south. The shallowest sequence of reflectors (down to 3.8 s near SP 1600, MR 181) is acoustically identical to the inferred Oronto/Bayfield unit on the northern flank; they are believed to be equivalent. The lowest part of this sequence (2.5-3.8 s at SP 1600-2100, MR 181-156) are interpreted as representing basalt flows interlayered with sedimentary rocks; similar to those found in the lower Oronto Group (Daniels, 1982). Immediately below this unit is a band (at 1-2.8 s near SP 2750, MR 125 and at 3.8-6.8 s near SP 1600, MR 181) of strong reflections which are thought to represent rocks of the Portage Lake Volcanics. For purposes of discussion and seismic correlation, the base of the Portage Lake Volcanics was arbitrarily placed along this marked change in reflectivity. The underlying sequence is layered, but the strength and continuity of individual reflectors is less than those within the Portage Lake unit. This lowermost Keweenawan unit is thought to be, at least in part, correlative with the Osler Group Volcanics. The Portage Lake Volcanics are about 5 km thick south of the Isle Royale fault and are believed to be absent to the north; suggesting that the fault scarp prevented northward spread of the basalt flows. The thickness of the underlying Osler Group does not appear to change across the fault, suggesting that the Isle Royale fault began as a hinge during Osler time and was later transformed into a normal fault during Portage Lake time. The fanning of these deposits

across the hinge line (SP 2450, MR 137) suggests that southward tilting of the basement continued until at least the end of Portage Lake time.

Near SP 2700 (MR 122), the contact between basement and rift deposits is interpreted to be the southward dipping (at approx. 13^{o}) reflections at 3.6 s. At the hinge line the dip increases to about 40^{o} and can be traced to a depth of about 27 km (9 s) at SP 2300 (MR 145). The truncated band of strong reflections at 6-6.5 s near SP 2400 (MR 139) are thought to come from pre-Keweenawan structures within the basement.

The arched reflectors beneath the deepest part of the rift are thought to be indicative of either complexly faulted basement blocks or Keweenawan intrusive rocks. Behrendt et al. (1988, 1989) have suggested that the complexity seen in the deepest reflections may be evidence of magmatic underplating from the underlying mantle. The Moho here may be as deep as 55 km (17 s).

The Southern Flank

Prestack migration of the CDP profile has shown that the reflectors within the poorly imaged Manitou structural zone (Figure 4 SP 1000-1500, MR 211-186) are continuous, and form a buckle with sharply increasing dips. A prominent angular unconformity at 1.2 s between SP 1100-1300 (MR 206-195) is interpreted to be overlain by rocks of the Jacobsville Sandstone; providing new evidence that Jacobsville Sandstone is stratigraphically equivalent to the Bayfield Group. The unconformity indicates that tilting and uplift of the Portage Lake Volcanics and Oronto Group began well before Jacobsville time. Tilting and uplift is believed to have been caused by reverse movement on the Keweenaw fault, which truncates the north dipping reflectors on the south near SP 1050 (MR 209). On Keweenaw Point the fault dips steeply northward and displays north-side-up reverse displacement. South of the fault, there is a wedge of reflectors which dip and thicken northward. Projection onto land indicates that these are, at least in the upper part, Jacobsville Sandstone. Units of the Oronto Group may be

present in the deeper parts of the wedge, but such units have not been recognized in outcrop south of the Keweenaw fault. The strong reflections near the base of the wedge may represent basalt flows.

Along the southern flank, the Moho is believed to be represented by the northward dipping band of reflectors at 12-15 s.

Data Acquisition and Processing

A detailed account of the field parameters and station locations for the entire GLIMPCE experiment is given in Hutchinson et al., (1988). During the shooting of line A refraction, 31 stations, 5 of which were Ocean Bottom Seismometers (OBSs), recorded the energy released from a 127 liter (7780 in^3) tuned airgun array. Figure 3 shows the position of line A and the locations of the wide-aperture recording stations. All the OBSs, except for A8, which only recorded data at source-receiver offsets of greater than 80 km, are included in this analysis. After examining the data recorded at onshore stations to the north and south of the profile and determining that the major features of all sections recorded at a given end were similar, sites SUP4 (north shore) and C1 (south shore) were chosen as being representative profiles from each end. Uninterpreted record sections from the six sites used in this analysis can be found in Appendix A.

The airguns were fired at a fixed time interval of two minutes, providing an average horizontal shot spacing of 330 meters. Shooting on a fixed time schedule allowed the self-contained OBSs to be programmed to record during specific time windows. Except in the case of OBS-A2, for which the hydrophone record was used because of its superior signal-to-noise ratio, only the vertical component records were used in this analysis. The OBSs were deployed, and initially located, by workers onboard a US Coast Guard vessel working in tandem with the shooting vessel. Initial plotting of the OBS data revealed that the site locations based on the navigation of the Coast Guard vessel were wrong. It became necessary to relocate the OBSs by inverting the first-break travel times of the direct water wave (Creager and Dorman, 1982). Unfortunately, the shallowness of the lake restricted confident picks of the water wave to the 5 to 7 closest shots for each instrument.

INSTRUMENT		OBS-A2	OBS-C4	OBS-C9	OBS-C3
LATITUDE (N)		48.26550	47.95688	47.71128	47.14079
LONGITUDE (W)		-87.26939	-87.36752	-87.43908	-87.59501
WATER DEPTH (m)		230	207	160	121
ERROR ELLIPSE	SEMI-MAJOR (m)	27.4	33.3	41.9	30.8
	SEMI-MINOR (m)	15.5	17.2	20.0	17.8
OFFSET FROM TRACKLINE (m)		726	1,121	943	242

Table 2. Estimated locations of the ocean bottom seismometers (OBS) deployed along line A of GLIMPCE resulting from least-squares inversion of water wave arrival times. Plots of these locations, the original Coast Guard locations and travel time circle solutions are given in appendix B.

The location and depth of the OBSs, their offset from the track line, and the dimensions of the error ellipses calculated as part of the inversion are listed in table 2. Appendix C contains figures which illustrate the OBS locations as determined initially by the Coast Guard vessel, the inversion method, and by a graphical travel time circle method.

The small size of the error ellipses listed in table 2 suggest that the instruments are well located, however, the curvature of the track line (over 5 to 7 shots) is insufficient to insure a unique solution. Therefore, it is possible that the instruments are located diametrically on the opposite side of the shot track line. The problem is well illustrated by the results given by the graphical travel time method (Appendix C) which shows two locations for each OBS on opposite sides of the track line.

After relocating the OBSs as described above, fresh plots of the record sections revealed a 0.07 second timing discrepancy between OBS-C4 and the other OBSs. The reason for the discrepancy remains unknown, however, it does appear to be constant for every shot, regardless of offset. In order to draw all of the reciprocal travel times into agreement, 0.07 seconds was added to each shot recorded by OBS-C4.

To improve signal quality, the wide-aperture data was frequency filtered and deconvolved (see Appendix A for processing parameters). An example of the beneficial effect that deconvolution has on the wide-aperture data is shown in Figure 5. The Figure shows a portion of the record section from OBS-C4 before and after deconvolution. As can be readily seen, the pronounced "ringing" present in the raw data is greatly diminished by deconvolution and the wide-angle reflection located at about 70 to 80 km offset is more clearly seen. Comparable signal enhancement was achieved following deconvolution of the data recorded at each of the other wide-aperture stations.

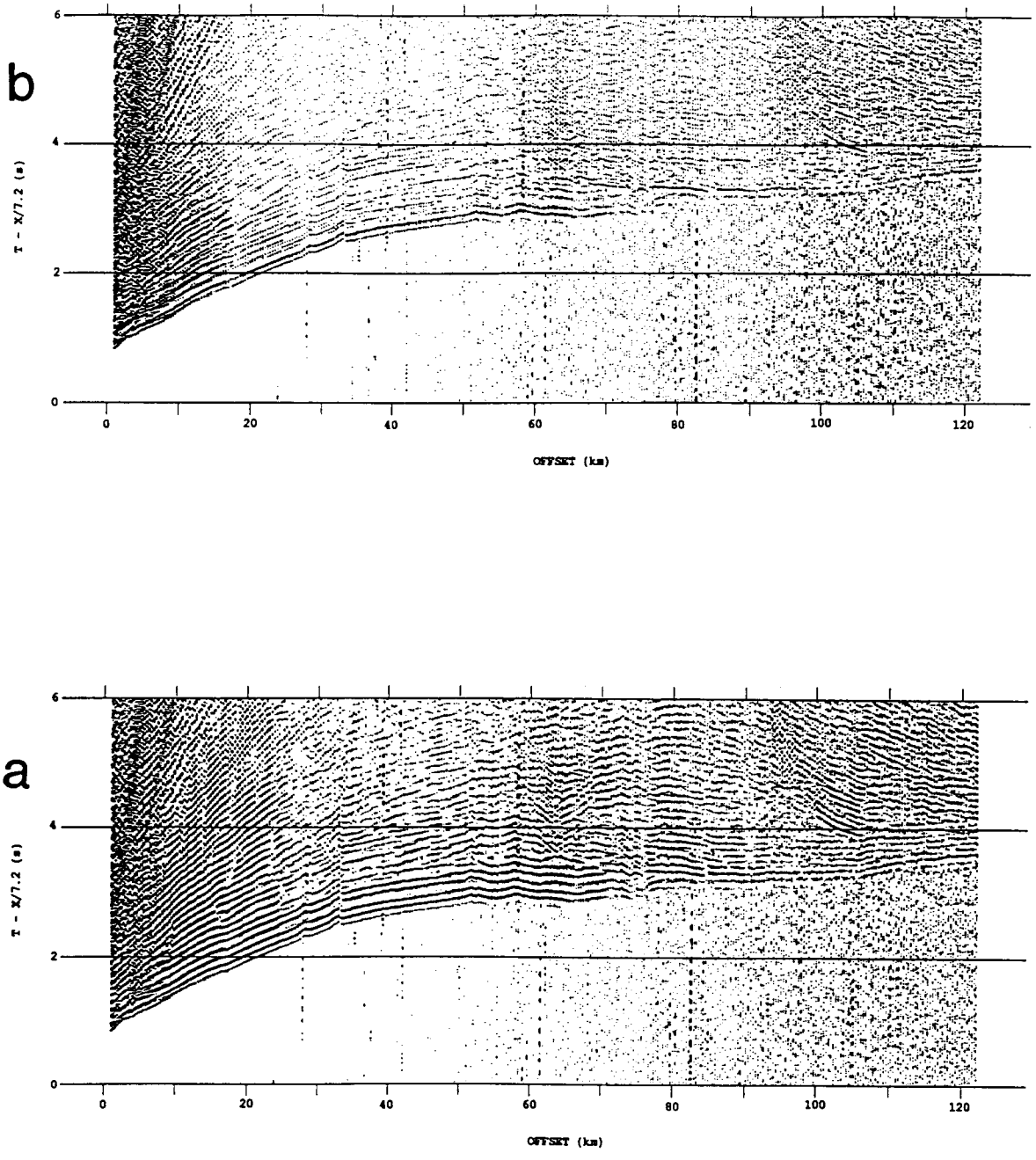

Figure 5. a) Portion of record section from OBS-C4 after frequency filtering (5-30 Hz) but prior to deconvolution, **b)** same record section following deconvolution based on a trace-by-trace 4 second design window hung approximately 0.1 s ahead of the first arrival travel time curve. The filter length and prediction distance were 0.24 s and 0.048 s respectively. The data were sampled at 0.008 s..

Seismic Model: Introduction

Constraints

The goal of geophysical modeling is to construct a geologically sensible model which satisfies all of the geological and geophysical constraints simultaneously. However, modeling is inherently non-unique and any number of models may satisfy the given constraints. Fortunately, the number of reasonable models decreases rapidly as the number of independent constraints increases. The following constraints contributed to the development of the velocity model presented below.

- The travel times and amplitudes of reflected and refracted rays shot through the model should be consistent with the travel times and amplitudes of reflected and refracted arrivals recorded at the six wide-aperture stations.
- The position of any reflective interfaces in the model should be consistent with the position of reflections observed on the CDP profile.
- The model must satisfy any known geologic controls provided by mapped outcrops and drillholes.
- The model should either support the results from previous investigations or adequately explain any discrepancies.
- The calculated gravity anomaly response of the model should be consistent with the observed gravity anomaly.

Although the magnetic field associated with the MRS could be used as an additional constraint, problems with estimating the effects of remanent magnetism associated with such a large body of syn-volcanic material precluded any serious attempt to model it. The magnetic profile along line A is shown in Figure 4.

Modeling approach

The first step in developing a seismic model was the velocity analysis of the wide-aperture data. This was accomplished by performing a 1-D tau-sum recursion on the digitized first-break travel time curve from each instrument. The recursions were done using a computer algorithm based on the formulations of Diebold and Stoffa (1981) and Vera and Diebold (1984).

The resulting velocity-depth functions were converted to two-way travel time (twtt) and projected onto the CDP reflection profile. Keeping in mind that the velocity analysis assumes flat lying laterally homogeneous beds, reflections on the CDP profile were used to map prominent velocity breaks between the instruments. Conversion of the reflection picks back to depth provided an initial 2-D seismic model. This initial model was then iteratively refined by interactive 2-D forward ray tracing.

Comparison of the 1-D velocity-depth functions with those at each instrument site in the final velocity model is shown in Figure 6. It should be noted that the 1-D velocity-depth functions are unsmoothed and are therefore non-monotonic with depth. Such features are part of the error response of the recursion method (Diebold, submitted) and are to be expected.

In general, the 1-D velocity-depth functions are similar to those in the final model until a depth between 5-10 km beneath the OBSs. These departures probably indicate the depth at which lateral velocity variations become important. By comparison, the better match for the two landbased stations, SUP4 and C1, at these depths suggests that lateral velocity variations are not as important within the Archean crust which forms the flanks of the rift. The shallow mismatch at site SUP4 is unimportant because the large minimum offset at this station precludes any good near surface control. The low velocity zone beneath OBS-C9, at a depth of about 32 km in the model, is not very well constrained. The feature corresponds to continental crust which sits adjacent to a downward tapering central

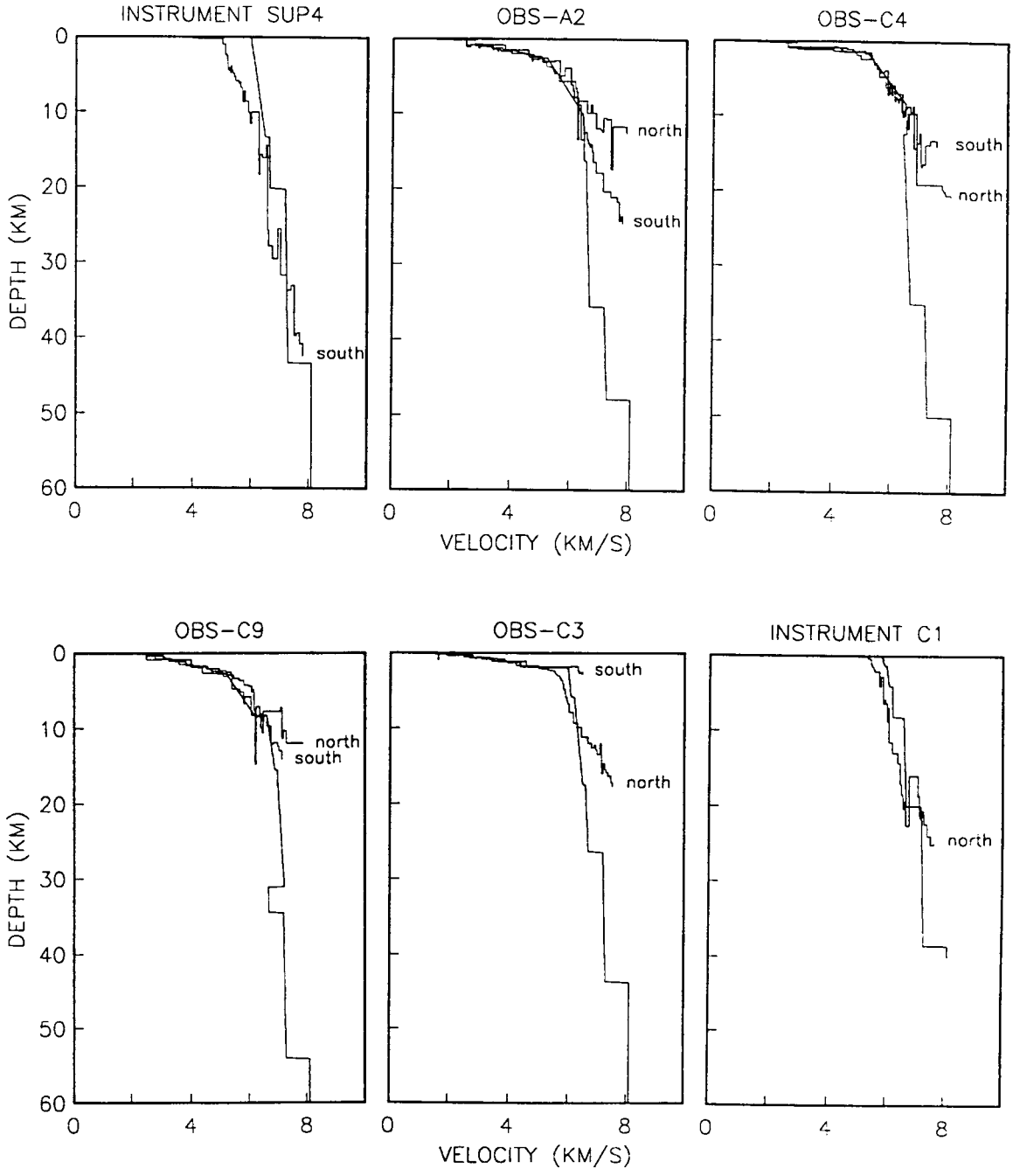

Figure 6. Comparison plots showing results of 1-D tau-sum recursion and final velocity-depth functions at each of the station locations in the model. North and south refer to the direction of offset from each instrument. The 1-D velocity-depth functions are unsmoothed.

half-graben containing higher velocity material (Figure 7a). This region of the model is discussed more fully in the layer-by-layer discussion given below.

Overview of the model

The seismic model is 275 km long and extends to a depth of 60 km (Figure 7a). The details of the upper 5 km of the model are shown in Figure 7b. The model's orgin is located at the northernmost site (SUP8) deployed along line A of GLIMPCE (Hutchinson et al., 1988). The locations of the six wide-aperture stations used in this study are shown in Figures 3 and 7. Although the track line appears to be nearly normal to the regional structural trends, as suggested by the mapped geology, a general assumption of two-dimensionality is clearly not valid for the entire crust as indicated by the potential field anomalies (O'Hara, 1982; Hinze et al., 1982). Therefore, some of the features in the model may actually correspond to structures located to the side of the trackline at slightly shallower depths.

In order to facilitate discussion, the use of the word range refers to positions along the seismic model shown in Figure 7. It should not be confused with the term offset which will only be used when describing distances relative to a specific instrument. Positive and negative offsets designate southward and northward offsets respectively. Ranges and offsets will always be given in kilometers and all seismic velocities are p-wave velocities in units of kilometers per second.

Ignoring the uppermost layer, which corresponds to the waters of Lake Superior, the seismic model comprises five distinct crustal layers (Figure 7) which generally represent: 1) the upper Keweenawan post-volcanic sedimentary sequence, 2) the upper Keweenawan transitional sequence and the lower and middle Keweenawan syn-volcanic sequence, 3) the Archean upper continental crust, 4) the lower crust, and 5) the upper mantle. In addition to these major crustal layers, the three uppermost layers each contain a

Figure 7. **a**) Velocity-depth model along line A of GLIMPCE showing p-wave velocities (km/s) at the top and bottom of each layer and sublayer. Layer 1 (sublayers 1a,1b,1c) corresponds to upper Keweenawan post-rift sedimentary sequence. Except for the shallow blocks directly beneath the IRFZ layer 2 (sublayers 2a,2b,2c,2d,2e) correspond to the middle and lower Keweenawan syn-rift volcanic and intercalated sedimentary sequence. Layer 3 (3a,3b,3c,3d,3e,3f) correspond to Archean upper crust. Layers 4 and 5 correspond to the lower crust and upper mantle respectively. Depths are relative to the surface of Lake Superior which is 83 meters above sea level. Dashed boundaries indicate the absence of a velocity contrast across that portion of the boundary. The vertical exaggeration is approximately 3. **b**) Detailed view of the upper 5 km of the velocity-depth model. The vertical exaggeration is approximately 31.

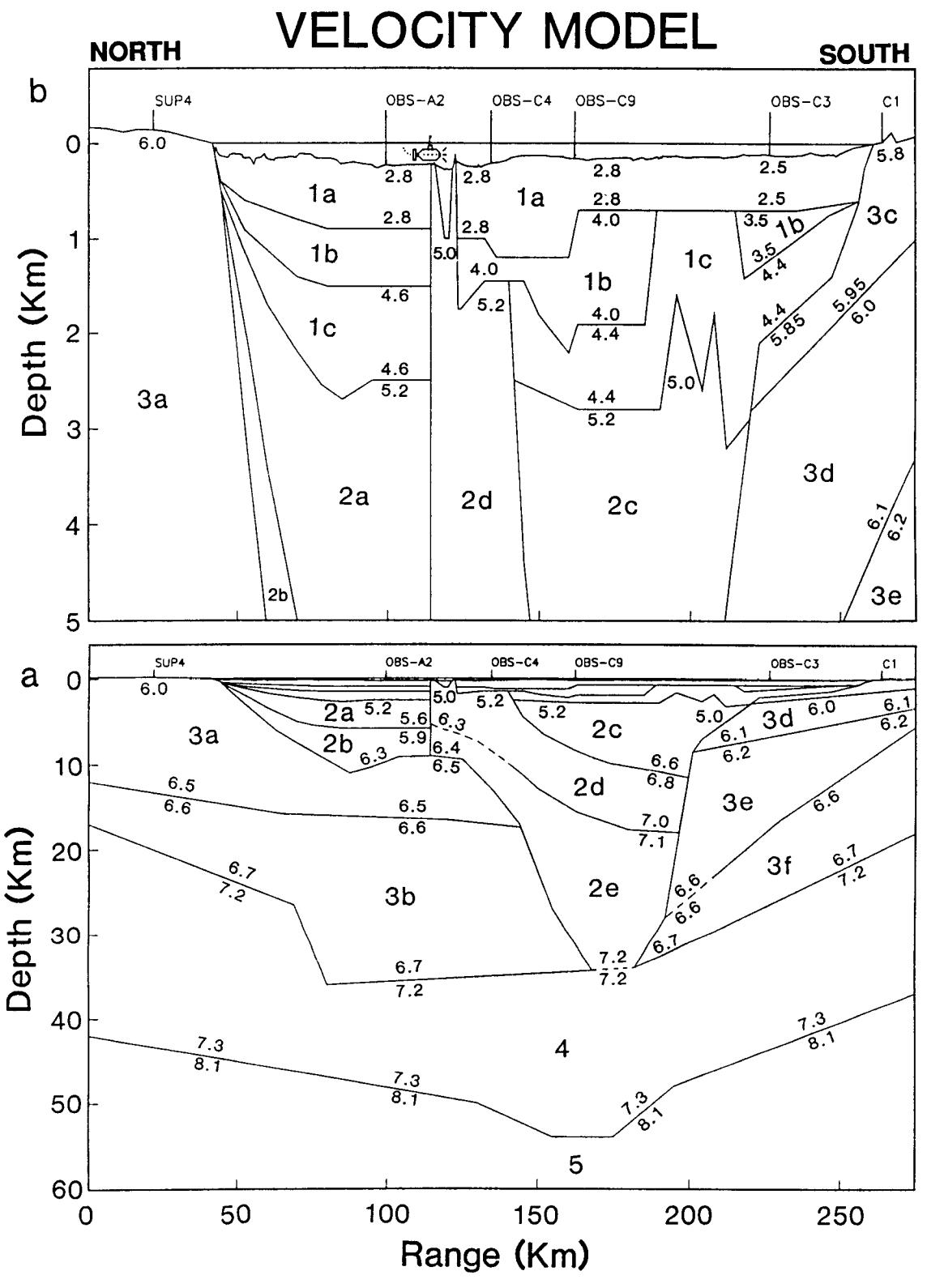
VELOCITY MODEL
NORTH
SOUTH
b
a
SUP4
OBS-A2
OBS-C4
OBS-C9
OBS-C3
C1
Depth (Km)
Range (Km)
1a
1b
1c
2a
2b
2c
2d
2e
3a
3b
3c
3d
3e
3f
4
5

Figure 7

small number of sublayers. Layer 1 comprises three sublayers (labeled 1a, 1b and 1c in Figure 7b), layer 2 has five sublayers (labeled 2a to 2e in Figure 7a), and layer 3 has six sublayers (labeled 3a to 3f in Figure 7a). Although many of these sublayers are interpreted below as corresponding to specific stratigraphic units, the ordering of the labels (i.e. 2a, 2b, 2c, 2d, 2e) does not necessarily denote stratigraphic order.

The match between the CDP profile and the seismic model is illustrated in Figure 8 in which the velocity-depth model (Figure 7a) has been converted to two-way travel time and then projected onto a copy of the migrated CDP profile. Considering that the model was constructed in part from information taken directly from the CDP profile, close agreement between them is not unexpected. However, the quality of the match does help to validate the model by demonstrating the model's ability to satisfy the constraints imposed by the CDP profile. Many of the details of the match between the CDP profile and the seismic model are discussed below in the layer-by-layer validation of the model.

By comparing Figure 4 with Figure 8, it is apparent that the geometry of the five crustal layers defined for the seismic model match similar crustal elements interpreted for the CDP profile by Cannon et al. (1989). For example, layer 1 in the seismic model matches the depth and extent of the upper Keweenawan section as interpreted by Cannon et al. very well. This includes the thinning of the upper Keweenawan section near both the IRFZ and Keweenaw fault, as well as the dip and landward projection of the upper Keweenawan section at the margins of the Lake Superior basin. The shape of layer 1 also matches some of the finer structural details interpreted by Cannon et al. such as the angular unconformity directly above the Manitou structural zone (Figure 4, SP 1100-1400, MR 205-190), and the position and sense of offset across the Isle Royale and Keweenaw faults.

The overall distribution of the syn-volcanic sequence interpreted by Cannon et al. is matched quite well by layer 2 in the velocity model. In particular, the shapes of sublayer 2d and 2e correspond very well with the inferred distribution of the Portage

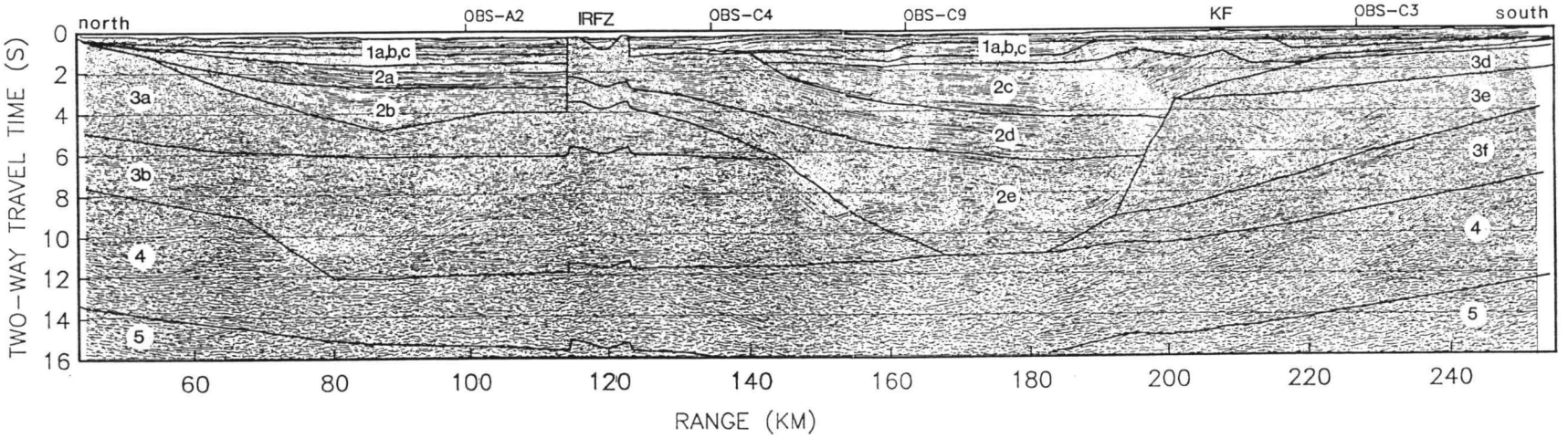

Figure 8. Comparison of velocity-time model and the migrated common depth point (CDP) profile. The labels correspond to the model layers in Figure 7.

Lake volcanics and the lower Keweenawan (Osler ?) volcanics, respectively. The handles of these ladle-shaped sublayers closely match the drape of these sequences across the hingeline which forms the northern boundary of the central half-graben. To avoid later confusion, it should be pointed out that the uppermost portion of sublayer 2d which projects upward beneath the IRFZ, is interpreted below as comprising upper Keweenawan sedimentary rocks rather than volcanic rocks. This complex region of the model is discussed in greater detail below in a section devoted to the IRFZ.

Although Cannon et al. (1989) do not delineate an upper and lower continental crust, the boundary between layers 3 and 4 approximately follows the dip and position of a number of complex reflections seen in the lower portions of the CDP profile. Taken together, the total extent of layers 3 and 4 is largely the same as that of the Archean crust as interpreted from the CDP profile (Cannon et al., 1989). The fact that the position of the modeled Moho, represented by the boundary between layers 4 and 5, does not agree very well with the interpretation of the CDP profile, highlights a higher degree of uncertainty associated with the edges and lower portions of the model. Such uncertainties in the model are discussed in more detail below.

The modeling of travel times and crossover distances is best illustrated by ray diagrams and travel time curves. Figures 9 thru 12 show ray diagrams (part a), and travel time curves (part b), for the close offset arrivals recorded at the four OBS sites. These figures illustrate the ray paths in the upper 5 km of the model (Figure 7b). Similar diagrams for the larger offset arrivals at all six stations are shown in Figures 14 to 19 (parts a and b). Modeling of critical points and velocity gradients is demonstrated by the synthetic wide-aperture data sections shown as part c of Figures 14 to 19. These synthetic sections illustrate the ability of the model to qualitatively predict the spacial and temporal variations in seismic amplitude observed in the data sections. A more quantitative comparison of the observed and calculated amplitudes is precluded by the fact that the seismographs were not calibrated to record absolute ground motion.

The synthetic sections were generated from amplitude information gained by shooting multiple sets of rays through the model with a take-off angle difference of 0.1 degree. Each set of rays was governed by a ray code describing a specific raypath. Appendix B contains copies of the synthetic sections which have been scaled to match the uninterpreted data sections in Appendix A. The source time function used to generate the synthetic sections is also listed in Appendix B. The ray diagrams show approximately every third ray used to generate the synthetic sections. The travel time curves, which overlay the data sections, were calculated at the same time as the amplitudes used to create the synthetic sections. The labeling of the travel time branches is explained in the figure captions. The details of each of these figures will be addressed in the layer-by-layer discussion given below.

Seismic Model: Layer-by-Layer Validation and Interpretation

Layer 1

The uppermost crustal layer contains three sublayers, labeled 1a,1b and 1c in Figure 7b. The velocity and thickness of the sublayers beneath each instrument is fairly well constrained by the slopes and crossover distances observed in the near surface data (Figures 9 to 12). The thinning and termination of individual sublayers as they approach the edges of the Lake Superior basin are not well constrained; the overall thinning and termination of layer 1, however, can be inferred from the mapped geology (Wold and Hinze, 1982) and the CDP reflection profile (Cannon et al., 1989).

The ranges of p-wave velocities exhibited by each of these sublayers are 2.5-2.8, 3.5-4.0, and 4.4-4.6 km/s respectively. The variations in p-wave velocity are a function of range (not depth), with lower velocity material generally residing on the southern flank of the rift. Based on previously reported velocities of upper Keweenawan rocks (Table 1) and information from the CDP profile (Figure 4), the sublayers are interpreted as corresponding to sedimentary rocks of the Bayfield-Jacobsville Group (1a and 1b) and the Oronto Group (1c). Correlation of sublayer 1a with the Jacobsville Sandstone is also supported by the fact that Jacobsville Sandstone crops out on the south shore and on the nearby Keweenaw peninsula (Figure 2). This same correlation for the segment of sublayer 1a north of the IRFZ, is supported by observations made during a recent submersible survey of the Superior Shoal (Manson and Halls, 1989). The three sublayers are observed beneath each OBS, except for OBS-C4, which apparently has only sublayers 1a and 1b directly beneath it.

The rocks in sublayer 1a have p-wave velocities of 2.8 km/s north of the Keweenaw fault (beneath OBS's A2, C4 and C9) and 2.5 km/s south of the Keweenaw fault (beneath OBS C3). Interestingly, these velocities are considerably lower than those

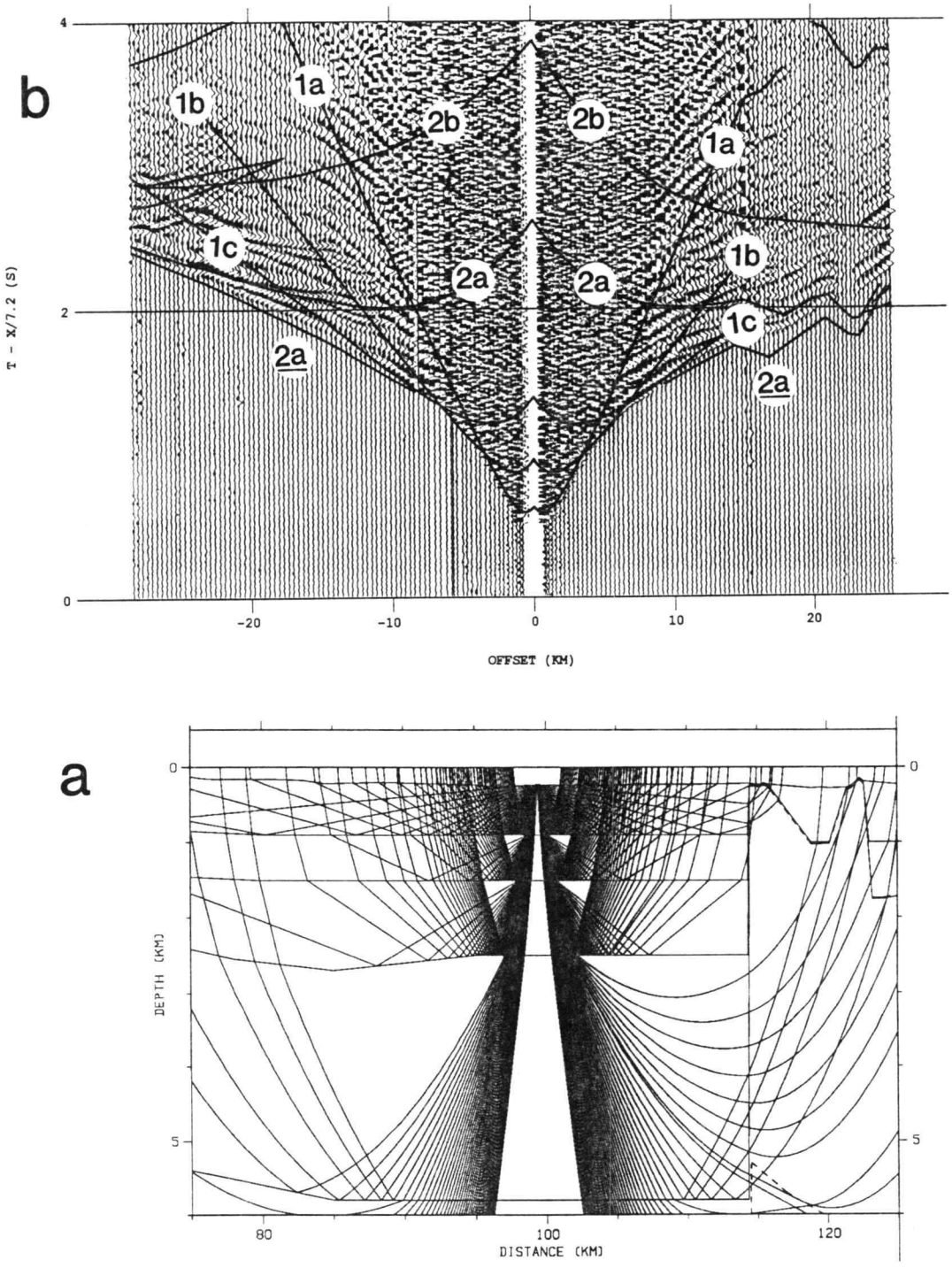

Figure 9. **a**) Near surface (0-6 km) ray diagram for OBS-A2. See figure 15 for discussion of ray density. **b**) Record section from OBS-A2 with calculated travel time curves overlaid. See appendix A for scaling and filtering parameters. The branch labels refer to the layer or sublayer (shown in figure 7) in which the corresponding rays bottom out. Underlined labels refer to purely refracted first arrivals.

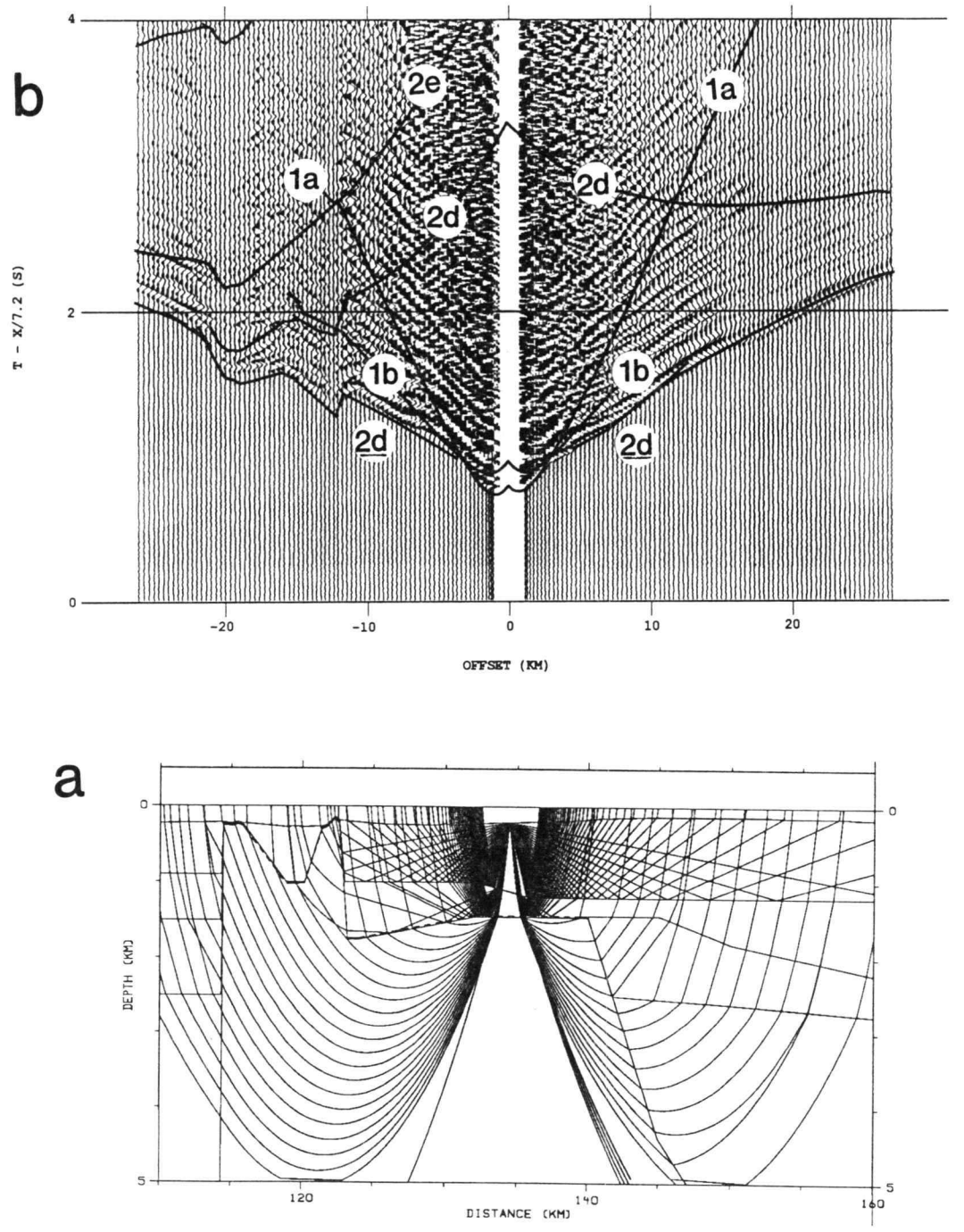

Figure 10. **a**) Near surface (0-5 km) ray diagram for OBS-C4. See figure 15 for discussion of ray density. **b**) Record section from OBS-C4 with calculated travel time curves overlaid. See appendix A for scaling and filtering parameters. The branch labels refer to the layer or sublayer (shown in figure 7) in which the corresponding rays bottom out. Underlined labels refer to purely refracted first arrivals.

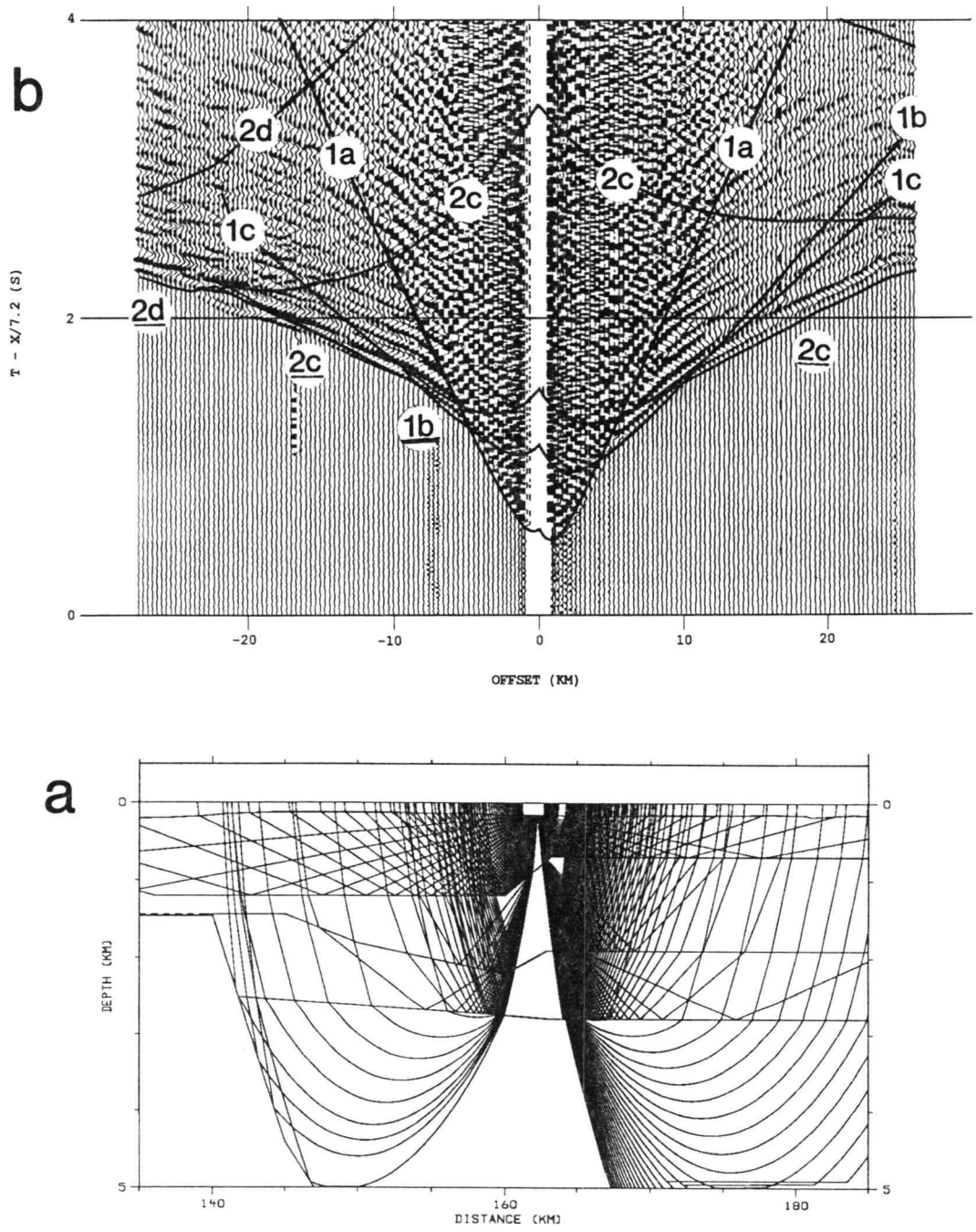

Figure 11. **a**) Near surface (0-5 km) ray diagram for OBS-C9. See figure 15 for discussion of ray density. **b**) Record section from OBS-C9 with calculated travel time curves overlaid. See appendix A for scaling and filtering parameters. The branch labels refer to the layer or sublayer (shown in figure 7) in which the corresponding rays bottom out. Underlined labels refer to purely refracted first arrivals.

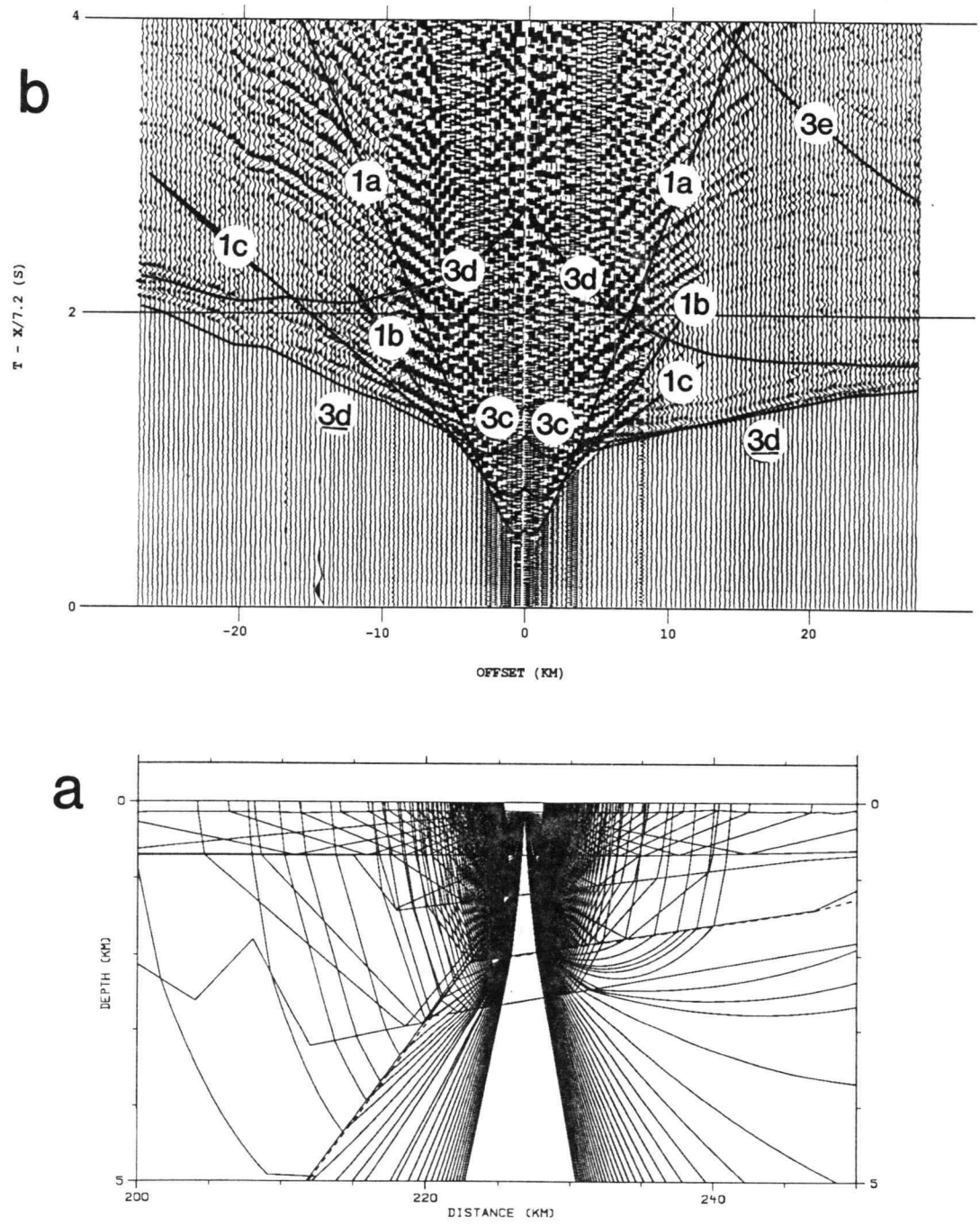

Figure 12. **a**) Near surface (0-5 km) ray diagram for OBS-C3. See figure 15 for discussion of ray density. **b**) Record section from OBS-C3 with calculated travel time curves overlaid. See appendix A for scaling and filtering parameters. The branch labels refer to the layer or sublayer (shown in figure 7) in which the corresponding rays bottom out. Underlined labels refer to purely refracted first arrivals.

previously reported for any layer within Lake Superior (see Table 1). One possible explanation for this discrepancy may be that, with the exception of the landbased survey shot by Mooney et al. (1970), all of the refraction profiles shot in the vicinity of Lake Superior prior to GLIMPCE had shot spacings which precluded good near-surface control. A contributing factor may be that the geometry of an OBS survey inherently creates a time delay in the arrival of the direct water wave (Kennett, 1976). This delay provides a broader offset window over which a relatively thin 2.5-2.8 km/s refractor may yield a first arrival segment. Incidentally, the lowest velocities reported by Mooney et al. (see Table 1) for the uppermost Keweenawan section are consistent with those reported here for sublayer 1a.

The 0.5 km thickening of sublayer 1a south of OBS-C4 and north of OBS-C9 is constrained by the complimentary asymmetry seen in the travel-time curves from these two instruments. Although the high degree of asymmetry seen in the record section for OBS-C9 (Figure 11b, offsets -4 to 4 km) was originally thought to be a manifestation of a mislocated instrument, the asymmetry is now believed to be due to a shallow structural feature directly beneath the instrument. The lack of asymmetry in the water wave arrival rules out any significant instrument mislocation. The exact nature of the structural feature beneath OBS-C9 is unknown, but a narrow zone of diffractions and minor offsets in near surface reflectors observed on the CDP profile (SP 1970) suggests the presence of a minor fault. The concept of a fault is supported by a similar offset in sublayer 1b which is required to properly model the second set of wide-angle reflections recorded at this site (labeled 1b on Figure 11b). The thickening of sublayer 1a north of OBS-C9 suggests that the fault was active during Jacobsville time; possibly developing in response to either late stage subsidence across the hinge line imaged on the CDP profile (Figure 4) or motion along the nearby IRFZ.

The two segments of sublayer 1b, located on the northern flank and over the central basin, are comprised of rocks having a p-wave velocity of approximately 3.8 and

4.0 km/s, respectively. Within the wedge shaped segment of sublayer 1b south of the Keweenaw fault, the rocks display a p-wave velocity of approximately 3.5 km/s. The thinning and shallowing of sublayers 1b and 1c south of the Keweenaw fault is required in order to properly model the high apparent velocities evident in the southern branch recorded at OBS-C3 (Figure 12b). The absence of sublayer 1b and the complex shape of sublayer 1c just north of the Keweenaw fault is discussed below in a section devoted to the Keweenaw fault.

Because sublayer 1c yields relatively few first arrivals (Figure 9 to 12), constraining its thickness and velocity beneath each OBS was not as easy as for sublayers 1a and 1b. On the northern flank of the rift, beneath OBS-A2, sublayer 1c contains rocks displaying a p-wave velocity of approximately 4.6 km/s. South of OBS-C4, sublayer 1c contains rocks having a p-wave velocity of approximately 4.4 km/s. Variations in the thickness of this sublayer between recording stations is constrained primarily by the timing of refracted arrivals coming from layer 2. For example, the thickness of sublayer 1c directly beneath OBS-A2 is fairly well constrained by the crossing-over of the refracted arrivals, however, the thickening of sublayer 1c north of OBS-A2 is only suggested by the later arrival of refracted rays coming from shots to the north of the instrument relative to those coming from shots to the south of the instrument. Obviously, the timing of these arrivals could be equally accommodated by laterally varying the velocity in sublayer 2a or by varying the thickness of sublayers 1a and 1b. The absence of sublayer 1c from beneath OBS-C4 is indicated by the apparent lack of a wide-angle reflection from an appropriate interface (Figure 10), however, the presence of a relatively thin member of sublayer 1c cannot be ruled out. Like sublayers 1a and 1b, the thicknesses and velocities modeled for sublayer 1c are consistent with results from previous investigations (Table 1).

The Keweenaw Fault

The overall thinning of layer 1 near the Keweenaw fault is supported by information from the CDP profile and by a small amplitude (20 to 40 ms), time advance anomaly whose onset is best observed on the record sections from OBS-C9 (Figure 17b, 26 km offset) and OBS-C4 (Figure 16b, 51 km offset). In addition to the time advance anomaly, the shallowing of the volcanics associated with layer 2 is supported by a strong maximum in the magnetic profile over the fault (Figure 4), and by the fact that the fault is mapped as a high angle reverse fault on the nearby Keweenaw Peninsula (Wold and Hinze, 1982).

The pinching out of sublayer 1b and the shallowing of sublayer 1c near the Keweenaw fault is constrained primarily by the pinching out and shallowing of reflectors observed on the CDP profile (Figure 8, MR 185-210). In particular, the shape and position of the lower boundary of sublayer 1c (MR 186-205) corresponds quite well with an angular unconformity directly above the Manitou structural zone (Figure 4) (Cannon et al., 1989). Interestingly, if the seismic model presented here is accurate, it would place upper Oronto Group rocks above the angular unconformity rather than Jacobsville rocks as interpreted by Cannon et al. (1989). It would also suggest the presence of another unconformity at the top of sublayer 1c, corresponding to an erosional surface which developed during Bayfield-Jacobsville time. The presence of a second unconformity would suggest that reverse motion on the fault was two-phased, with the earliest movement occuring during Oronto deposition and the second after the start of Bayfield-Jacobsville deposition. A second phase of movement along the fault is also suggested by the apperent folding of the deeper angular unconformity. The presence of an unconformity between the Bayfield-Jacobsville Group and the Oronto Group is supported by the fact that over much of the Bayfield syncline, Bayfield Group rocks have low dips and the Oronto Group rocks have steeper dips (Ojakangas and Morey, 1982b).

Obviously, without having an instrument sited directly above the Manitou structural zone, there are any number of models which would fit the wide-aperture observations equally well. Included in the list of possible models is one which has only Bayfield-Jacobsville rocks above the deeper unconformity. The geometry of such a model would be essentially identical to the interpretation of the CDP profile set forth by Cannon et al., (1989). The model presented in this thesis is preferred because it provides a superior match to the CDP profile, especially near SP 1450 (MR 188) where the reflectors corresponding to the base of sublayer 1b appear to pinch out. It should be noted, however, that the pinching out of these reflectors may be a processing artifact caused by variations in water depth and near surface velocity variations.

The Isle Royale Fault Zone (IRFZ)

The model becomes quite complex near the IRFZ (Figure 7b, MR 114-122). The modeling of two narrow higher velocity blocks within the IRFZ is supported by a large amplitude (50 to 100 ms) double-peaked time-advance anomaly observed at every station. For example, the anomaly is readily observed on OBS-A2 (Figure 9b) at offsets of 15 to 25 kms, and on OBS-C4 (Figure 10b) at offsets of -11 to -21 kms; both of these offsets correspond to rays emerging from the IRFZ. The fact that the anomaly is associated with rays emerging from the IRFZ at every station requires that it be due to a near surface feature directly beneath the fault zone.

The nature of the material comprising the higher velocity blocks is unknown but the recent discovery of Jacobsville Sandstone along the walls of steep-sided glacially carved canyons in this area (Manson and Halls, 1989), suggests that the uppermost portion of the blocks may be Jacobsville Sandstone. If the narrow blocks are indeed upper Keweenawan sedimentary rock, their higher p-wave velocities suggests that hydrothermal alteration may have more fully indurated the upper Keweenawan section along two fault splays. Such an interpretation is supported by the fact that hydrothermal

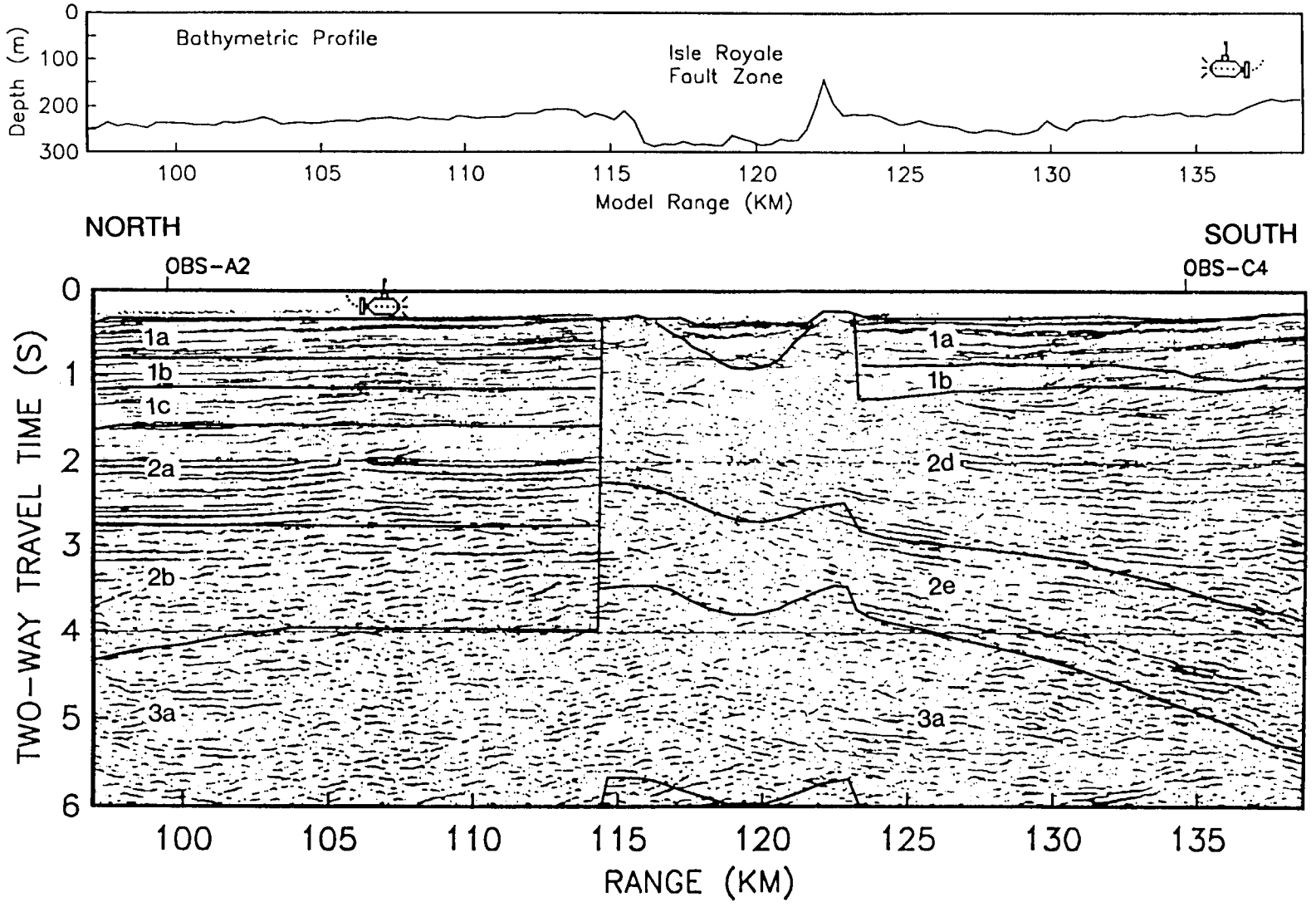

Figure 13. Detailed comparison of velocity-time model and migrated CDP profile in the vicinity of the Isle Royale fault zone.

alteration of the upper Keweenawan section is a common feature along the Keweenaw fault (White, 1971; Wold and Hinze, 1982; Van Schmus and Hinze, 1985) and that comparable p-wave velocities have been reported for indurated upper Keweenawan sedimentary rocks (Halls, 1969). Figure 13 shows an enlargement of the migrated CDP profile near the IRFZ with the seismic model (converted to twtt) superimposed. The clear correlation between the higher velocity blocks in the model, the two narrow diffraction zones on the CDP data and the narrow bathymetric trough supports the idea that the blocks are fault controlled features. It is quite conceivable that two narrow zones of more highly indurated sedimentary rock could be responsible for both the observed diffractions and the pronounced bathymetric relief.

Although it is possible that the higher velocity blocks (and the narrow zone of diffractions) may correspond to igneous intrusions, the fact that the Jacobsville Sandstone is devoid of cross-cutting intrusions of any kind (Kalliokoski, 1982) argues against it. In addition, the absence of a distinct positive gravity anomaly (Figure 4) across this narrow feature argues against the presence of high density igneous rocks at shallow depths. Although the lack of a distinct gravity anomaly may be due to the level of resolution imposed by the 8 km gravity data collection grid (O'Hara, 1982), it may also indicate a low density contrast between the higher velocity blocks and the surrounding sedimentary rock. Considering that the upper Keweenawan sedimentary rocks display a fairly broad range of p-wave velocities for a given density (Halls, 1969), a low density contrast would tend to support the idea that the higher velocity blocks correspond to hydrothermally altered sedimentary rocks, rather than higher density igneous intrusions. Finally, a recent submersible survey revealed no evidence of late Keweenawan igneous activity in the vicinity of the IRFZ (Manson and Halls, 1989; Halls, per. comm., 1989).

The velocity of the material between the two blocks is fairly well constrained. A superb fit of the time-advance anomaly recorded by OBS-C4 (Figure 10b) can be

accomplished by assigning the material between the blocks the same velocity (2.8 km/s) and thickness (1 km) as the uppermost sublayer beneath OBS-C4. Extending sublayer 1a between the two high velocity blocks is also supported by the presence of reflectors on the CDP profile (between the diffractions) which resemble those directly beneath OBS-C4 (Figure 13). In addition, analysis of refracted arrivals from the multichannel CDP profile indicate the presence of low velocity (2.8-3.9 km/s) material within the fault zone (Cannon et al., 1989). Although the exact travel time fits are not as good for the other more distant sites, the general character of the anomaly is fairly well modeled at each of the wide-aperture sites. Additional modeling of the IRFZ, which includes modeling of the magnetic profile, may help to resolve some of the details of this structure.

The pinching out of sublayer 1c south of OBS-C4 corresponds well with the shallowing and pinching out of reflectors just south of the hinge line on the CDP profile (Figure 8, MR 142). The apparent truncation of sublayer 1c south of OBS-C4 suggest that the Bayfield-Jacobsville sedimentary rocks represented by sublayers 1a and 1b, rest unconformably upon middle Keweenawan volcanic rocks represented by sublayer 2d. The inferred unconformity appears to be a late Oronto to middle Bayfield-Jacobsville erosional surface, which brackets the dates inferred for the unconformities associated with the Keweenaw fault discussed earlier. Taken together, these observations indicate that tilting and uplift associated with reverse movement on the Keweenaw and Isle Royale faults took place at approximately the same time.

Layer 2

The second crustal layer, representing the bulk of the middle and lower Keweenawan syn-rift volcanic rocks and intercalated sediments, comprises five sublayers labeled 2a to 2e on Figure 7a. Unlike the sublayers in layer 1, the sublayers in layer 2 contain vertical velocity gradients in which seismic velocity increases with depth. The

presence of a velocity gradient is generally indicated by a progressive increase in apparent velocity with no prominent crossovers being observed in the data.

Restricted to the northern flank of the rift, sublayers 2a and 2b correspond closely to the Osler volcanic sequence and the lower Proterozoic sequence inferred from the CDP data by Cannon et al. (1989) (compare Figures 4 and 8). The top of sublayer 2a sits above the set of strong reflectors interpreted by Cannon et al. as representing the top of the Osler Group. This is a surprising interpretation considering that the boundary between sublayers 1c and 2a corresponds to a fairly substantial velocity contrast, and one would expect the boundary to coincide with a fairly strong reflector on the CDP profile. Since the depth to this interface is constrained only by data recorded by OBS-A2 (see layer 1 discussion above), the most likely explanation for this incongruity is that the boundary observed by OBS-A2 is off the line of section (and slightly shallower) than the one observed on the CDP profile. Another possible explanation is that OBS-A2 is mislocated (see field parameter discussion above); however, the high degree of symmetry evident in the close offset data restricts any instrument mislocation to be perpendicular to the track line.

The rocks comprising sublayer 2a are modeled as having p-wave velocities which range from 5.2 to 5.6 km/s. The depth to the base of sublayer 2a is contrained by the modeling of a wide-angle reflection observed by OBS-A2 at about -20 km offset (labeled 2a on Figure 9b). The reflection appears to come from the unconformity which Cannon et al. interpret as marking the base of the Osler volcanics on the northern flank of the rift (Figure 4). Both the amplitude and travel time curve modeled for this reflection north of the instrument (Figure 15) closely match those observed in the record section. Although a reflection from this interface should also be observed for shots south of OBS-A2, the structural complexity of the IRFZ apparently disrupts any coherent arrival from this interface.

Sublayer 2b contains rocks which display velocities ranging from 5.9 to 6.3 km/s. The thickness of this sublayer south of OBS-A2 is fairly well constrained by the abrupt decrease in the amplitudes of refracted first arrivals observed at OBS-C4 (-55 to -60 km offset, Figure 16b). Likewise, the thickening of sublayer 2b to fill the buried syncline imaged on the CDP profile north of OBS-A2 (85 to 90 km, Figure 4) is constrained by the abrupt decrease in first arrival amplitudes observed on instrument SUP4 (Figure 14b at about 93 km offset). The ray diagrams for these instruments (Figures 14a and 16a) indicate that the drop in amplitude is due to a defocusing of the rays as they encounter the lower gradient present in sublayer 3a. The model does a fairly good job predicting these drops in first arrival amplitudes (Figures 14c and 16c). The geology of the rocks within this sublayer is open to interpretation. Based on the unconformity imaged on the CDP profile, Cannon et al. (1989) suggest these rocks to be pre-Osler deposits. Whether the rocks correspond to pre-rift sediments or early syn-rift volcanics cannot be determined from the seismic data, however, their higher p-wave velocities, relative to the overlying Osler volcanics, tends to support an igneous interpretation. However, the possibility that the rocks correspond to higher p-wave velocity metasedimentary rock cannot be ruled out.

Sublayer 2c covers the uppermost portion of the central half-graben and extends across the Keweenaw fault, onto the southern flank of the rift (Figure 7b, MR 137 - 222). The seismic velocity of the rocks along the top of this sublayer range from 5.0 near the Keweenaw fault, to 5.2 km/s beneath OBS-C9. Along its base, the velocity increases from north to south; reaching a maximum of 6.6 km/s near the thickest point. Based on the observed p-wave velocities and information gained during the modeling of the gravity profile (discussed later, Figure 21), the upper portion of sublayer 2c is thought to represent upper Keweenawan (Oronto ?) sedimentary rocks; whereas, the lower portion probably contains a transitional sequence comprising a mixture of

Figure 14. a) Full model ray diagram for site SUP4 (model range 22.12 km) . The figure shows approximately every third ray used to calculate the synthetic section shown in part c. **b)** Record section from site SUP4 with calculated travel time curves overlaid. See appendix A for scaling and filtering parameters. The branch labels refer to the layer or sublayer (shown in figure 7) in which the corresponding rays bottom out. Underlined labels refer to purely refracted rays. The travel time curves, were calculated at the same ray density as the synthetics. **c)** Synthetic record section for site SUP4. See appendix B for calculation and plotting parameters.

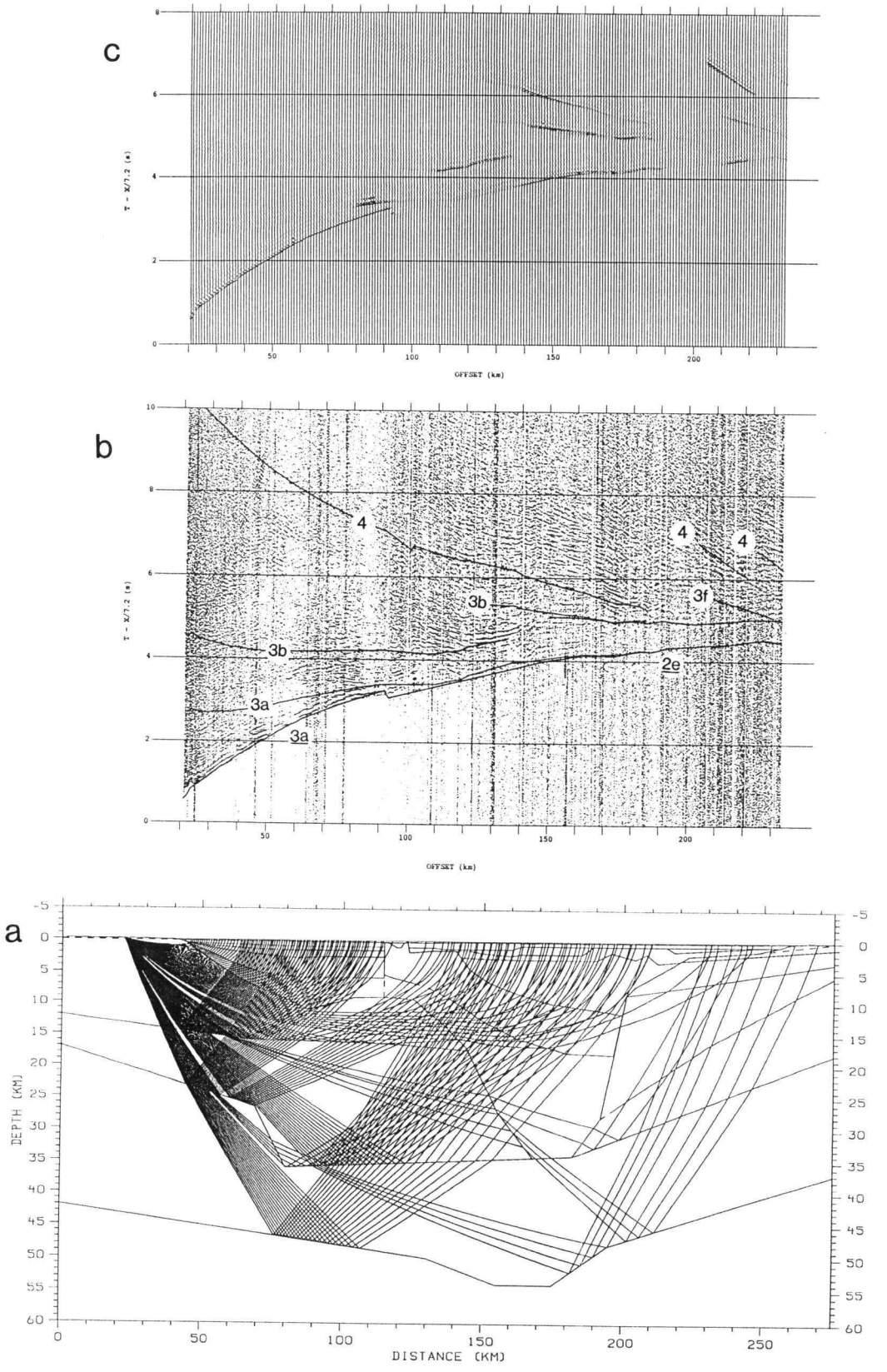

Figure 14

Figure 15. a) Full model ray diagram for OBS-A2 (model range 99.42 km). The figure shows approximately every third ray used to calculate the synthetic section shown in part c. **b)** Record section from OBS-A2 with calculated travel time curves overlaid. For the sake of record clarity the section is shown without the wiggle. See appendix A for scaling and filtering parameters. The branch labels refer to the layer or sublayer (shown in figure 7) in which the corresponding rays bottom out. Underlined labels refer to purely refracted rays. The travel time curves, were calculated at the same time as the synthetics. **c)** Synthetic record section for OBS-A2. See appendix B for calculation and plotting parameters.

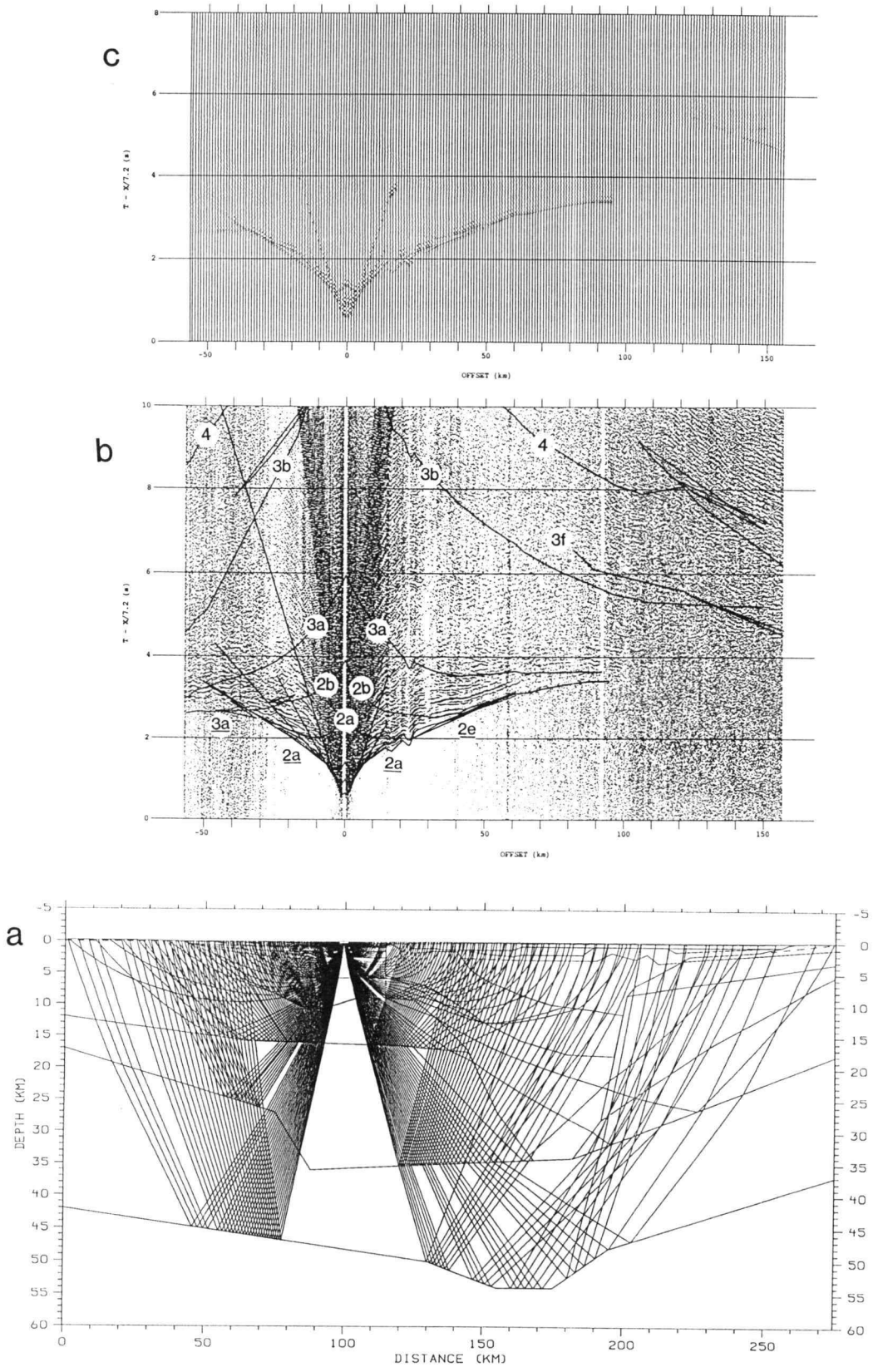

Figure 15

Figure 16. a) Full model ray diagram for OBS-C4 (model range 134.46 km). The figure shows approximately every third ray used to calculate the synthetic section shown in part c. **b)** Record section from OBS-C4 with calculated travel time curves overlaid. For the sake of record clarity the section is shown without the wiggle. See appendix A for scaling and filtering parameters. The branch labels refer to the layer or sublayer (shown in figure 7) in which the corresponding rays bottom out. Underlined labels refer to purely refracted rays. The travel time curves, were calculated at the same time as the synthetics. D1 and D2 refer to diffractions originating at the top (range 199.5 km, depth 11.5 km) and bottom (range 196.4 km, depth 18.0 km) of sublayer 2d were they intersect the Keweenawan fault (KF). **c)** Synthetic record section for OBS-C4. See appendix B for calculation and plotting parameters.

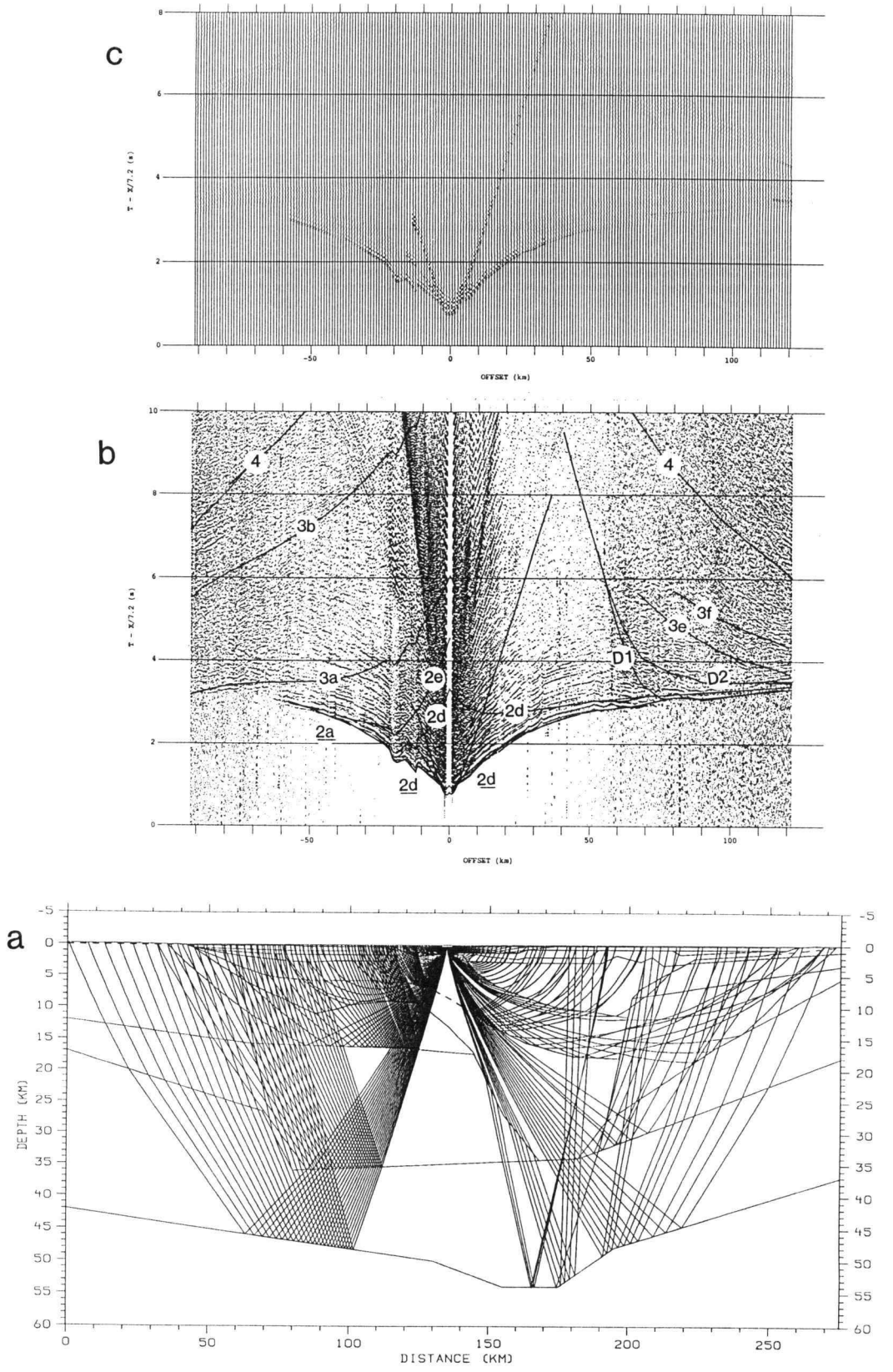
c
T - X/7.2 (s)
OFFSET (km)
b
4
3b
4
3f
3e
D1
D2
3a
2e
2d
2d
2a
2d
2d
T - X/7.2 (s)
OFFSET (km)
a
DEPTH (KM)
DISTANCE (KM)

Figure 16

Figure 17. a) Full model ray diagram for OBS-C9 (model range 162.27 km). The figure shows approximately every third ray used to calculate the synthetic section shown in part c. **b)** Record section from OBS-C9 with calculated travel time curves overlaid. For the sake of record clarity the section is shown without the wiggle. See appendix A for scaling and filtering parameters. The branch labels refer to the layer or sublayer (shown in figure 7) in which the corresponding rays bottom out. Underlined labels refer to purely refracted rays. The travel time curves, were calculated at the same time as the synthetics. D1 and D2 refer to diffractions originating at the top (range 199.5 km, depth 11.5 km) and bottom (range 196.4 km, depth 18.0 km) of sublayer 2d were they intersect the Keweenawan fault (KF). **c)** Synthetic record section for OBS-C9. See appendix B for calculation and plotting parameters.

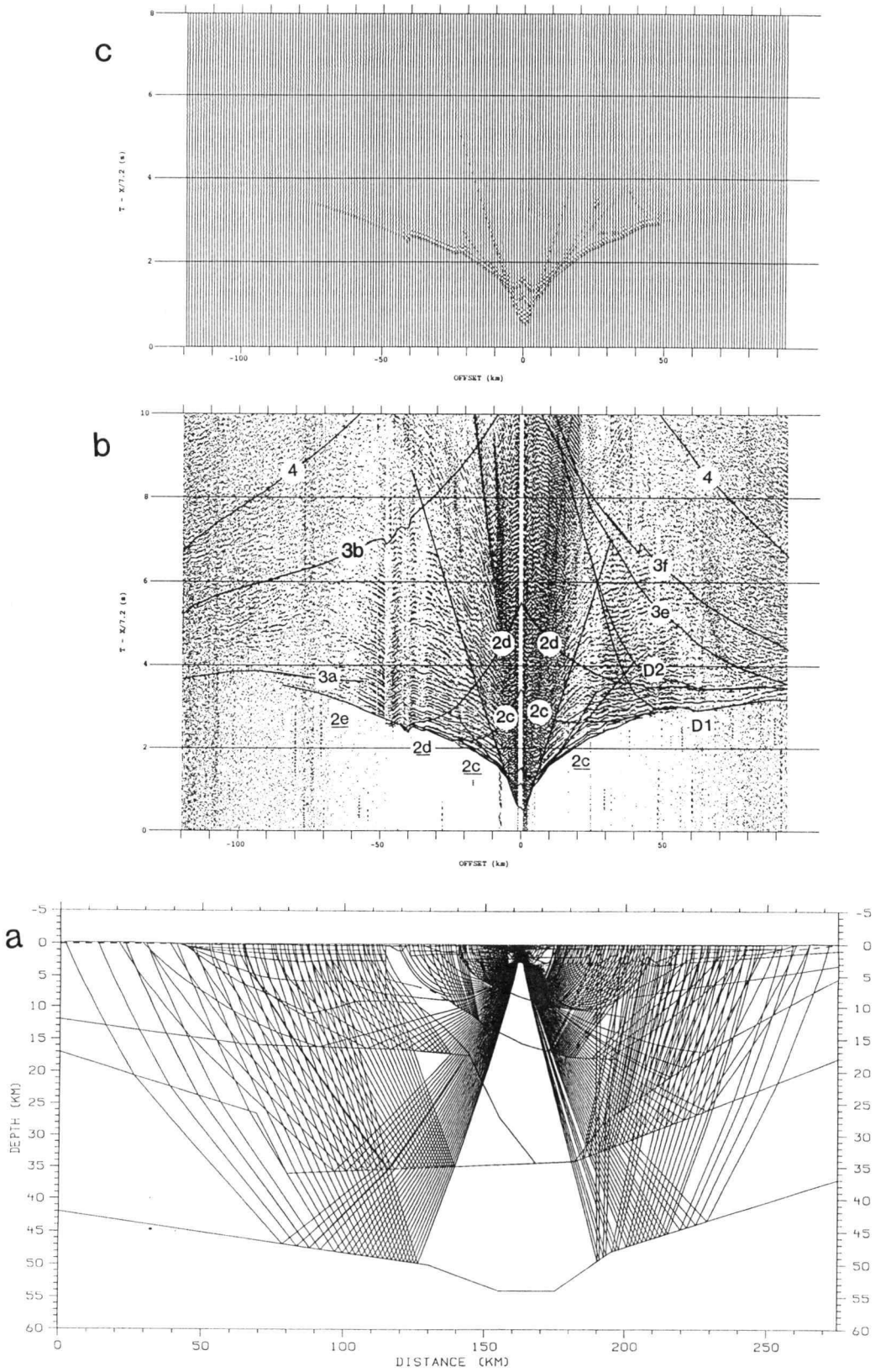
c
T - X/7.2 (s)
OFFSET (km)
b
4
3b
3a
2e
2d
2c
3f
3e
D2
D1
a
DEPTH (KM)
DISTANCE (KM)

Figure 17

Figure 18. a) Full model ray diagram for OBS-C3 (model range 226.76 km). The figure shows approximately every third ray used to calculate the synthetic section shown in part c. **b)** Record section from OBS-C3 with calculated travel time curves overlaid. For the sake of record clarity the section is shown without the wiggle. See appendix A for scaling and filtering parameters. The branch labels refer to the layer or sublayer (shown in figure 7) in which the corresponding rays bottom out. Underlined labels refer to purely refracted rays. The travel time curves, were calculated at the same time as the synthetics. **c)** Synthetic record section for OBS-C3. See appendix B for calculation and plotting parameters.

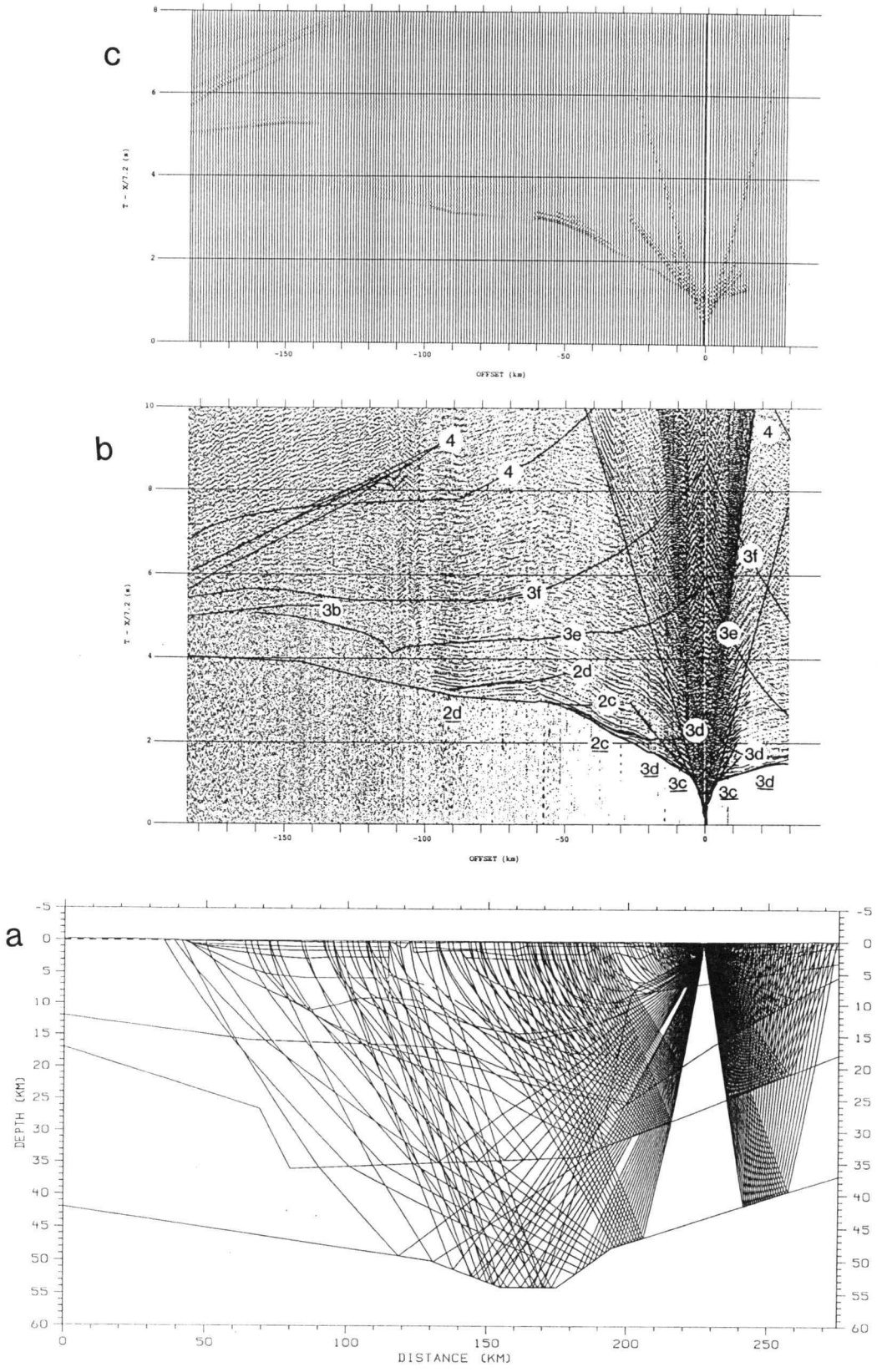

Figure 18

Figure 19. a) Full model ray diagram for site C1 (model range 263.97 km). The figure shows approximately every third ray used to calculate the synthetic section shown in part c. **b)** Record section from site C1 with calculated travel time curves overlaid. See appendix A for scaling and filtering parameters. The branch labels refer to the layer or sublayer (shown in figure 7) in which the corresponding rays bottom out. Underlined labels refer to purely refracted rays. The travel time curves, were calculated at the same ray density as the synthetics. **c)** Synthetic record section for site C1. See appendix B for calculation and plotting parameters.

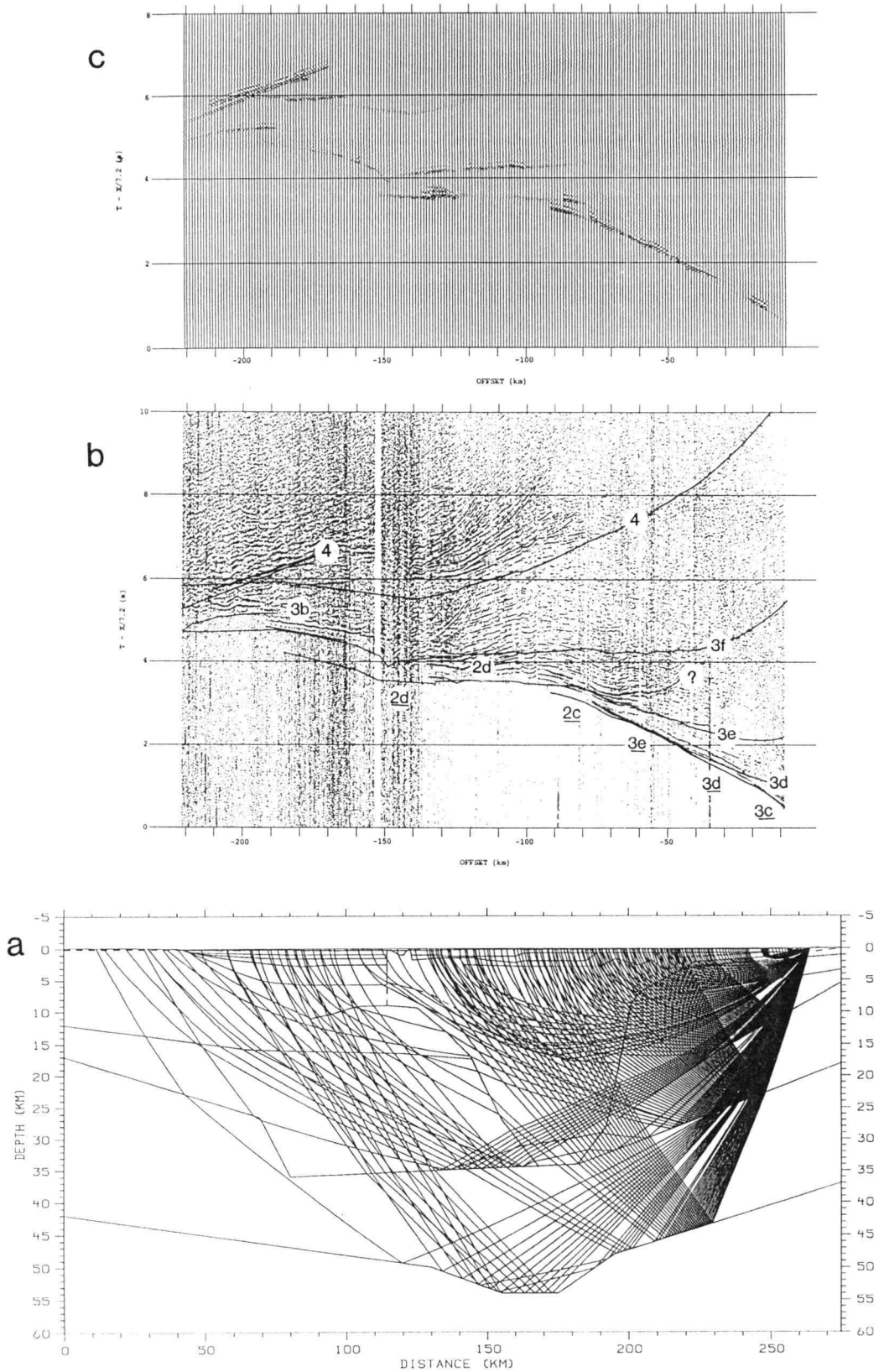

Figure 19

sedimentary and volcanic rocks. This interpretation is fully consistent with the interpretation of the CDP profile (Figure 4) put forth by Cannon et al., (1989).

The model does a fairly good job at predicting both the travel times and amplitudes of rays which reflect off the base of this sublayer and are recorded at OBS-C9 and OBS-C3. For example, the position of the boundary is constrained by the post-critical reflections observed at OBS-C9 at offsets of about -21 and 27 km (labeled 2c on Figure 17b). The proper modeling of the high amplitudes associated with the critical angle is shown in Figure 17c. As seen from OBS-C3 (Figure 18), the model predicts this same wide-angle reflection to be observable only through a very narrow offset window (-50 to -60 km). Such a restricted window may help to explain the narrow zone of high amplitudes recorded at this site at an offset of approximately -57 km.

Termination of the lower boundary of this sublayer against the Keweenaw fault is supported by the drop in amplitudes of first arrivals observed at OBS-C9 at approximately 52 km offset (Figure 17b). The model predicts that offsets greater than this (i.e. from 52 km to the southern edge of the model) constitute a shadow zone for both purely refracted rays as well as for rays reflected from the base of sublayer 2c. The low amplitude first arrivals observed on the record section beyond 50 km offset can be modeled as diffracted energy originating from the point where the lower boundary of sublayer 2c terminates against the fault (event labeled "D1" on Figure 17). Although lowering the gradient within sublayer 2c will permit rays to penetrate the shadow zone, doing so adversely affects the travel times and amplitudes of all the arrivals. However, additional modeling of the velocity gradients immediately adjacent to the fault might result in a model which permits some rays to penetrate the shadow zone.

The diffraction labeled "D2" originates from the point where the base of sublayer 2d terminates against the fault. For comparison, the same two diffraction points have been modeled for OBS-C4 (Figure 16). Although the amplitudes modeled for these diffractions are considerably lower than those observed on the corresponding record

sections, this is partly because the diffractions have been normalized so their peak amplitude is equal to the average modeled amplitude of refracted rays arriving at approximately the same offsets. Interestingly, the modeled travel time curves for these two diffractions appear to bracket a region of diffracted energy above the Keweenaw fault (~ 55 km offset on Figure 17b and ~ 83 km offset on Figure 16b). This zone of diffracted energy may be evidence that fairly energetic seismic waves may be trapped along lava flows within the Portage Lake sequence (sublayer 2d). Another possible explanation may be that either the dip or seismic character of the fault changes near the base of sublayer 2d. Less dip on the fault would tend to force any potential diffraction point northward, towards the center of the half-graben. The seismic character of the fault may change with depth in such a way that its ability to act as a seismic discontinuity is diminished.

Sublayer 2d is bound by the Isle Royale and Keweenaw faults with the majority of it resting beneath sublayer 2c. The shallowing of sublayer 2d beneath OBS-C4 closely resembles a 2-D seismic model proposed for the uppermost crust in this area by Luetgert (unpublished manuscript). Figure 8 shows that the upper and lower bounds of sublayer 2d closely match the shape and extent of the Portage Lake Volcanics interpreted from the CDP profile by Cannon et al. (1989). This interpretation is fully consistent with the range of velocities modeled for this sublayer. It should be remembered, however, that the base of the Portage Lake Volcanics on the CDP profile was arbitrarily placed along a pronounced change in reflectivity (Cannon et al., 1989). Therefore, any attempt to measure the amount of offset across the IRFZ, based on the apparent offset of the Osler Volcanics, would be very speculative.

Directly beneath the IRFZ the p-wave velocities assigned to this sublayer range from 5.0 to 6.4 km/s, corresponding to a vertical velocity gradient of approximately 0.3 s^{-1}. This relatively high gradient is needed in order to properly model the variations in amplitude of first arrivals emerging in the vicinity of the IRFZ as recorded at OBS-A2

(Figure 15c, 14 to 30 km offset) and OBS-C4 (Figure 16c, -10 to -35 km offset). Again, more detailed modeling of the IRFZ is needed in order to better resolve the velocities and gradients in the immediate vicinity of the fault zone. The velocity gradient gradually decreases southward until it reaches a minimum of approximately 0.03 s^{-1} within the central half-graben. Here the p-wave velocities range from 6.8 to 7.0 km/s.

In addition to modeling the first arrivals, a post-critical reflection off the base of this sublayer observed at OBS-C4 (labeled 2d on Figure 16b) was used to help constrain the velocity and thickness of sublayer 2d. As can be seen in the synthetic section for this instrument (Figure 16c), the model not only predicts a minor build up of amplitudes associated with the wide-angle reflection (critical offset at ~ 70 to 75 km), it also predicts lower amplitudes for the purely refracted first arrivals.

Although the model predicts that reflections from this same interface should be observable at OBS-C9 (Figure 17b), OBS-C3 (Figure 18b), and site C1 (Figure 19b), matching these arrivals to discrete events on the respective data sections is unclear. The fact that the reflections for both OBS-C3 and OBS-C9 are modeled as low amplitude pre-critical arrivals (Figures 17c and18c), helps to explain the absence of easily recognizable events on the corresponding record sections. The erroneous high amplitudes of the reflected and refracted arrivals modeled for site C1 (labeled 2d and 2d respectively on Figure 19b) indicates that the velocity gradient in the upper part of sublayer 2d may be too large.

Sublayer 2e sits entirely beneath sublayer 2d and extends to a depth of approximately 34 km. The ladle-shape of this sublayer matches the drape of lower Keweenawan volcanics across the hinge line and the lower portion of the central half-graben as imaged on the CDP profile (Figure 8). The velocities within this sublayer range from approximately 6.4 to 6.5 km/s near the IRFZ, and from 7.0 to 7.2 km/s within the central half-graben, implying the presence of relatively large lateral velocity gradients. Except for a few rays which pass through the uppermost portions of this sublayer

(labeled 2e on Figures 14a, 15a, and 17a) , there are no first arrivals which bottom out within this sublayer. The lower portion of this sublayer is constrained by information taken from the CDP profile and by wide-angle reflections which pass through the sublayer but are associated with interfaces located in crustal layers 3 and 4 (see events labeled 3b, 3f and 4 on Figures 14b to 19b). The velocities assigned to this region are those which, by trial and error, were found to provide the best fit for most of the wide-angle reflections.

Due to the uncertainties associated with the modeling of wide-angle reflections, there is some room for debate regarding the velocities that have been assigned to this sublayer. Since it would be exceedingly difficult to explain velocities greater than those present in the lower crust (i.e. layer 4), the velocities shown in Figure 7 probably represent an upper limit. Yet, lowering the velocity within the central half-graben to 7.0 km/s adversely affects the amplitudes of the wide-angle reflections coming from the base of sublayer 2d and delays the arrival time of some of the wide-angle reflections associated with layers 3 and 4. Attempts to accommodate the time delays by placing the reflective interfaces at shallower depths or increasing the velocities outside the half-graben adversely affects the critical angles and amplitudes which have been accurately modeled for many of the wide-angle reflections. If the model presented here is accurate, the acceptable range of p-wave velocities that may be assigned to the lower portions of the half-graben is approximately 7.0 to 7.2 km/s, suggesting that the region comprises metabasalts and/or a high percentage of mafic/ultramafic intrusions (Mooney and Brocher, 1987; McCarthy and Thompson, 1988; Behrendt et al., 1988, 1989).

Layer 3

Layer 3 contains six sublayers, labeled 3a to 3f in Figure 7a. Taken together, the distribution of these sublayers closely matches the upper portions of the Archean crust as imaged on the CDP profile (compare Figures 4 and 8). The two uppermost sublayers (3a

and 3c) crop out along the line of section and have been mapped as part of the Archean granite-greenstone belt of the Superior Province (Figure 2). The p-wave velocity within sublayer 3a ranges from 6.0 to 6.5 km/s. The p-wave velocities within sublayer 3c are slightly lower, ranging from 5.8 to 5.95 km/s. These velocities are fully consistent with those measured for similar near surface rocks (Steinhart, 1961; Steinhart et al., 1961; Mooney et al., 1970).

Sublayer 3b sits directly below sublayer 3a at a depth of approximately 12 to 15 km and comprises rocks displaying velocities ranging from 6.6 to 6.7 km/s. Reflections from the boundary between sublayers 3a and 3b are observed as post-critical arrivals at site SUP4 (labeled 3a on Figure 14b). Extension of this interface north of approximately 65 km is unconstrained by the seismic data. Modeling of the interface south of about 85 km is also poorly constrained because only pre-critical reflections from this interface are observable at OBS-A2 (Figure 15), OBS-C4 (Figure 16), and OBS-C9 (Figure 17) Interestingly, the only segment of this interface that is constrained (imaged by SUP4 between 65 to 85 km), rests directly beneath the "Pre-Osler" basin imaged on the CDP profile (Figure 4). Although it is possible that this interface is structurally related to the overlying basin, possibly representing a shear zone developed during the early extensional phase of the rift, such an interpretation would be fairly speculative. The boundary is so poorly imaged by both the wide-aperture and CDP data that for it to have played a major role in developing the basin seems unlikely.

The abrupt thinning of sublayer 3b north of 70 km (Figure 7a), is constrained by a range-limited, high amplitude, wide-angle reflection that is only observed at the GLIMPCE stations sited on the north shore (Figure 3). On the record section from site SUP4, the event can be seen at approximately 100 to 140 km offset (labeled 3b, Figure 14b); corresponding to rays reflecting from the southernmost limit of the interface (approximately 60 to 70 km). Although the concurrent thickening of layer 4 in this region is also supported by a coincident high in the gravity profile (Figure 4), extension

of layer 4 much north of about 60 km is not supported by the gravity reponse of the seismic model (discussed below) Additional modeling of this region of the model, reported by Tréhu et al. (in prep.), shows thickening of the lower crust to be limited to approximately 60 to 90 km.

Post-critical reflections from the deeper segment of this interface, south of 70 km, are observed at site SUP4 (Figure 14b, 120 to 230 km offset), OBS-C3 (Figure 18b, -130 to -180 km offset), and C1 (Figure 19b, -185 to -220 km offset). The amplitudes for these arrivals appear to be well modeled, however, the low signal-to-noise ratio recorded at OBS-C3 at offsets greater than 100 km makes comparison with its record section more difficult. This interface is discussed further in the section below covering layer 4.

Sublayer 3c is a poorly constrained feature because the minimum offset (9 km) recorded at site C1 precludes any near surface control. The sublayer was included in the model in an attempt to boost the amplitudes of first arrivals recorded at site C1 and OBS-C3 (see events labeled 3c on Figures 12b, 18b and 19b). Although the modeled amplitudes are far from perfect (Figures 18c and 19c), without sublayer 3c they are much worse. The problem does appear to be restricted to the near surface because trying to do away with sublayer 3c by raising the gradient within sublayer 3d, adversely affects the amplitudes of first breaks modeled for instruments north of the Keweenaw fault. Additional modeling of the near surface gradient in this region is needed in order to resolve this minor mismatch.

Sublayer 3d rests directly beneath sublayer 3c and has been assigned p-wave velocities which range from 6.0 to 6.1 km/s. Although the travel times of reflections from the base of this sublayer are well modeled at site C1 and OBS-C3 (event 3d on Figures 18b and 19b), the modeled amplitudes appear to be slightly low, suggesting that the velocity contrast between sublayers 3d and 3e (6.1 to 6.2 km/s) may be too low.

The p-wave velocities assigned to sublayer 3e range from 6.2 km/s along the top (and southern edge) to 6.6 km/s near its deepest point adjacent to the central half-graben.

Figure 8 shows that the boundary at the base of this sublayer corresponds well with a band of northward dipping reflectors on the CDP profile. The model accurately predicts that reflections from this interface should be observed at site OBS-C3 as a low amplitude pre-critical arrival (event labeled 3e on Figure 18b). At site C1, the model accurately predicts the travel times for this reflection, but the build-up of amplitudes at the critical angle appears to occur at too large an offset, suggesting that the velocity contrast between sublayers 3e and 3f may be too low. The fact that this interface projects downward (at about 16^0 north dip) towards the base of the central half-graben suggests that it may have played an important role in the development of the MRS; possibly serving as a detachment surface during the early stages of rifting. Extension of this interface south of approximately 240 km is unconstrained by the seismic data.

A puzzling high amplitude wide-angle reflection is observed by every instrument sited on the south shore of Lake Superior (Figure 3). On the record section from site C1, the event is seen at approximately -50 km offset (labeled ? on Figure 19b). Several attempts to model this event, while preserving the timing and amplitudes of the other wide-angle reflections modeled for this instrument, have all failed. The dramatic upward curvature of the arrival requires the reflecting interface to dip southward, but modeling high amplitude reflections off a southward dipping interface requires a large velocity contrast across the interface. Unfortunately, the CDP profile shows no evidence of a southward dipping interface that could be responsible for such an energetic arrival. The most likely explanation for this puzzling event is that it represents an out-of-plane reflection. The presence of a large (-90 mGal) gravity low centered in nearby Keweenaw Bay (O'Hara, 1982) is a clear indicator of structural complexity in this area.

Sublayer 3f has been assigned p-wave velocities which range from 6.6 to 6.7 km/s. The model predicts post-critical reflections from the base of this sublayer to be observable at sites SUP4 (Figure 14), OBS-A2 (Figure 15), and OBS-C1 (Figure 19). In particular, it predicts that the reflection should be observed as a post-critical first arrival at

site C1 (-165 to -220 km offset on Figure 19b). Considering the complexity of the model, the high degree of accuracy seen in the modeling of the travel times and amplitudes of this arrival at site C1 lends a great deal of confidence to the model in general. Although poor signal quality hampers the comparison of the modeled travel times and amplitudes with the record sections from the other sites, the slopes of the travel time curves appear to match the apparent velocities observed on the respective record sections. Extension of this interface south of approximately 220 km is unconstrained by the seismic data. The modeling of reflections from the deepest portion of this interface is discussed further in the section below.

Layers 4 and 5

Layers 4 and 5 extend entirely across the lower half of the seismic model and are interpreted to represent the lower crust and upper mantle respectively. The velocities assigned to these layers (Figure 7a) are consistent with the results from previous investigations of continental crust (Smith et al., 1966; Mooney and Brocher, 1987; McCarthy and Thompson, 1988). This region of the model is based on the modeling of wide-angle reflections and is supported by a direct image of the region obtained using wide-angle migration techniques (Tréhu et al., 1989a). In addition, the results of a travel time inversion for interface position (Tréhu et al., 1989b; Lutter and Nowack, 1990) provided critical insight into the position of the interface between sublayer 3b and layer 4 and between layers 4 and 5.

One of the most interesting geophysical phenomena of the rift is revealed by the wide-angle reflections coming from the top of the lower crust. In the model, the top of the lower crust is represented as the base of sublayers 3b and 3f. A wide-angle reflection coming from the base of sublayer 3f is most readily observed at station C1 (labeled 3f on Figure 19b). As mentioned above, this reflection is modeled as a post-critical first arrival at offsets greater than about -165 km. The half second of delay observed between this

arrival and the closer offset first arrivals appears to be a direct result of the rather large lateral velocity variations present in the model. In a classic layer cake model such delays would generally be interpreted as evidence for a low velocity zone (LVZ) (Diebold, 1988). In this case, the lower velocity continental crust on the far side of the high velocity half-graben acts as the lateral equivalent of a LVZ. Although the model predicts that the same phenomena should be observable from the site occupied by OBS-A2 (Figure 15), a low signal-to-noise ratio obscures the view. The larger offset between instrument SUP4 and the half-graben prevents the same phenomenon from being observed at that site for reflections coming from the base of sublayer 3b (Figure 14). The phenomenon might have been seen at SUP4 had the survey been continued southward on land.

On the northern flank, the depth and dip of the Moho, represented by the boundary between layers 4 and 5, is constrained by wide-angle reflections observed at station SUP4. Figure 14 shows that the model predicts a set of three en echelon wide-angle reflections (labeled 4) coming from various segments of the Moho. Although the low amplitude of the furthest arrival (pre-critical) makes it difficult to evaluate, the model does a fairly good job predicting both the timing and amplitude of the two nearest arrivals (115 to 180 km, 205 to 210 km). Similarly, two en echelon wide-angle reflections can be modeled for site C1 on the southern flank. Unlike for site SUP4, the model does a better job predicting the timing and amplitude of the furthest event. Surprisingly, the near offset event appears to arrive too soon and with too little amplitude. Simply deepening the interface does not really help because it forces the critical offset even further away. As presently modeled, the depth and dip of the Moho in this region is consistent with the beam-steering solution reported by Jefferson et al. (1989) and Meyer et al. (1989). The delayed high amplitude arrivals from the southern Moho may be evidence of constructive interference between peg-leg multiples within a mafic/sialic interlayered lower crust (McCarthy and Thompson, 1988). The gravity response of the seismic model (discussed below) indicates that the lower crust needs to be much thinner south of the central half-

graben. Thinning of the lower crust in this region may provide a better travel time and amplitude match for the near offset Moho reflections modeled at site C1.

Because of the scarcity of rays which pass through the region of the model directly below the central half-graben, the velocity of the rocks in this region is not well constrained. However, based on the high velocities modeled for the rocks filling the central half-graben and the flanking lower crust, the rocks in this region are most likely to have p-wave velocities in excess of 7.0 km/s. Based on the modeling results from a number of GLIMPCE investigators, Tréhu et al., (in prep) have interpreted the lower crust in this region as representing a zone of extensive intrusion into a pre-rift Archean lower crust. Petrologic interpretations based on the modeling of both P and S wave arrivals may provide additional insight into the nature of the lower crust in this region.

RMS Fits

Because the first-break arrival times observed at each station must be satisfied by the same velocity model, the combined root mean square (rms) fit for all of the stations provides a fundamental measure of the validity of the model. Rather than comparing the arrival times of each calculated ray to the observed travel time curve directly, which would bias the rms estimate by the density of calculated rays arriving at a given offset, the rms fit was determined by comparing spline fits of the calculated and observed travel time curves. The fitted curves were compared at equivalent offsets every half kilometer. The calculation was done for each instrument out to the maximum offset at which reliable first-break arrival times could be picked. Details of the rms calculation for each instrument are summarized in Table 3. Equal weighting of the rms fit from each instrument gives an overall rms fit of 0.07 seconds.

Site	Offsets (Km)	RMS (sec)
SUP4	+22 to +140	0.076
OBS-A2	-40 to +90	0.052
OBS-C4	-66 to +120	0.064
OBS-C9	-87 to +93	0.080
OBS-C3	-100 to +29	0.065
C1	-135 to -9	0.103
Average		0.073

Table 3. Summary of RMS fits. See text for explanation of calculations.

Comparison of Forward and Inverse Models

A formal inversion of the first break travel time curves used in this study was done by Lutter et al. (1989) using the method described by Lutter et al. (1990). The inversion assumes that the velocity structure is smooth and that all of the first arrivals are due to pure refractions. Figures 20a and 20b show the isovelocity contours that resulted from 63 node and 250 node inversions respectively. The contours have been overlaid on grayscale images of the forward model presented above. Although the inversion results are quite smooth and show very little detail, the isovelocity contours closely match the velocity structure shown in the forward model. For example, Figure 20a shows that both models predict high velocity (7.0 km/s) material to reside within the upper portions of the central half-graben and Figure 20b shows that both models image high velocity uplifts coincident with the IRFZ and the Keweenaw fault. The close agreement between the forward and inverse models lends considerable support to the forward model.

It should be pointed out that the first arrival inversion becomes unconstrained at depths greater than approximately 18 km. The approximate depth from which the deepest refracted rays are observed. In the forward model the velocity structure below 18 km is based primarily on the modeling of wide-angle reflections and is supported by a direct image of the region obtained using wide-angle migration techniques (Tréhu et al., 1989a) and by an inversion of wide-angle reflection travel times for interface position (Lutter and Nowack, 1990).

Although both the forward and inverse models show essentially the same velocity distribution, it is important to remember that both results are based upon the same first arrival picks and that there is a degree of uncertainty associated with the furthest offset picks. Obviously, these uncertainties also represent uncertainties in the p-wave velocities

assigned to the lower crust which, in turn, has implications for the petrology of the central half-graben and lower crust.

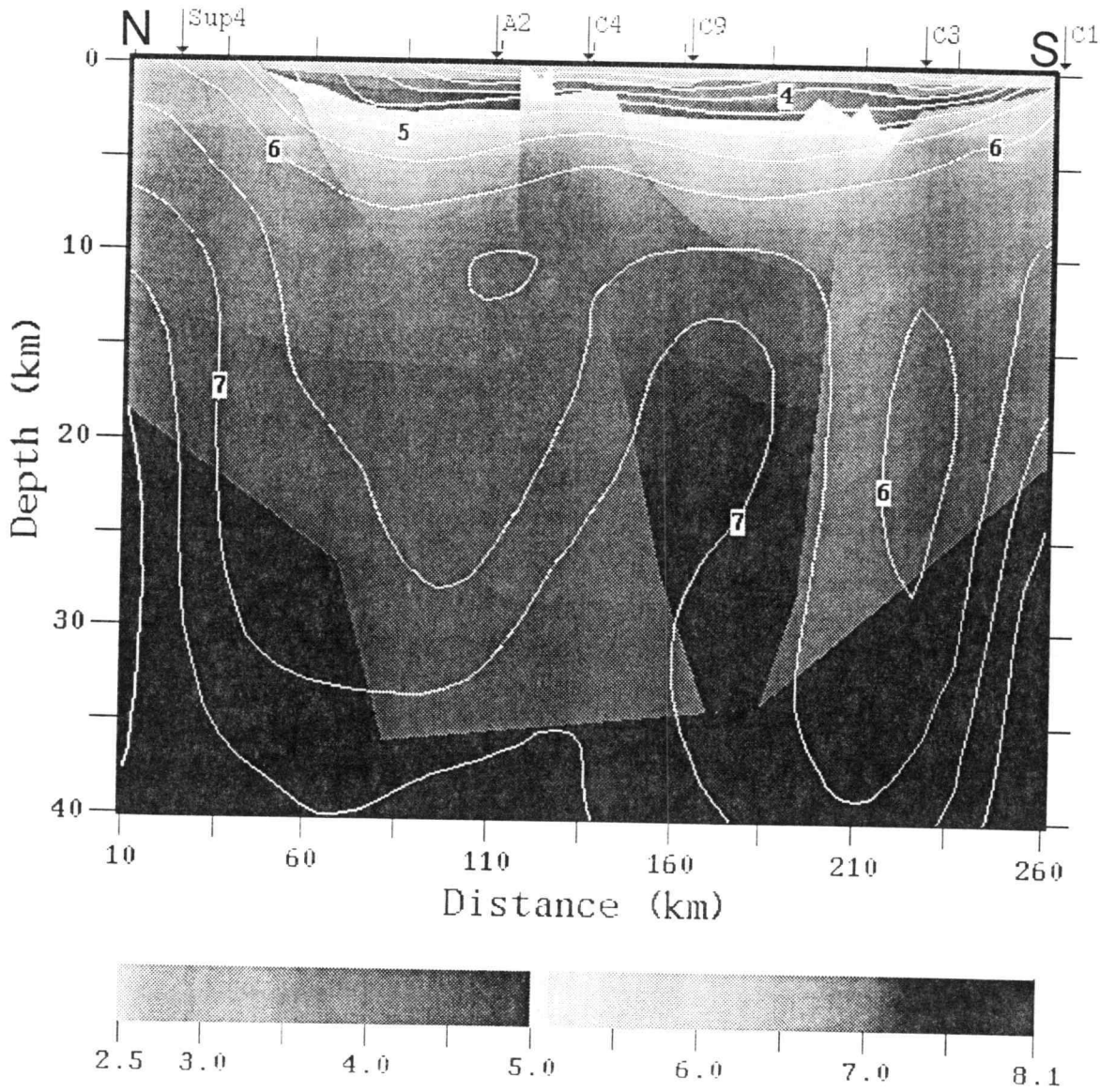

Figure 20a. Comparison of the forward model (grayscale) and the velocity contours resulting from the 63-node formal inversion of Lutter et. al., (1989a). Contour are labeled in units of km/s. The vertical exaggeration is approximately 5.

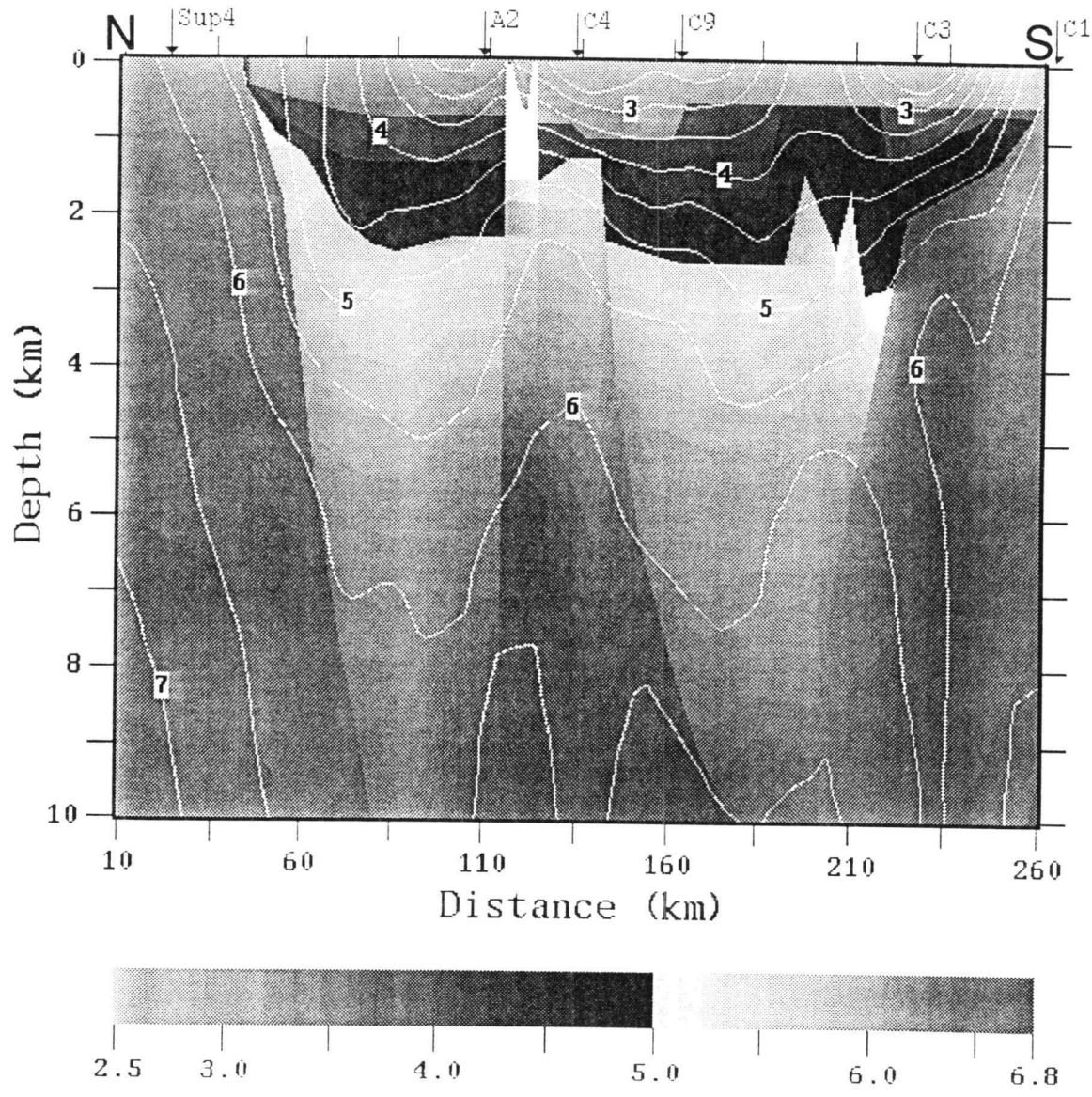

Figure 20b. Comparison of the forward model (grayscale) and the velocity contours resulting from the 250-node formal inversion of Lutter et. al., (1989a). Contours are labeled in units of km/s. The vertical exaggeration is approximately 20.

Gravity Response of the Seismic Model

Gravity profiles across the MRS are characterized by a pronounced high flanked by strong lows. Numerous studies have correlated the central high with high density rift-related volcanics and intrusives, and have attributed the flanking lows to lower density sedimentary basins (Thiel, 1956; Ocola and Meyer, 1973; Chase and Gilmer, 1973; Hinze et al., 1982; Chandler et al., 1989; Hutchinson et al., submitted). The observed Bouguer gravity anomaly along profile A (Figures 4 and 21b) contains this characteristic signature but has an additional high over the northern end of the profile. The fact that this northern high is actually the flank of a large, circular high centered approximately 60 km west of the profile highlights the 3-dimensional complexity of the lower crust in this region, and underscores the inadequacies (and possible biases) inherent in 2-dimensional gravity models for this region.

Figure 21a shows a 2-dimensional gravity model which was constructed by assigning a density to each of the layers and sublayers in the seismic model presented above. The geometry of the gravity model is essentially the same as the seismic model, with the only modifications to the sublayers shown in Figure 7 being: 1) sublayer 2c has been divided into two smaller polygons with slightly different densities, 2) sublayers 2a and 2b have been assigned the same density and appear as a single polygon, and 3) the narrow block of sublayer 2d which projects upwards beneath the IRFZ has been defined as a separate polygon with a density of 2.5 gm/cm.

The division of sublayer 2c into two smaller polygons provides a better match to the higher frequency low which is superimposed on the central gravity high. As mentioned above in the seismic interpretation, the upper portion of sublayer 2c is believed to represent upper Keweenawan (Oronto) sedimentary rocks while the lower portion is thought to comprise a transitional sequence of sedimentary and volcanic rocks.

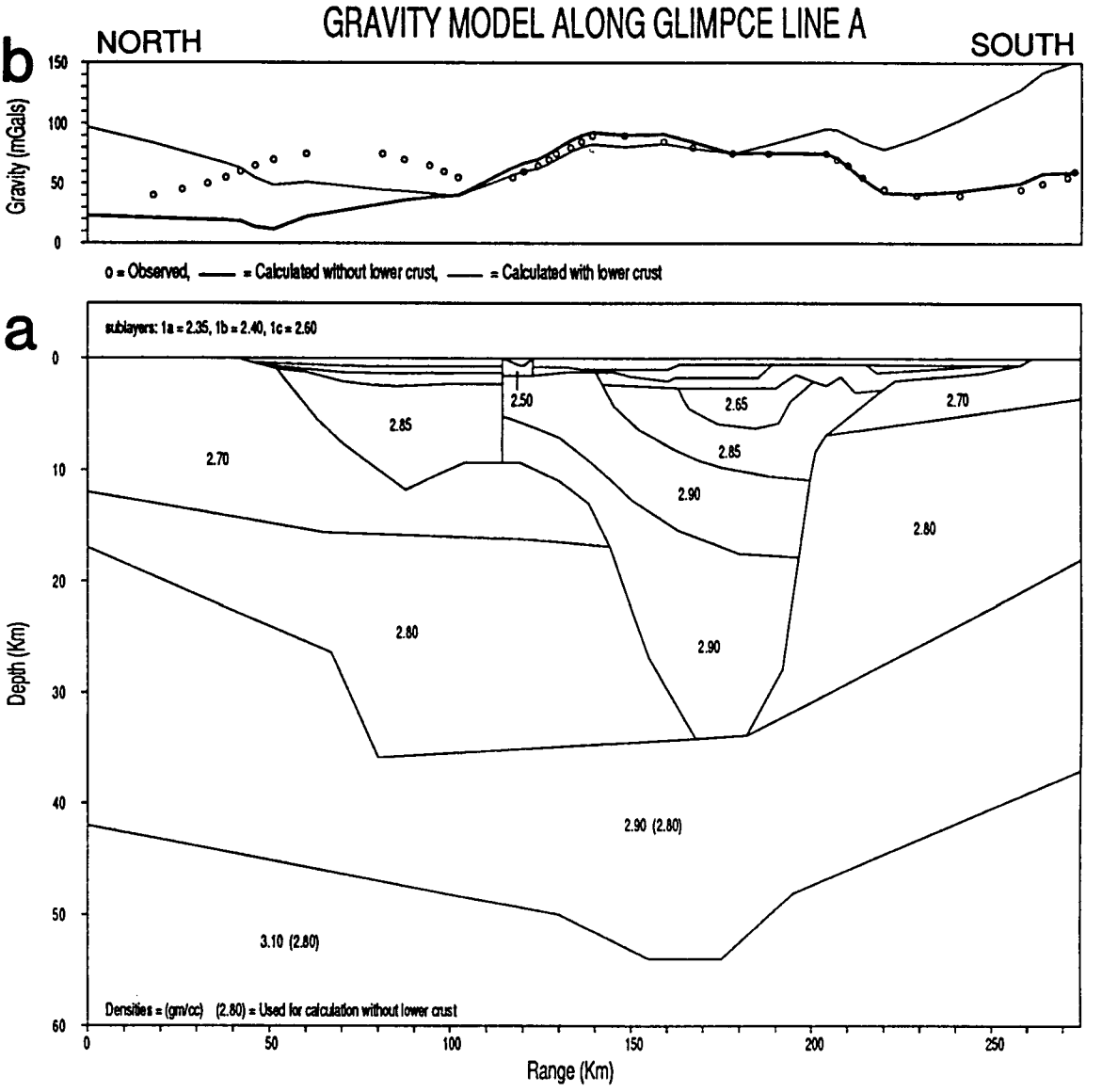

Figure 21. a) Gravity model along line A of GLIMPCE derived from the seismic model. **b)** Gravity response of the model showing Bouguer anomalies calculated with and without the lower crustal layers. The observed Bouguer gravity anomaly is from O'Hara (1982). The vertical exaggeration is approximately 3.

Reference	Jacobsville Bayfield Gp	Oronto Group	Volcanics undifferentiated	Archean crust	Comment
Theil (1956)	2.30 ± .06	2.36 ± .12			Measured
Bacon (1966)	2.25	2.66	2.88	2.70	Measured
White (1966a,b)	2.30 - 2.37	2.44 - 2.62	2.90 - 2.95	2.67	Measured
Steinhart and Smith (1966)	2.30 - 2.36	2.43 - 2.54	2.70 - 2.80		Measured
Steinhart et al. (1968)	2.30	2.66			Measured
Weber and Goodacre (1966)			2.97	2.70	Measured
Oray (1971)	2.41	2.65	2.95	2.70	Measured
Jolly and Smith (1972)			2.85 - 3.31		Measured[1]
Hinze et al. (1982)	2.40	2.60	2.95	2.70	Modeled
Serpa et al. (1984)			2.90	2.67	Modeled
Zhu and Brown (1986)	2.40	2.65	2.95	2.70	Modeled
Hutchinson et al., (1990)	2.30 - 2.35	2.65	2.85 - 2.92	2.70/2.90	Modeled[2]
	2.40	2.76	2.95 - 2.98	2.70/2.90	Modeled[3]
This study	2.35 - 2.40	2.60 - 2.65	2.85 - 2.90	2.70 - 2.90	Modeled

Table 4. Density (gm/cm^3) of rocks from the vicinity of the midcontinent rift . Comment notes: 1) From metamorphosed flow tops; 2) Rift flank values, densities for upper/lower Archean crust given; 3) Central basin values, densities for upper/lower Archean crust given. Figure is modified after Hutchinson et al., (1990).

Such a division is fully consistent with the interpretation of the CDP profile (Figure 4). The division of this sublayer does not appear in the seismic model because the dividing interface is not directly observable from any of the large aperture sites. Reflections from this inferred interface would only be observable by an instrument sited directly above the interface (i.e between approximately 165 to 190 km). The fact that sublayer 2c contains a fairly large vertical velocity gradient (approximately 0.2 s^{-1}) supports the decision to subdivide it for the gravity calculations which assume isodensity polygons. Table 4 summaries the densities of rocks that have been either measured or modeled in the vicinity of Lake Superior, as well as the density assignments used in this investigation.

Two gravity response curves were calculated for the seismic model (Figure 21b) using a computer algorithm based on the formulations of Talwani et al. (1959). The thin curve shows the gravity response of the entire model while the bold line shows the gravity response of the model minus the effect of the lower crustal layers. The second curve, which was calculated by setting the density of layers 4 and 5 to 2.8 gm/cm^3, demonstrates that the central gravity high can be entirely attributed to high-density rocks occupying the central half-graben imaged on the CDP reflection profile. Based on p-wave velocities approaching 7.0 to 7.2 km/s, the rocks in the lower portion of the central half-grabe probably comprise meatbasalts and/or a high percentage of mafic/ultramafic intrusions (Mooney and Brocher, 1987; McCarthy and Thompson, 1988; Behrendt et al., 19888, 1989; Cannon et al., 1989; Hutchinson et al., submitted). Including the mass of the lower crust in the calculation dramatically changes the gravity response over the flanks of the rift. On the northern flank, the thickening of the lower crust north of 80 km begins to accommodate the northern gravity high but fails to generate a distinct maximum. Because the observed northern gravity high is due to an off-profile body, exact matching of this feature by a gravity model constructed from a two-dimensional velocity model is not to be expected. On the southern flank, the calculated gravity curve indicates that the mass of the lower crust to be grossly over estimated.

Further gravity modeling of the lower crust , as reported by Tréhu et al. (in prep), shows that the northern gravity high can be successfully modeled by restricting the thickening of the lower crust to a region directly beneath the northern gravity high (approximately 60 to 90 km), and that the excess mass on the southern flank can be accommodated by thinning the lower crust immediately south of the central half-graben. Their model shows essentially the same Moho relief as that shown in Figure 21a, suggesting that a high density lower crust "rift-pillow" can compensate for the topography of the Moho. In order to more fully understand the mass balance within the lower crust in this region, future gravity modeling should incorporate the flexural response of the lithosphere (Cohen and Meyer, 1966; McGinnis, 1970; Nyquist and Wang, 1986, 1988, 1989; Peterman and Sims, 1988).

Discussion

The geological model illustrated in Figure 22 was constructed directly from the seimic model shown in Figure 7a. The position of the wide-aperture stations whose record sections where used in this study are indicated along the top of the figure. As mentioned earlier, the edges and lower corners of the seismic model are unconstrained by the seismic data, and therefore do not appear in this figure. For the sake of clarity, the three sublayers comprising layer 1 in the seismic model appear as a single layer in this figure. The upper portion of sublayer 2c, which was inferred from the gravity model (Figure 21a) to contain lower density upper Keweenawan (lower Oronto) sedimentary rock, appears as a separate layer. Figure 22 shows a deep central half-graben filled with dense mafic rock flanked and overlain by rift-related sedimentary basins. Although numerous models of the MRS contain similar crustal geometries (Craddock et al., 1963; King and Zietz, 1971; Craddock, 1973; Ocola and Meyer, 1973; McSwiggen et al., 1987; Chandler et al., 1989, Hutchinson et al., submitted), none of them have been able to image the rift to such great depths or with such clarity. The enhanced image of the midcontinent rift presented in this thesis is a direct benefit of having a coincident set of reflection and wide-aperture seismic profiles to help constrain the modeling.

The Northern Flank

What appears in Figure 22 to be a relatively simple basin structure on the northern flank of the rift (centered at about 85 km), was interpreted by Cannon et al., (1989) as containing a pre-Osler (Lower Proterozoic ?) basin resting unconformably beneath a much broader basin (Figure 4) containing lower Keweenawan Osler volcanics. The wide-aperture data support this interpretation by imaging a crustal boundary which appears to coincide with the angular unconformity (Figure 8). Although this interface is clearly evidenced by a wide-angle reflection recorded by OBS-A2, the p-wave velocities

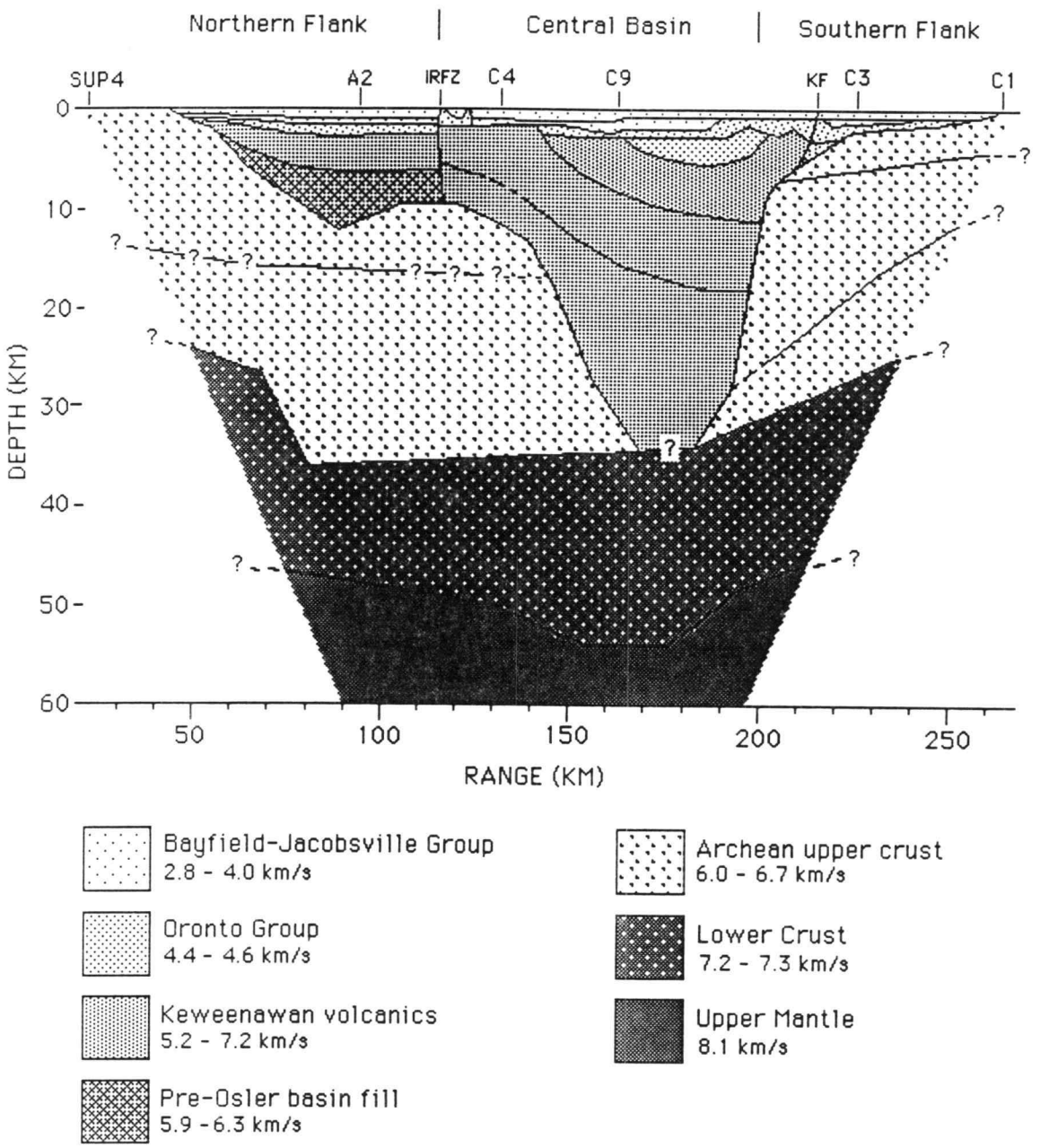

Figure 22. Geological/seismic model along line A of GLIMPCE. SUP4, A2, C4, C9, C3 and C1 denote postions of wide-aperture stations whose record sections were used in this study. IRFZ and KF denote the approximate surface position of the Isle Royale fault zone and the Keweenaw fault, respectively. The vertical exaggeration is approximately 2.5.

determined for the underlying rock (5.9-6.3 km/s) provide limited insight into the geology of the buried basin fill. The high p-wave velocities, coupled with the fact that the CDP profiles show a few continous reflections in this region, suggest they comprise pre-Osler volcanics and/or meta-sediments. The structural and genetic relationship between this basin and the central half-graben remains unclear; however, the imaging of a subhorizontal boundary (base of sublayer 3a in Figure 7a) 2 to 3 km directly beneath this basin may be evidence of a low angle fault which may have played a role in the opening of the pre-Osler basin. Unfortunately, the modeling of this interface is constrained only by a relatively low amplitude wide-angle reflection recorded by instrument SUP4 on the north shore of the lake. Therefore, the exact dip and southward extension of this interface is poorly constrained. The absence of any significant tilting or deformation of the overlying Keweenawan strata indicates that development of the pre-Osler basin was fully arrested before the onset of the major phase of rifting. The basin may be related to a much earlier rifting event (1340 ma versus 1100 ma) believed to be associated with deposition of the Sibley Group (Ojakangas and Morey, 1982a) which outcrops north of the lake.

Although Figure 22 shows the upper Keweenawan sedimentary sequence as a single unit, at least three distinct sublayers can be discriminated based on wide angle reflections recorded at each of the OBS sites. Based on the reported p-wave velocities of upper Keweenawan rocks (Table 1), the three sublayers correlate fairly well to either Oronto Group rocks or Bayfield-Jacobsville Group rocks. Obviously, the thickness and p-wave velocities of these units are best constrained in the immediate vicinity of each of the OBSs. On the northern flank of the rift, these post-rift sediments were determined to have p-wave velocities of 2.8, 3.5 and 4.6 km/s, and a maximum combined thickness of approximately 3 km. The velocities, thicknesses, and inferred geology of these units agree with, and support, the interpretation of the CDP profile by Cannon et al. (1989).

The Central Basin

Approximately 3 to 5 km of upper Keweenawan sedimentary rock (2.8 - 5.2 km/s) overlie an 8 km thick sequence of middle Keweenawan volcanics and interflow sediments (5.2-6.5 km/s) within the central rift graben imaged on the CDP profile (Figures 4 and 8). Beneath this sequence is a 6 to 8 km thick sequence of 6.6 - 7.0 km/s material thought to represent middle to lower Keweenawan volcanics and/or metavolcanics The velocity of the material at the base of the rift graben is not well constrained (approximately 7.0 - 7.2 km/s) but is believed to represent an additional 10 to 12 km of lower Keweenawan meta-volcanics/intrusions that extend to the base of the graben observed on the CDP profile.

Angular discordance between the upper Keweenawan sedimentary units and the underlying volcanics in the vicinity of the IRFZ and the Keweenaw fault indicate that tilting and uplift associated with reverse motion along these faults took place sometime between late Oronto and early Bayfield time. The timing of this uplift agrees well with previous estimates (Morey and Ojkangas, 1982; Kalliokoski, 1982). Unfortunately, the modeling results provide no additional insight to the exact timing of the uplift. There is, however, some evidence that uplift along the Keweenaw fault may have been two-phased, with additional uplift taking place after the onset of Bayfield-Jacobsville deposition. The interested reader should refer to the section of thesis covering the Keweenawan fault for a more detailed discussion.

A 50 - 100 ms time advance anomaly associated with the IRFZ is observed on the record sections from every wide-aperture station. This anomaly has been modeled as shallow high velocity blocks located directly beneath the fault zone. The blocks appear to be fault controlled structures and are believed to represent highly indurated upper Keweenawan sediments which may have formed by hydrothermal processes confined to the fault zone. Hydrothermally altered upper Keweenawan sediments outcrop along the Keweenaw fault and Halls (1969) reports significantly higher velocities for indurated

upper Keweenawan sedimentary rocks. Although the possibility that the blocks correspond to some sort of igneous intrusion can not be ruled out, the gravity field and observations made during recent submersible dives (Manson and Halls, 1989) argue against it. The amount of relative offset across the IRFZ is difficult to assess because the inferred base of the Portage Lake volcanics was set arbitrarily to coincide with a marked change in reflectivity seen in the CDP profile (Cannon et al., 1989). Again, the interested reader should refer to the main body of the thesis for a more detailed discussion of the IRFZ.

The densities (Table 4) and high p-wave velocities determined for the material within the central half-graben imaged on the CDP profile confirm the primarily mafic composition of the graben fill. The total thickness of the graben fill exceeds 30 km. Based on a p-wave velocity of approximately 7.0-7.2 km/s, the rocks in the lower portion of the central half-graben probably comprise metabasalts and/or a high percentage of mafic/ultramafic intrusions (Mooney and Brocher, 1987; McCarthy and Thompson, 1988; Behrendt et al., 1988, 1989). The two southward dipping interfaces within the central half-graben are evidenced by wide angle reflections recorded at sites C1, OBS-C3, OBS-C9 and OBS-C4. The position of the two boundaries closely match the upper and lower bounds of the Portage Lake volcanic sequence as inferred from the CDP data by Cannon et al. (1989).

Hutchinson et al. (submitted) have estimated the total volume of extrusive basalt contained within the MRS (deposited over a period of approximately 15 m.y.) to be approximately 1.3×10^6 km^3. Such enormous volumes and high rates of basaltic magmatism are generally associated with major flood basalt provinces (McKenzie and White, 1989; Richards et al., 1989; Hutchinson et al., submitted). Large volumes of extrusive magmatism are also commonly found along some passive continental margins. In particular, thick sequences of seaward dipping reflectors have been observed near the ocean-continent boundary on many passive margins and have been interpreted to

represent massive subaerial basalt flows that occurred during the transition from rifting to seafloor spreading (e.g. Hinze, 1981; Mutter et al., 1984; Mutter, 1985; White et al., 1987; Mutter et al., 1988; Klitgord et al., 1988). The similarity between these seaward dipping reflectors and the basalt flows imaged along line A of GLIMPCE suggests that the MRS may have reached this stage of development when rifting was suddenly aborted. Cannon et al.(1989) also recognized the high degree of structural similarity between the MRS and recent passive continental margins in noting that, "the area nearly evolved into an ocean basin with true oceanic crust near its axis".

The Southern Flank

The modeling of the wide-aperture data generally support the interpretation of the CDP profile south of the Keweenaw fault (Cannon et al., 1989). In this region, the model indicates a wedge of upper Keweenawan sediments which dip and thicken northward. Although Figure 22 shows no Keweenawan volcanics south of the Keweenaw fault, minor occurances of basalt in this region cannot be completely ruled out. Modeling of the wide-aperture data from OBS-C3 indicates a thin wedge of Oronto Group rocks immediately south of the Keweenaw fault. Since Oronto Group rocks are not seen in outcrops south of the lake, Cannon et al. (1989) could only speculate on their occurance south of the Keweenaw fault.

The Archean Crust

The Archean crust depicted in Figure 22 is part of the granite-greenstone terrane of the Superior province. The terrane, which comprises a significant portion of the North American craton, formed 2.6 to 3.1 Gyr ago and remained relatively stable until Keweenawan time, at which time it was rifted into its present geometry. Based on the horizontal and undeformed character of the overlying Upper Keweenawan sedimentary sequence, the region appears to have remained relatively stable since the end of the

Proterozoic. Without the benefit of piercing points it is difficult to accurately estimate the amount of crustal extension which has occurred; however, the approximate width of the central half-graben (~ 55 km) tends to support previous estimates of 50 to 60 km of extension across the rift in the vicinity of Lake Superior (Klasner et al., 1982; Chandler, 1983).

The subhorizontal interfaces imaged within the Archean crust are evidenced by wide-angle reflections recorded at several of the wide aperture stations. The exact nature of these boundaries remains unknown, however, their riftward dip suggests they may have played a key role during rifting. In particular, the boundary which projects towards the southern base of the central half-graben (the base of sublayer 3e in Figure 7a) may have served as a low-angle detatchment surface during early extension of the brittle upper crust. The dip of these interfaces matches the riftward dip of the reflective grain of the crust imaged on the CDP profile (Figure 8). Cannon et al. (1989) suggest this reflective grain could be caused by ductile necking of the rocks caused by crustal extension. However, the modeling results do not rule out the possibility that some or all of these intracrustal boundaries actually correspond to ancient pre-rift structures.

The Lower Crust and Moho

For the most part, the seismic model presented above supports the structural interpretation of the upper crust along line A of GLIMPCE put forth by Cannon et al (1989). In particular, the geometry of the Keweenawan rocks, and their relationship to the surrounding Archean upper crust is essentially the same as that inferred from the CDP profile. Based on the known geological constraints and their interpretation of the CDP profile, Cannon et al. (1989) described four stages of rift development which adequately explain most of the near surface expression of the rift in the vicinity of Lake Superior (Figure 23). A brief description of these stages are given below.

1) Broad scale crustal sagging and extension. During the lower Keweenawan thinning and extension of the Archean crust is accomodated by low-angle normal faults in the brittle upper crust and by pure shear of the ductile lower crust. Intense wide-spread volcanism, fueled by partial melting of an upwelling asthenosphere, dominated the early development of the rift.

2) Asymmetric rift valley formation with continued crustal extension. During the middle Keweenawan most volcanism is confined to a central rift valley bounded by normal faults. Normal motion centered primarily along the Keweenawan fault led to the development of the asymmetric central half-graben and the thick wedge of "seaward" dipping reflectors. Crustal sagging continued and contributed to the enormous thickness of the graben fill. Sediments eroded from the flanks of the rift contributed to the filling of the graben.

3) Thermal collapse followed by sedimentation. When rifting was aborted towards the end of the middle Keweenawan, volcanism waned, and deposition became progressively more clastic (Oronto Group). A broad sedimentary basin developed in response to the thermal collapse. Development of this basin was compounded by sediment loading.

4) Tectonic inversion by high-angle reverse movement along graben-bounding normal faults. Following the deposition of the Oronto Group sedimentary sequence, the central half-graben was uplifted and the original graben-bounding normal faults were transposed to reverse faults. The tilting and uplift is evidenced by a regional angular unconformity at the base of the upper Keweenawan Bayfield-Jacobsville Group rocks (not shown in Figure 23). Deposition of these rocks marked a final period of renewed regional subsidence.

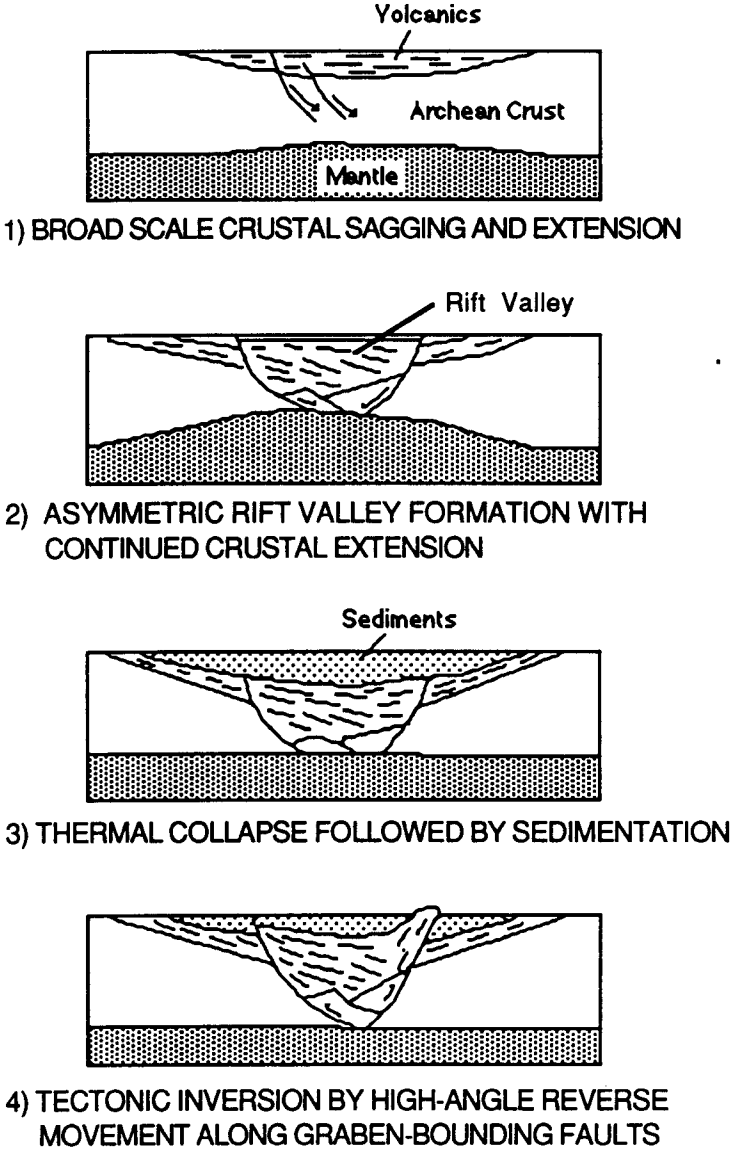

Figure 23. Schematic depiction of the development of the midcontinent rift in the Lake Superior region after Cannon et al. (1989).

The modeling results presented in this thesis are at variance with Cannon et al.'s (1989) depiction of the Moho as either a broadly upwelling or essentially planar contact (Figure 23), a feature which is most commonly seen beneath Phanerozoic continental rifts (Mooney and Brocher, 1987; McCarthy and Thompson, 1988). The wide-aperture data indicate the Moho to have considerable topographic relief beneath the rift and what appears to be a 15 to 20 km thick layer of, highly intruded and/or underplated lower crust beneath the axis of the rift. The nature of the lower crust evidenced by the wide-aperture data is more similar to models of some passive continental margins, in which thick layers of both extrusive and intrusive material have been added to the crust at the continent-ocean boundary (Tréhu et al., 1989; White and McKenzie, 1989).

Tréhu et al. (in prep) interprete the lower crust (layer 4) beneath central Lake Superior as corresponding to Archean crust which became heavily intruded by mafic material during rifting. They use the fact that this layer is not well imaged by the CDP data as possible evidence that the upper region of this layer comprises a zone of random igneous intrusion rather than simple underplated crust. Imaging of this boundary by the large aperture data is explained by the modeling results of Gibson and Levander (1988), who showed that a zone of random velocity heterogeneities at depth can appear layered in large aperture data.

Interestingly, if rifting had not aborted and a "Keweenawan Ocean" had formed, the top of this heavily intruded/underplated lower crust could correspond to the landward dipping reflectors imaged on reflection profiles from the Grand Banks by de Voogd and Keen (1987). In their model of continental rifting (Keen and de Voogd, 1988), the top of landward dipping reflectors seen beneath continent-ocean boundaries are interpreted as corresponding to intruded/underplated lower crust whose upper boundary is continous with the top of oceanic crust formed within the expanding rift (Figure 24).

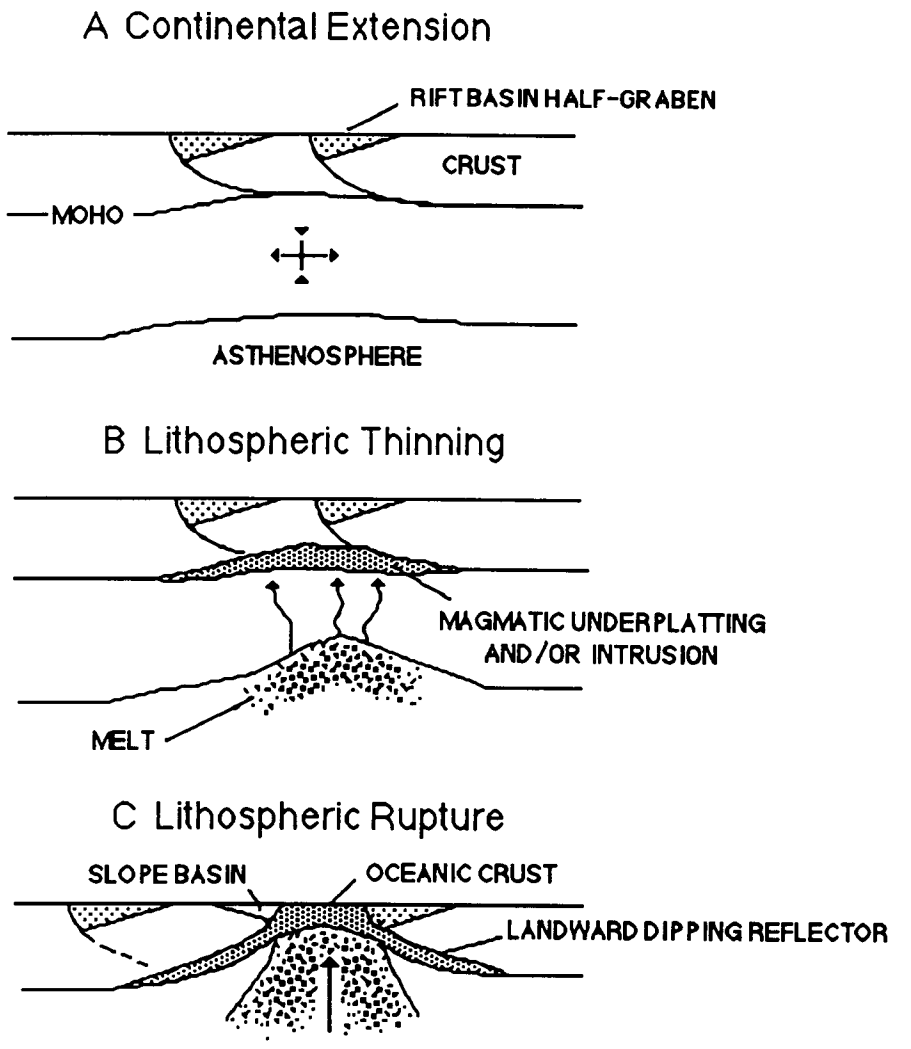

Figure 24. Conceptual model of continental breakup and formation of first oceanic crust after Keen and de Voogd (1988) **a)** Half-graben develop during extension of the continental lithosphere and the asthenosphere begins upwelling in response to lithospheric thinning. **b)** As lithospheric thinning progresses partial melt generated in the upwelling asthenosphere migrates to the Moho where it may intrude and/or underplate the lower crust. Some of the melt may also find its way to the surface to erupt there. **c)** At the time of breakup, the continental lithosphere ruptures and steady state seafloor spreading is established. The partial melting, differentiation, and migration of basaltic magma which creates the oceanic lithosphere, represents the end point of a process of continental underplating which began when the continental lithosphere thinned. According to this model the landward dipping reflector corresponding to the top of the intruded/underplated lower crust should be continous with the top of the newly created oceanic lithosphere.

Recent geophysical (Cannon et al., 1989; Hutchinson et al., submitted), isotopic (Nicholson and Shirey, submitted) and dynamic modeling (Brown and Beaumont, 1989; Beaumont and Brown, 1989) studies of the MRS all support the concept of an asthenospheric thermal anomaly/mantle plume being associated with the development of the MRS. Hutchinson et al.(submitted), go so far as to refer to the feature as the "Keweenawan hot spot". Although such an interpretation for the development of the MRS is not new (Burke and Dewey, 1973), the combined results of these studies and others (McKenzie and White, 1989; Chandler et al., 1989) offer an incredibly broad range of supporting evidence.

References

Anzoleaga, R., 1971, Crustal structure in western Lake Superior from the integration of seismic and gravity data., *[Ph.D thesis]: Univ. Wisconsin, Madison, Wisconsin.* 53 pages.

Bacon, L.O., 1966, Geologic structure east and south of the Keweenaw fault on the basis of geophysical evidence, *in* Steinhart, J.S., and Smith, T.J., eds., The Earth beneath the Continents, *Am. Geophy. Union, Geophysical Monograph 10,* p.42-55.

Beaumont, C., and Brown, K.C., 1989, Finite element models of the dynamics of the midcontinent rift beneath Lake Superior, *EOS, Transactions, Amer. Geophy. Union,* v.70, p.275.

Behrendt, J.C., Green, A.G., Cannon, W.F., Hutchinson, D.R., Lee, M.W., Milkereit, B., Agena, W.F., and Spencer, C., 1988, Crustal structure of the midcontinent rift system: Results from GLIMPCE deep seismic reflection profiles, *Geology*, v.16, p.81-85.

Behrendt, J.C., Hutchinson, D.R., Lee, M., Tréhu, A.M, Thornber, C.R., Cannon, W., and Green, A., 1989, Seismic reflection (GLIMPCE) evidence of deep crustal and upper mantle intrusions and magmatic underplating associated with the midcontinent rift system of North America, *EOS, Transactions, Amer. Geophy. Union*, v.70, p.272.

Berry, M.J., and West, G.F., 1966, An interpretation of the first-arrival data of the Lake Superior experiment by the time-term method, *Bull. Seismol. Soc. Am.*, v.56, p.141-171.

Black, W.A., 1955, Study of the marked positive gravity anomaly in the northern midcontinent region of the United States. *Geol. Soc. Am. Bull.*, v.66, p.1531.

Brown, K.C., and Beaumont, C., 1989, Kinematic models of the midcontinent rift beneath Lake Superior constrained by GLIMPCE data, *EOS, Transactions, Amer. Geophy. Union*, v.70, p.275.

Brown, L., Jensen, L., Oliver, J., Kaufman, S., and Steiner, D., 1982, Rift structure beneath the Michigan basin from COCORP profiling, *Geology*, v.10, p.645-649.

Brown, L., Serpa, L., Setzer, T., Oliver, J., Kaufman, S., Lillie, R., and Steiner, D., 1983, Intracrustal complexity in the United States midcontinent: Preliminary results from COCORP surveys in northeastern Kansas, *Geology*, v.11, p.25-30.

Burke, K., and Dewey, J.F., 1973, Plume-generated triple-junctions: Key indicators in applying plate tectonics to old rocks, *Jour. Geology*, v. 81, p. 406-433.

Butler, B.S., and Burbank, W.S., 1929, The copper deposits of Michigan, *U. S. Geol. Survey Prof. Paper 144*, 238 pages.

Cannon, W.F., Green, A.G., Hutchinson, D.R., Lee, M., Milkereit, B., Behrendt, J.C., Halls, H.C., Green, J.C., Dickas, A.D., Morey, G.B., Sutcliffe, R., and Spencer, C., 1989, The North American midcontinent rift beneath Lake Superior from GLIMPCE seismic reflection profiling, *Tectonics*, v.8, p.305-332.

Chandler, V.W., 1983, Correlation of magnetic anomalies in east-central Minnesota and northwestern Wisconsin: Constraints on magnitude and direction of Keweenawan rifting, *Geology*, v.11 p.174-176.

Chandler, V.W., McSwiggen, P.L., Morey, G.B., Hinze, W.J., and Anderson, R.R., 1989, Interpretation of seismic reflection, gravity, and magnetic data across middle Proterozoic mid-continent rift system, Northwestern Wisconsin, Eastern Minnesota, and Central Iowa, *Am. Ass. Petrol. Geol. Bull.*, v.73, p.261-275.

Chase, C.G., and Gilmer, T.H., 1973, Precambrian plate tectonics: The midcontinent gravity high, *Earth Planet. Sci. Letters*, v.21, p.70-78.

Cohen, T.J., and Meyer, R.P., 1966, The midcontinent gravity high: Gross crust structure., *in* Steinhart, J.S., and Smith, T.J., eds., The Earth beneath the Continents, *Am. Geophy. Union, Geophysical Monograph 10,* p.141-165.

Creager, C.C., and Dorman, L.M., 1982, Location of instruments on the seafloor by joint adjustment of intrument and ship positions, *J. Geophys. Res.,* v.87, p.8379-8388.

Daniels, P.A., 1982, Upper Precambrian sedimentary rocks: Oronto Group, Michigan-Wisconsin, *in*: Wold, R. J., and Hinze, W. J., eds., Geology and Tectonics of the Lake Superior Basin, *Geol. Soc. Am. Memoir,* v.156, p. 107-133.

Davidson, D.M., 1982, Geological evidence relating to interpretation of the Lake Superior Basin structure,*in*: Wold, R. J., and Hinze, W. J., eds., Geology and Tectonics of the Lake Superior Basin, *Geol. Soc. Am. Memoir,* v.156, p.5-14.

Davis, D.W., and Sutcliffe, R.H., 1985, U-Pb ages from the Nipigon plate and northern Lake Superior, *Geol. Soc. Am. Bull.*, v.96, p.1572-1579.

de Voogd, B., and Keen, C.E., 1987, Lithoprobe east: Results from reflection profiling of the continental margin: Grand Banks Region, *Geophy. J. R. Astron. Soc.*, v.89, p.195-200.

Dickas, A.B., 1986, Comparative Precambrian stratigraphy and structure along the midcontinent rift, *Am. Ass. Petrol. Geol. Bull.*, v.70, p.225-238.

Diebold, J.B., and Stoffa, P., 1981, The traveltime equation, tau-p mapping, and inversion of common midpoint data., *Geophysics*, v.46, p.238-254.

Diebold, J.B., (submitted), Low velocity zones in tau-sum inversion, *Geophysics*.

Donaldson, J.A., and Irving, E., 1972, Grenville Front and rifting of the Canadian Shield, *Nature*, v.237, p.139-140.

Fadaie, K., Teskey, D., Thomas, M.D., Hood, P., and Green, A.G., 1988, Quantitative gravity and magnetic modeling of GLIMPCE seismic lines A and C across Lake Superior, *EOS, Transactions, Amer. Geophy. Union*, v.69, p.1313.

Fowler, J.H., and Kuenzi, W.D., 1978, Keweenwan turbidites in Michigan (Deep borehole red beds): A foundered basin sequence developed during evolution of a protoceanic rift system, *J. Geophy. Res.*, v.83, p.5833-5843.

Gibbs, A.K., Payne, B., Setzer, T., Brown, L.D., Oliver, J.E., and Kaufman, S., 1984, Seismic-reflection study of the Precambrian crust of central Minnesota, *Geol. Soc. Am. Bull.*, v.95, p.280-294.

Gibson, B.S., and Levander, A.R., 1988, Lower crustal reflectivity patterns in wide-angle seismic recordings, *Geophy. Res. Letters*, v.15, p.617-620.

Gordon, M.B., and Hempton, M.R., 1986, Collision-induced rifting: The Grenville orogeny and the Keweenawan rift of North America, *Tectonophysics*, v.127, p. 1-25.

Green, J.C., 1977, Keweenawan plateau volcanism in the Lake Superior region, *Geol. Ass. Canada Special Paper*, v.16, p.407-422.

Green, J.C., 1982, Geology of Keweenawan extrusive rocks, *in*: Wold, R. J., and Hinze, W. J., eds., Geology and Tectonics of the Lake Superior Basin, *Geol. Soc. Am. Memoir,* v.156, p.47-55.

Green, A.G., Milkereit, B., Davidson, A., Spencer, C., Hutchinson, D.R., Cannon, W.F., Lee, M.W., Agena, W.F., Behrendt, J.C., and Hinze, W.J., 1988, Crustal structure of the Grenville front and adjacent terranes, *Geology*, v.16, p.788-792.

Halls, H.C., 1969, Compressional wave velocities of Keweenawan rock specimens from the Lake Superior region, *Canadian J. Earth Sci.*, v.6, p.555-568.

Halls, H.C., 1982, Crustal thickness in the Lake Superior region, *in*: Wold, R. J., and Hinze, W. J., eds., Geology and Tectonics of the Lake Superior Basin, *Geol. Soc. Am. Memoir,* v.156, p.239-243.

Halls, H.C., and West, G.F., 1971, A seismic refraction survey in Lake Superior, *Canadian J. Earth Sci.*, v.8, p.610-630.

Halls, H.C., and Pesonen, L.J., 1982, Paleomagnetism of Keweenawan rocks, *in*: Wold, R. J., and Hinze, W. J., eds., Geology and Tectonics of the Lake Superior Basin, *Geol. Soc. Am. Memoir,* v.156, p. 173-201.

Hamblin, W.K., 1961, Paleogeographic evolution of the Lake Superior region from late Keweenawan to late Cambrian time., *Geol. Soc. Am. Bull.,* v.72, p.1-18.

Hinze, W.J., and Wold, R.J., 1982, Lake Superior geology and tectonics - overview and major unsolved problems, *in*: Wold, R. J., and Hinze, W. J., eds., Geology and Tectonics of the Lake Superior Basin, *Geol. Soc. Am. Memoir,* v.156, p.273-280.

Hinze, W.J., Wold, R.J., and O'Hara, N.W., 1982, Gravity and magnetic studies of Lake Superior, *in*: Wold, R. J., and Hinze, W. J., eds., Geology and Tectonics of the Lake Superior Basin, *Geol. Soc. Am. Memoir,* v.156, p.203-221.

Hinze, W.J., Braile, L.W., Keller, G.R., and Lidiak, E.G., 1988, Models for midcontinent tectonism: An update, *Reviews of Geophy.*, v. 26, p.699-717.

Hutchinson, D.R., Morel, P., Meyer, H., Asudeh, I., Ervin, P., Hajnal, Z., Karl, J., Mereu, R., Meyer, R., Sexton, J., Spencer, C., and Tréhu, A., 1988, A description of GLIMPCE, 1986, large offset seismic experiment from the Great Lakes, *U.S. Geological Survey open-file report 88-431*, 91p.

Hutchinson, D.R., and White, R.S., 1989, Origin of the midcontinent rift, *EOS, Transactions, Amer. Geophy. Union*, v.70, p.275.

Hutchinson, D.R., White, R.S., Cannon, W.F., and Schultz, K.J., submitted, Keweenaw Hot Spot: Geophysical evidence for a 1.1 Ga mantle plume beneath the midcontinent rift system, *J. Geophy. Res.*,

Jefferson, T.J., Karl, J.H., and Meyer, P.J., 1989, A model of the velocity distribution across the midcontinent rift: GLIMPCE line A, *EOS, Transactions, Amer. Geophy. Union*, v.70, p.274.

Jolly, W.T., and Smith, R.E., 1972, Degradation and metamorphic differentiation of the Keweenawan tholeiitic lavas of northern Michigan, USA: *J. Petrol.*, v.13, p.273-309.

Kalliokoski, J., 1982, Jacobsville sandstone., *in*: Wold, R. J., and Hinze, W. J., eds., Geology and Tectonics of the Lake Superior Basin, *Geol. Soc. Am. Memoir,* v.156, p.147-155.

Keen, C.E., and de Voogd, B., 1988, The continent ocean boundary at the rifted margin off eastern Canada: New results from deep seismic reflection studies, *Tectonics*, v.7, p.107-124.

Keller, G.R., Lidiak, E.G., Hinze, W.J., and Braile, L.W., 1983, The role of rifting in the tectonic development of the midcontinent, U.S.A., *Tectonophysics*, v.94, p.391-412.

Kennet, B.L.N., 1976, A comparison of travel-time inversions, *Geophy. J. R. Astr. Soc.*, v.44, p.517-536.

King, E.R., and Zietz, I., 1971, Aeromagnetic study of the midcontinent gravity high of central United States, *Geol. Soc. Am. Bull.*, v.82, p.2187-2208.

Klasner J.S., Cannon, W.F., and Van Schmus, W.R, 1982, The pre-Keweenawan tectonic history of southern Canadian Shield and its influence on formation of the Midcontinent Rift, *in*: Wold, R. J., and Hinze, W. J., eds., Geology and Tectonics of the Lake Superior Basin, *Geol. Soc. Am. Memoir,* v.156, p.27-46.

LePichon, X., and Barbier, R., 1987, Passive margin formation by low-angle faulting within the upper crust; the northern Bay of Biscay margin, *Tectonics*, v.6, p.246-250.

Lightfoot, G., 1972, The wreck of the Edmund Fitzgerald, *Warner Bros. Records Inc., a Warner Communications Company.*

Lippus, C.S., 1988, The seismic properties of mafic volcanic rocks of the Keweenawan supergroup and their implications, *[Master thesis]: Purdue University, West Lafayette, Indiana.*

Lister, G.S., Etheridge, M.A., and Symonds, P.A., 1986, Detachment faulting and the evolution of passive continental margins, *Geology*, v.14, p.246-250.

Luetgert, J.H., and Meyer, R.P., 1982, Structure of the western basin of Lake Superior from cross structure refraction profiles., *in*: Wold, R. J., and Hinze, W. J., eds., Geology and Tectonics of the Lake Superior Basin, *Geol. Soc. Am. Memoir,* v.156, p.245-255.

Luetgert, J.H., unpublished manuscript., Crustal studies in eastern Lake Superior, U.S. Geological Survey, Menlo Park, California.

Lutter, W.J., Tréhu, A.M., Nowack, R.L., and Shay, J.T., 1989, Inversion for crustal structure using first arrival refraction data from the 1986 Lake Superior GLIMPCE experiment, *EOS, Transactions, Amer. Geophy. Union*, v.70, p.274.

Lutter, W.J, Nowack, R.L., and Braile, L.W., 1990, Seismic imaging of upper crustal structure using travel times from the PASSCAL Ouachita experiment., *J. Geophy. Res.*, v.95, p.4621-4631.

Lutter, W.J., and Nowack, R.L., 1990, Inversion for crustal structure using reflections from the PASSCAL Ouachita experiment., *J. Geophy. Res.*, v.95, p.4633-4646.

Lyons, P.L., 1959, The Greenleaf anomaly, a significant gravity feature., Synp. Geophy. Kans., *Kansas State Geol. Surv. Bull.*, v.137, p.105-120.

Manson, M.L., and Halls, H.C., 1989, A submersible dive on Superior Shoal, central Lake Superior, *EOS, Transactions, Amer. Geophy. Union*, v.70, p.275.

McCarthy, J., and Thompson, G.A., 1988, Seismic imaging of extended crust with emphasis on the western United States, *Geol. Soc. Am. Bull.*, v.100, p.1361-1374.

McGinnis, L.D., 1970, Tectonics and gravity field in the continental interior, *J. Geophy. Res.*, v.75, p.317-331.

McGinnis, L.D., Cannon, W.F., Dickas, A.B., Ervin, C.P., Green, A., Hinze, W.J., Milkereit, B., Morey, G.B., Mudrey, M.G., Nyquist, J., Sexton, J.L., and Wang, H.F., 1989, Geophysical and tectonic study of sedimentary basins and the upper crust beneath Lake Superior, *EOS, Transactions, Amer. Geophy. Union*, v.70, p.272.

McSwiggen, P.L., Morey, G.B., and Chandler, V.W., 1987, New model of the midcontinent rift in eastern Minnesota and western Wisconsin, *Tectonics*, v.6, p.677-685.

McWilliams, M.O., and Dunlop, D.J., 1978, Grenville paleomagnetism and tectonics, *Canadian Journal of Earth Sciences*, v.15, p.687-695.

Merk, G.P., and Jirsa, M.A., 1982, Provenance and tectonic significance of the Keweenawan interflow sedimentary rocks, *in*: Wold, R. J., and Hinze, W. J., eds., Geology and Tectonics of the Lake Superior Basin, *Geol. Soc. Am. Memoir,* v.156, p.97-105.

Meyer, P.J., Karl, J.H., and Jefferson, T.J., 1989, Beamsteering applied to the GLIMPCE wide-angle data: Line A, *EOS, Transactions, Amer. Geophy. Union*, v.70, p.276.

Milkereit, B., Green, A.G., Morel-a-l'Huissier, P.A., Lee, M.W., and Agena, W.F., 1988, 1986 Great Lakes seismic reflection survey migrated data, *Geol. Surv. Canada Open file report*, v.1592, 33 pages.

Mooney, H.M., Craddock, C., Farnham, P.R., Johnson, S.H., and Voltz, G., 1970, Refraction seismic investigation of the northern midcontinent gravity high, *J. Geophy. Res.*, v.75, p.5056-5086.

Mooney, W.D., Andrews, M.C., Ginzburg, A., Peters, D.A., and Hamilton, R.M., 1983, Crustal structure of the northern Mississippi embayment and a comparison with other continental rift zones, *Tectonophysics*, v.94, p.327-348.

Mooney, W.D., and Brocher, T.M., 1987, Coincident seismic reflection/refraction studies of the continental lithosphere: A global review, *Reviews of Geophysics*, v.25, p.723-742.

Morel-a-l'Huissier, P., and Green, A.G., 1989, Modeling the GLIMPCE 1986 seismic refraction data recorded along seismic reflection line A, *EOS, Transactions, Amer. Geophy. Union*, v.70, p.277.

Morel-a-l'Huissier, P., and Tréhu, A.M., 1988, Modeling of GLIMPCE seismic refraction data across central Lake Superior, *EOS, Transactions, Amer. Geophy. Union*, v.69, p.1313.

Morey, G.B., and Green, J.C., 1982, Status of the Keweenawan as a stratigraphic unit in the Lake Superior region, *in*: Wold, R. J., and Hinze, W. J., eds., Geology and Tectonics of the Lake Superior Basin, *Geol. Soc. Am. Memoir*, v.156, p.15-25.

Morey, G.B., and Ojakangas, R.W., 1982, Keweenawan sedimentary rocks of eastern Minnesota and northwestern Wisconsin, *in*: Wold, R. J., and Hinze, W. J., eds., Geology and Tectonics of the Lake Superior Basin, *Geol. Soc. Am. Memoir*, v.156, p. 135-146.

Morey, G.B., and Sims, P.K., 1976, Boundary between two Precambrian W terranes in Minnesota and its geologic significance., *Geol. Soc. Am. Bull.*, v.87, p.141-152.

Mutter, J.C., Talwani, M., and Stoffa, P.L., 1982, Origin of seaward-dipping reflectors in oceanic crust off the Norwegian margin by "subaerial sea-floor spreading", *Geology*, v.10, p.353-357.

Mutter, J.C., Buck, W.R., and Zehnder, C.M., 1988, Convective Partial Melting: A model for the formation of thick basaltic sequences during the initiation of spreading, *J. Geophy. Res.*, v.93, p.1031-1048.

Nicholson, S.W., and Schulz, K.J., 1989, Petrologic and geochemical constraints on the development of the midcontinent rift in Western Lake Superior, *EOS, Transactions, Amer. Geophy. Union*, v.70, p.274.

Nicholson, S.W., and Shirey S.B., submitted, Evidence for a Precambrian mantle plume: A Sr, Nd, and Pb isotope study of the midcontinent rift system in the Lake Superior region, *J. Geophy. Res.*,

Nyquist, J.E., and Wang, H.F., 1986, Lithospheric flexure and evolution of the midcontinent rift, *in:* Mudrey, M.G., editor, Precambrian petroleum potential, Wisconsin and Michigan, *Geosci. Wis.*, v.11, p.19-21.

Nyquist, J.E., and Wang, H.F., 1988, Flexural modeling of the midcontinent rift, *J. Geophy. Res.*, v.93, p.8852-8868.

Nyquist, J.E., and Wang, H.F., 1989, Flexural modeling of the midcontinent rift and the Goodman Swell, *EOS, Transactions, Amer. Geophy. Union*, v.70, p.275.

O'Hara, N.W., 1982, Great Lakes region gravity and magnetic map sequence, *Geol. Soc. Am. Map and Chart Series,* MC-37 - MC 41.

Ocola, L.C., and Meyer, R.P., 1973, Central North American Rift System: Structure of the axial zone from seismic and gravimetric data, *J. Geophy. Res.*, v.78, p.5173-5194.

Ojkangas, R.W., and Morey, G.B., 1982a, Keweenawan pre-volcanic quartz sandstones and related rocks of the Lake Superior region, *in*: Wold, R. J., and Hinze, W. J., eds., Geology and Tectonics of the Lake Superior Basin, *Geol. Soc. Am. Memoir,* v.156, p.85-96.

Ojkangas, R.W., and Morey, G.B., 1982b, Keweenawan sedimentary rocks of the Lake Superior region: A summary, *in*: Wold, R. J., and Hinze, W. J., eds., Geology and Tectonics of the Lake Superior Basin, *Geol. Soc. Am. Memoir,* v.156, p.157-164.

Oray, E., 1971, Regional gravity investigation of the eastern portion of the northern peninsula of Michigan: *[PhD Thesis] Michigan State University, East Lansing, Michigan*, 86 pages.

Paces, J.B., and Davis, D.W., 1988, Implications of high precision U-Pb age dates on zircons from Portage Lake volcanic basalts on midcontinent rift subsidence rates, lava flow repose periods and magma production rates., paper presented at Institute on Lake Superior Geology 34th Annual Meeting, Marquette, Michigan.

Palmer, H.C., and Davis, D.W., 1987, Paleomagnetism and U-Pb geochronology of volcanic rocks from Michipicoten Island, Lake Superior, Canada: Precise calibration of the Keweenawan polar wnader track, *Precambrian Res.*, v.37, p.157-171.

Peterman, Z.E., and Sims, P.K., 1988, The Goodman Swell: A lithospheric flexure caused by crustal loading along the midcontinent rift system, *Tectonics*, v.7, p.1077-1090.

Richards, M.A, Duncan, R.A., and Courtillot, V.E.,1989, Flood basalts and hotspot tracks: Plume heads and tails., *Science*, v.246, p.103-107.

Rosendahl, B.R., 1987, Architecture of continental rifts with special reference to East Africa, *Ann. Rev. Earth Planet. Sci.*, v.15, p.445-503.

Serpa, L., Setzer, T., Farmer, H., Brown, L., Oliver, J., Kaufman, S., and Sharp, J., 1984, Structure of the southern Keweenawan rift from COCORP surveys across the midcontinent geophysical anomaly in northeastern Kansas, *Tectonics*, v.3, p.367-384.

Sims, P.K., Card, K.D., Morey, G.B., and Peterman, Z.E., 1980, The Great Lakes tectonic zone- A major crustal structure in central North America, *Geol. Soc. Am. Bull.* v.91, p.690-698.

Smith, T.J., Steinhart, J.S., and Aldrich, L.T., 1966, Crustal structure under Lake Superior, *in*: Steinhart, J.S., and Smith, T.J., eds., The Earth beneath the Continents, *Am. Geophy. Union, Geophysical Monograph 10,* p.181-197.

Steinhart, J.S., 1961, The continental crust from explosions: A review. *in* Steinhart, J.S., Meyer, R.P., eds., Explosion studies of continental structure., *Carnegie Institution of Washington, Washington, D.C., Publication 622,* p.7-73.

Steinhart, J.S., Meyer, R.P., and Wollard, G.P., 1961, Explosion studies of continental structure: Wisconsin-Upper Michigan, *in* Steinhart, J.S., Meyer, R.P., eds., Explosion studies of continental structure., *Carnegie Institution of Washington, Washington, D.C., Publication 622*, p.248-304.

Steinhart, J.S., 1964, Lake Superior seismic experiment: shots and travel times., *J. Geophys. Res.* v.69, p.5335-5352.

Steinhart, J.S., and Smith, T.J., 1966, The Earth beneath the Continents, *Am. Geophy. Union, Geophysical Monograph 10,* Washington, D.C..

Steinhart, J.S., Hart, S.R., and Smith, T.J., 1968, Heat flow, *Carnegie Institution of Washington, Washington, D.C., Yearbook 67,* p.130-140.

Talwani, M., Worzel, J.L., and Landisman, M., 1959, Rapid gravity computations for two-dimensional bodies with application to the Mendocino submarine fracture zone, *J. Geophys. Res.* v.64, p.49-59.

Thiel, E., 1956, Correlation of gravity anomalies with the Keweenawan geology of Wisconsin and Minnesota, *Geol. Soc. Am. Bull.*, v.67, p.1079-1100.

Tréhu, A.M., Milkereit, B., and Shay, J.T., 1989a, Structure of the lower crust beneath the midcontinent rift from migration of wide angle reflections, *EOS, Transactions, Amer. Geophy. Union*, v.70, p.277.

Tréhu, A.M., Lutter, W.J., and Nowack, R.L., 1989b, Structure of the lower crust beneath the midcontinent rift from inversion of wide angle reflection travel times for interface position, *EOS, Transactions, Amer. Geophy. Union*, v.70, p.1214.

Tréhu, A.M., Ballard, A., Dorman, L.M., Gettrust, J.F., Klitgord, K.D., and Schreiner, A., 1989c, Structure of the lower crust beneath the Carolina trough, U.S. Atlantic continental margin, *J. Geophys. Res.* v.94, p.10,585-10,600.

Tréhu, A.M.,Morel-a-l'Huissier, P., Hajnal, Z., Karl, J., Mereu, R., Meyer, R., Sexton, J., Shay, J., Chan, W.K., Epili, D., Jefferson, T., Shih, X.R., Wendling, S., Milkereit, B., Green, A., Hutchinson, D., in prep, Imaging the midcontinent rift beneath Lake Superior using large aperture seismic data, *Nature*

Van Schmus, W.R., and Hinze, W.J., 1985, The midcontinent rift system, *Ann. Rev. Earth Planet. Sci.,* v.13, p.345-383.

Van Schmus, W.R., Green, J.C., and Halls, H.C., 1982, Geochronology of Keweenawan rocks of the Lake Superior region: A summary, *in*: Wold, R. J., and Hinze, W. J., eds., Geology and Tectonics of the Lake Superior Basin, *Geol. Soc. Am. Memoir,* v.156, p.165-171.

Vera, E., and Diebold, J.B., 1984, Generalized inversions of discrete tau-p data. EOS, v.65, p.239.

Weber, J.R., and Goodacre, A.K., 1966, A reconnaissance underwater gravity survey of Lake Superior, *in* Steinhart, J.S., and Smith, T.J., eds., The Earth beneath the Continents, *Am. Geophy. Union, Geophysical Monograph 10,* p.56-65.

Weiblen, P.W., 1982, Keweenawan intrusive igneous rocks, *in*: Wold, R. J., and Hinze, W. J., eds., Geology and Tectonics of the Lake Superior Basin, *Geol. Soc. Am. Memoir,* v.156, p.57-82.

White, W.S., 1966a, Tectonics of the the Keweenawan basin, western Lake Superior region: *U. S. Geol. Survey Prof. Paper 524-E,* p. E1-E23.

White, W.S., 1966b, Geologic evidence for crustal structure in the western Lake Superior basin., *in* Steinhart, J.S., and Smith, T.J., eds., The Earth beneath the Continents, *Am. Geophy. Union, Geophysical Monograph 10,* p.28-41.

White, W.S., 1971, A paleohydrological model for mineralization of the White Pine copper deposit, northern Michigan, *Econ. Geology*, v.66, p.1-13.

White, R.S., Spence, G.D., Fowler, S.R., McKenzie, D.P., Westbrook, G.K., and Bowen, A.N., 1987, Magmatism at rifted continental margins, *Nature*, v.330, p.439-444.

White, R.S., and McKenzie, D.P., 1989, Magmatism at rift zones: the generation of volcanic continental margins and flood basalts, *J. Geophy. Res.*, v.94, p.7685-7729.

Wold, R.J., and Hinze, W.J., 1982, Geology and Tectonics of the Lake Superior Basin, *Geol. Soc. Am. Memoir* , v.156, 280 pages, 3 plates.

Woollard, G.P., 1943, Transcontinental gravitational and magnetic profile of North America and its relation to geologic structure. *Geol. Soc. Am. Bull.*, v.54, p.747-790.

Zhu, T., and Brown, L.D., 1986, Consortium for Continental Reflection Profiling Michigan surveys: Reprocessing and results, *J. Geophy. Res.*, v.91, p.11,477-11,495.

Appendices

Appendix A: Uninterpreted Record Sections

Uninterpreted copies of the wide aperture record sections. The data for each record section displayed in this thesis have been frequency filtered (5-30 Hz) and subjected to deconvolution based on a trace-by-trace 4 second design window hung approximately 0.1 s ahead of the first breaks. The filter length and prediction distance were 0.24 s and 0.048 s respectively. With such a short prediction distance the filter behaved essentially as a spiking deconvolution. The data were sampled at 0.008 s and has been plotted at a reduction velocity of 7.2 km/s. Trace amplitudes have been scaled by a factor of range/10km for offsets greater than 10 km. All of the record sections, except those for OBS-A2, show the vertical component of motion recorded by each instrument. For OBS-A2, the hydrophone component is shown. For the sake of record clarity the full record sections shown in this appendix and in figures 14-19 are shown without the wiggle.

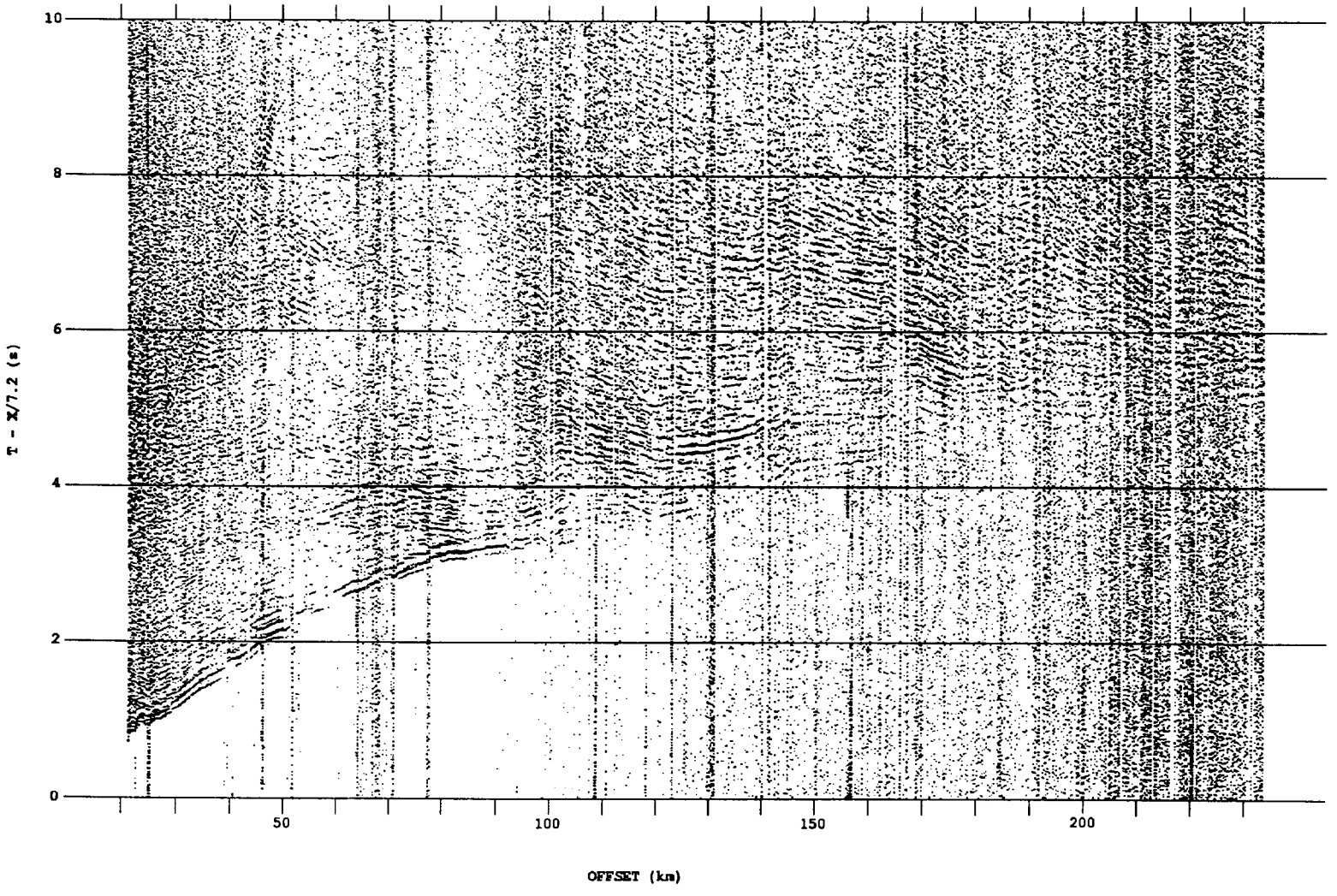

Figure 25. Record section from instrument SUP4

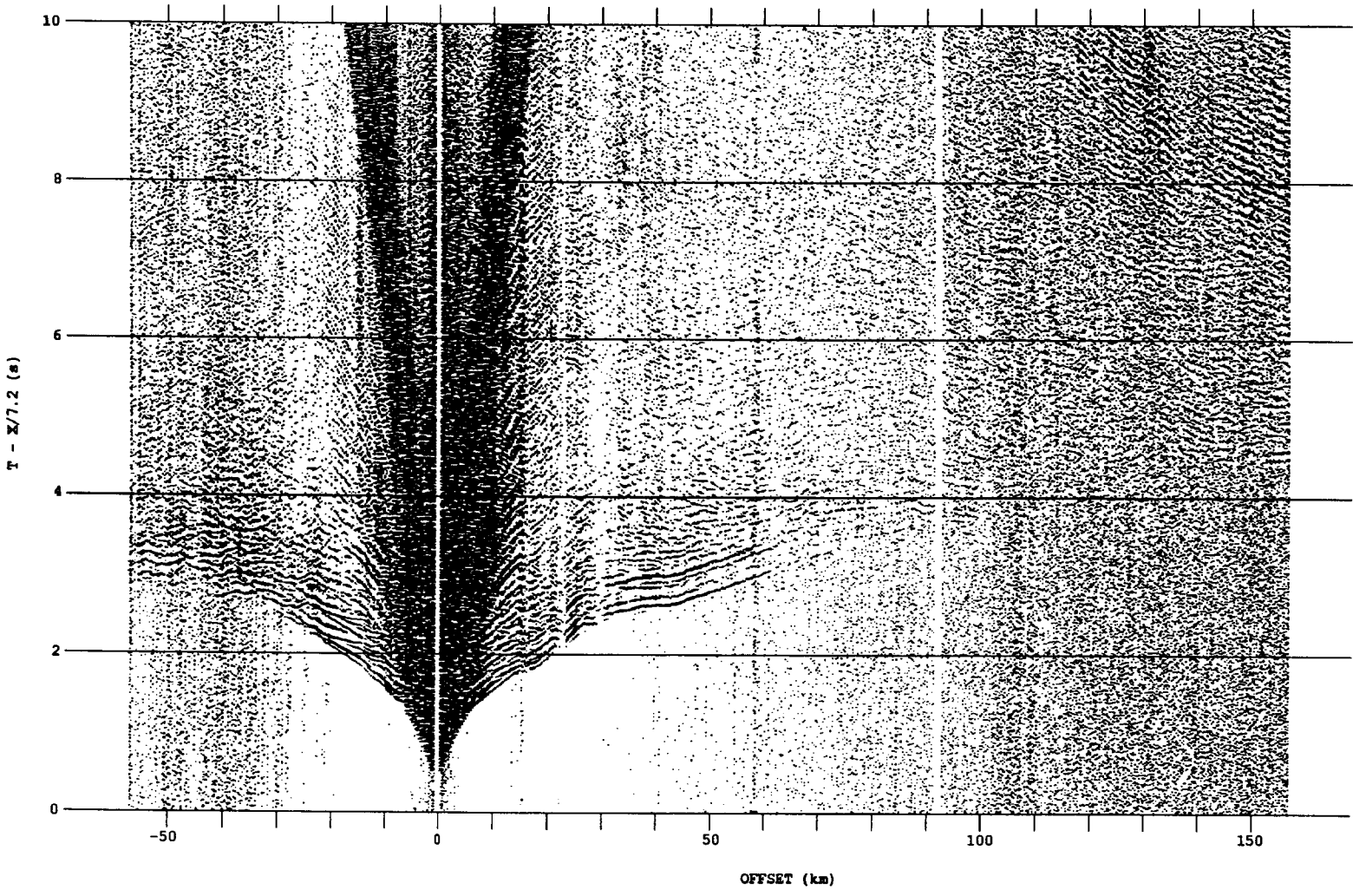

Figure 26. Record section from OBS-A2

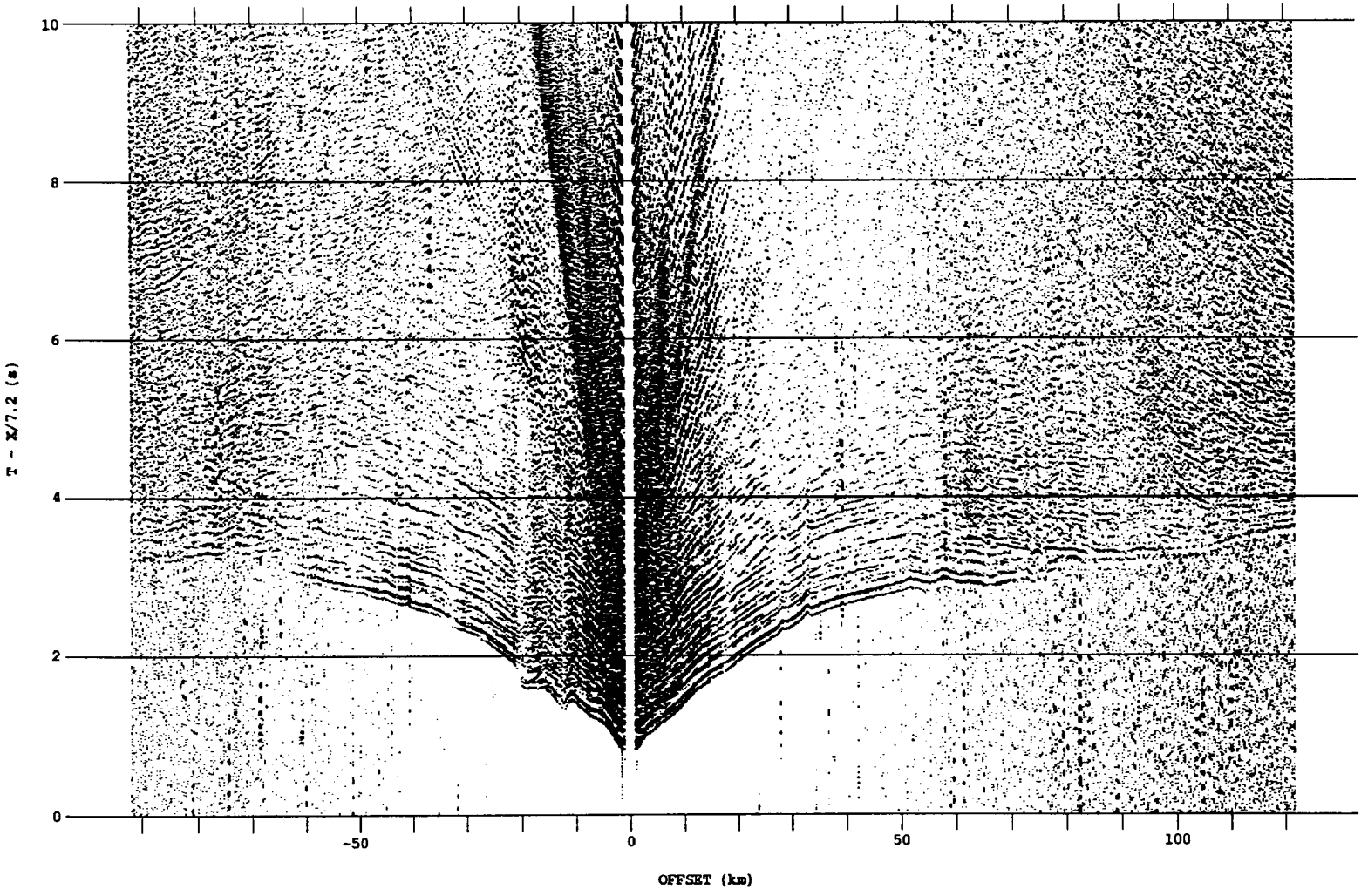

Figure 27. Record section from OBS-C4

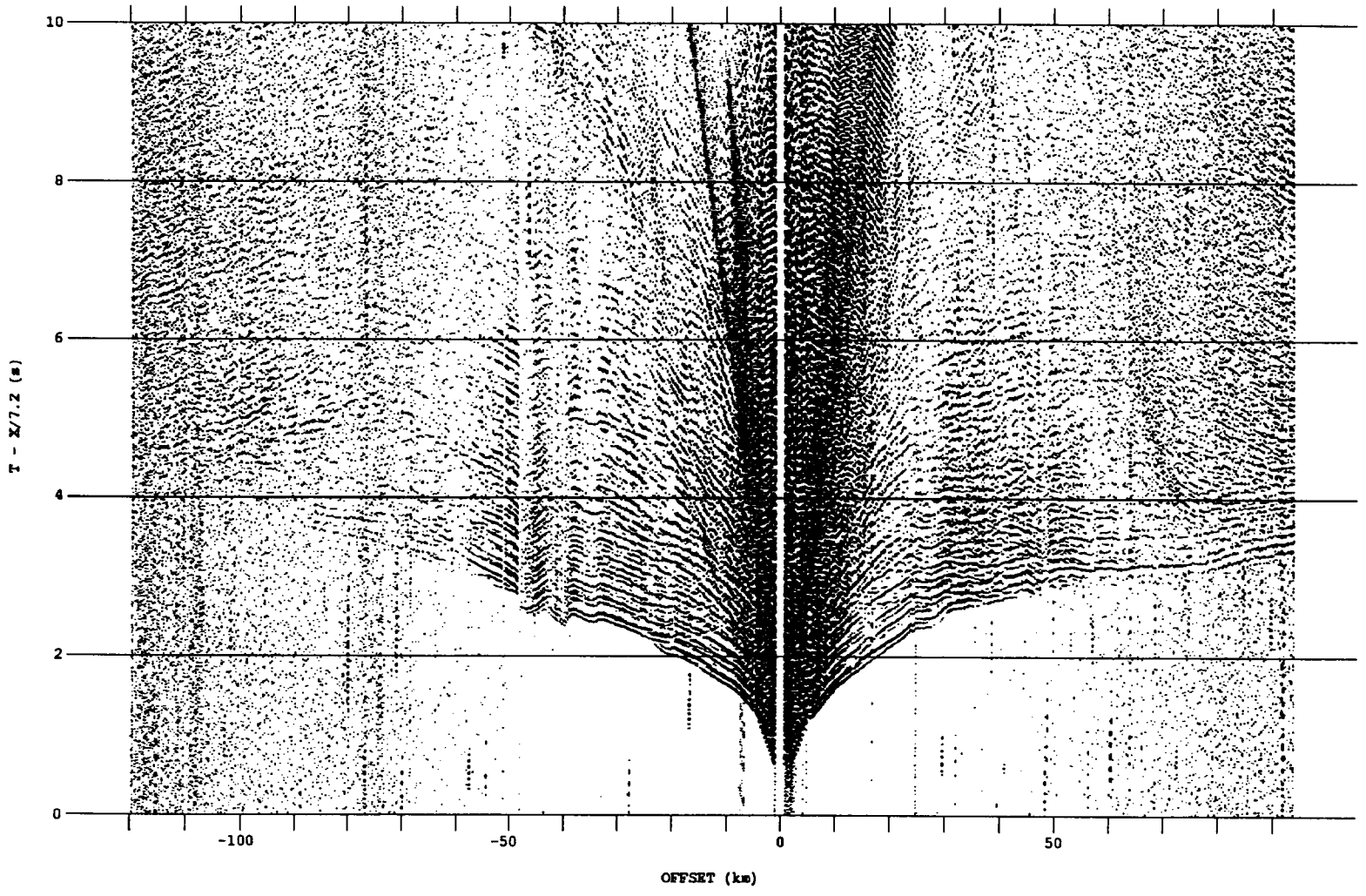

Figure 28. Record section from OBS-C9

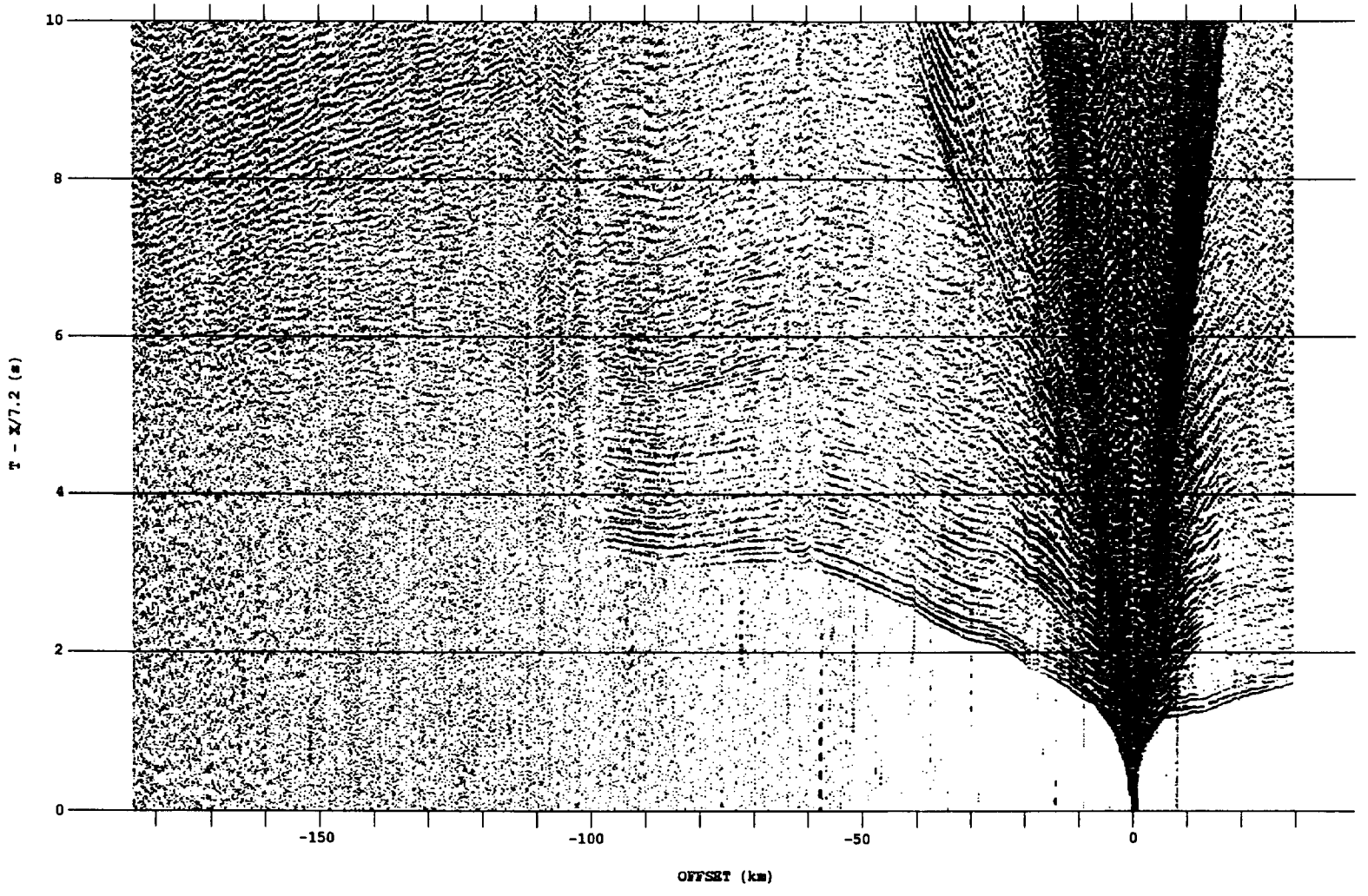

Figure 29. Record section from OBS-C3

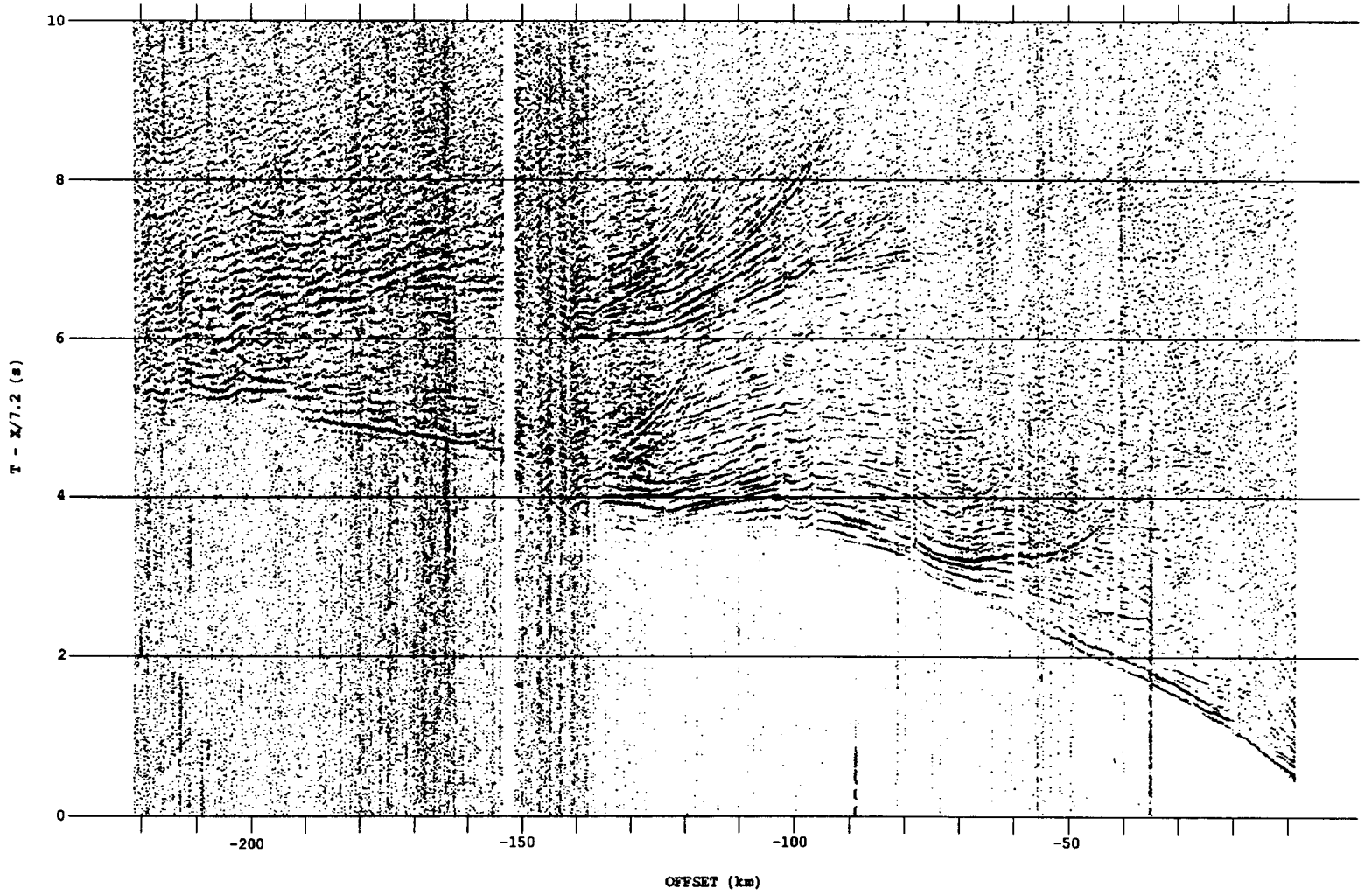

Figure 30. Record section from instrument C1

Appendix B: Synthetic Record Sections

Copies of the synthetic record sections plotted at the same scale as the data sections shown in appendix A. The amplitudes for all of the synthetic record sections displayed in this thesis were calculated from rays shot by ray code. Except for rays confined to sublayer 1a, the amplitudes for each travel time branch were calculated from rays shot approximately every 0.1 degree of take-off angle. The rays for branch 1a were shot approximately every 1.0 degree of take-off angle..Trace amplitudes have been scaled by a factor of range/10km for offsets greater than 10 km. The source time function used to create the synthetic record sections is given below. The source time function is sampled at 8 milliseconds.

0.00	5.52	0.42	-21.15	-9.78	20.44	23.69	8.13	-7.69	-14.48
-12.52	-6.70	-2.02	0.82	3.80	4.96	5.84	8.61	8.19	2.04
-4.95	-8.87	-8.83	-5.28	-0.68	2.21	3.54	3.66	2.23	1.07
1.16	0.86	-0.28	-1.25	-1.75	-1.77	-1.36	-0.75	0.12	0.92
0.89	0.52	0.59	0.86	0.65	0.04	-0.56	-0.80	-0.83	-0.51
-0.09	0.22	0.31	0.32	0.26	0.28	0.12	0.08	-0.05	-0.13
-0.38	-0.19	-0.16	0.16						

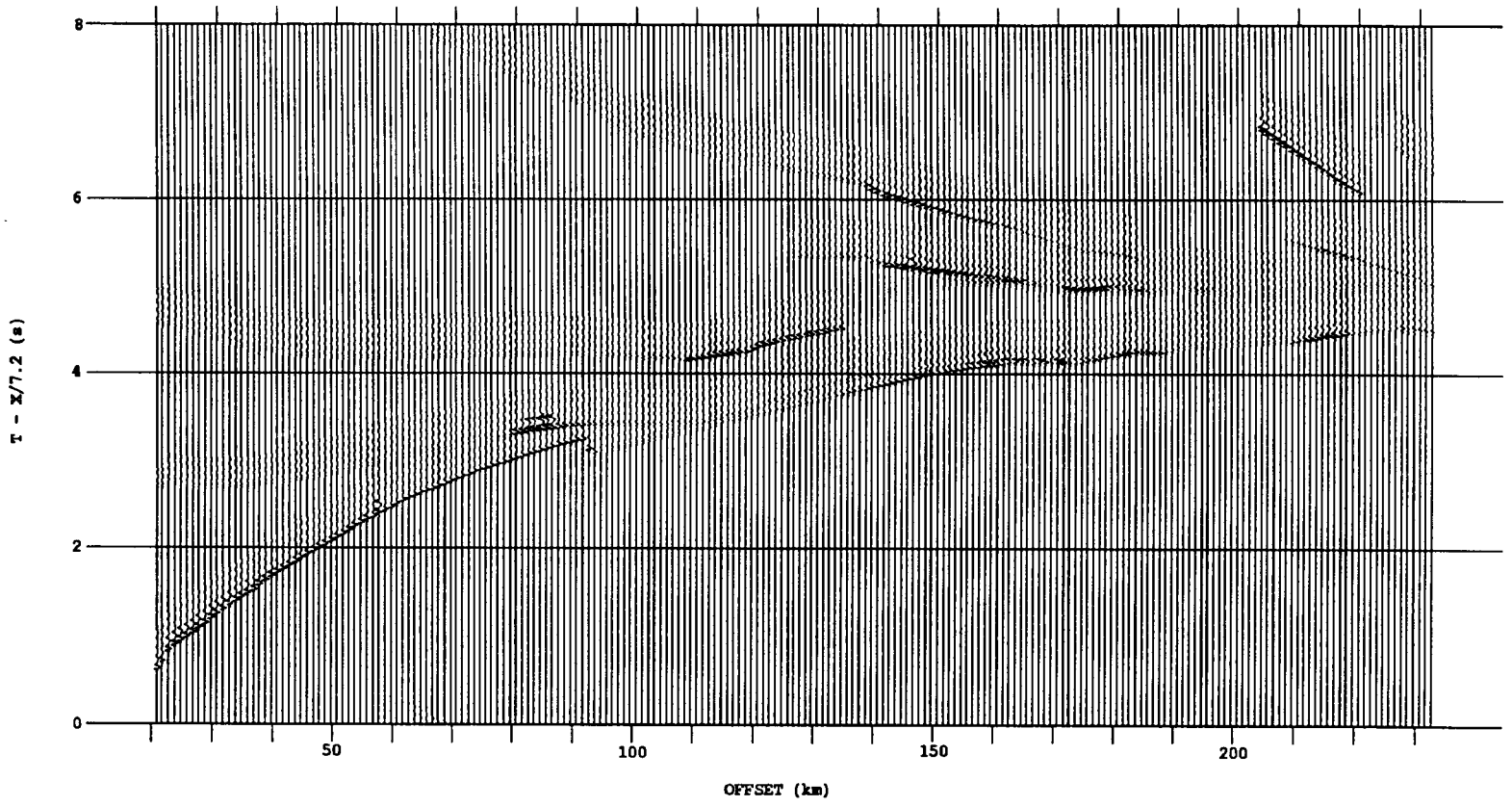

Figure 31. Synthetic section calculated for instrument SUP4

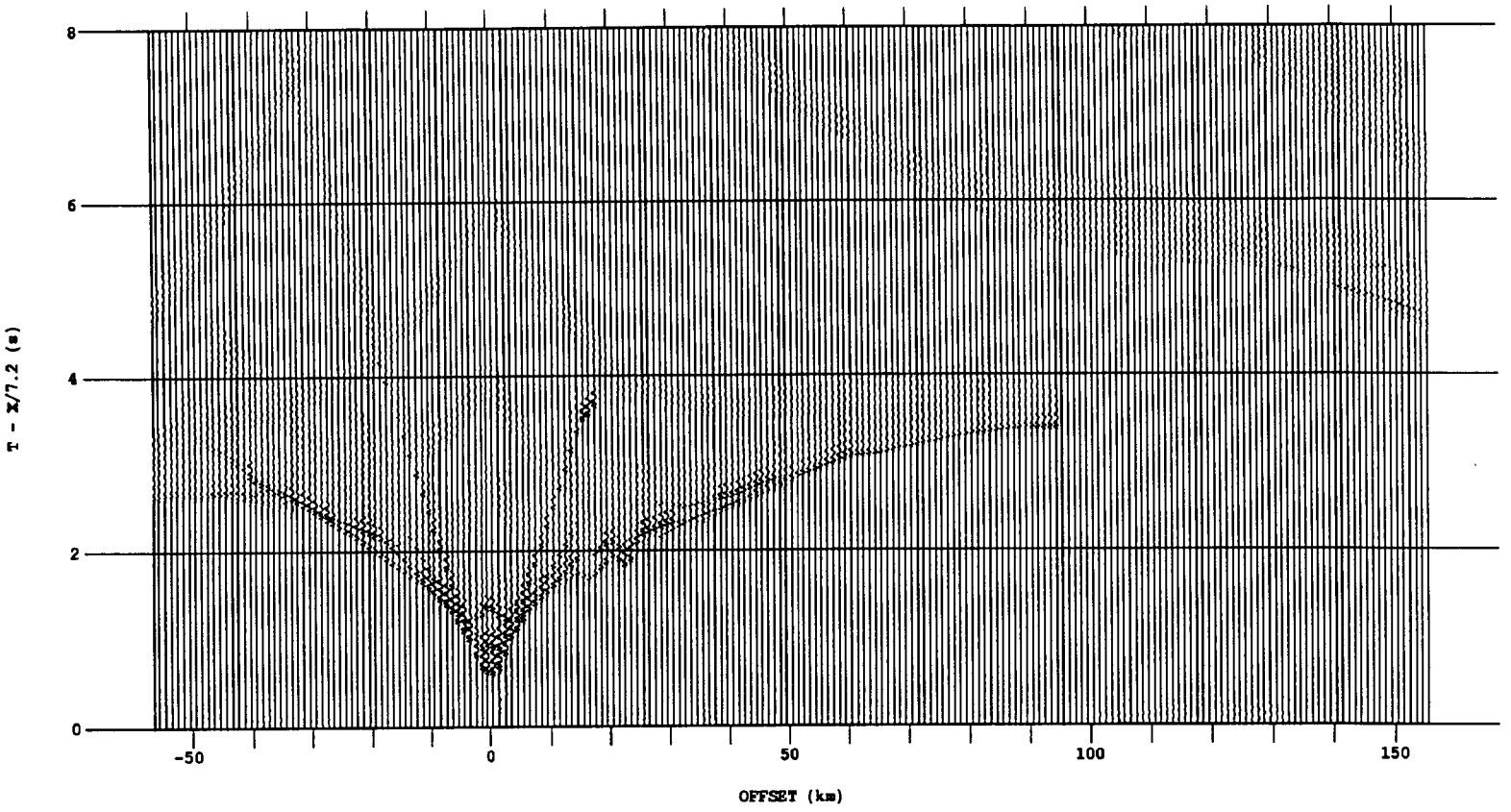

Figure 32. Synthetic section calculated for OBS-A2

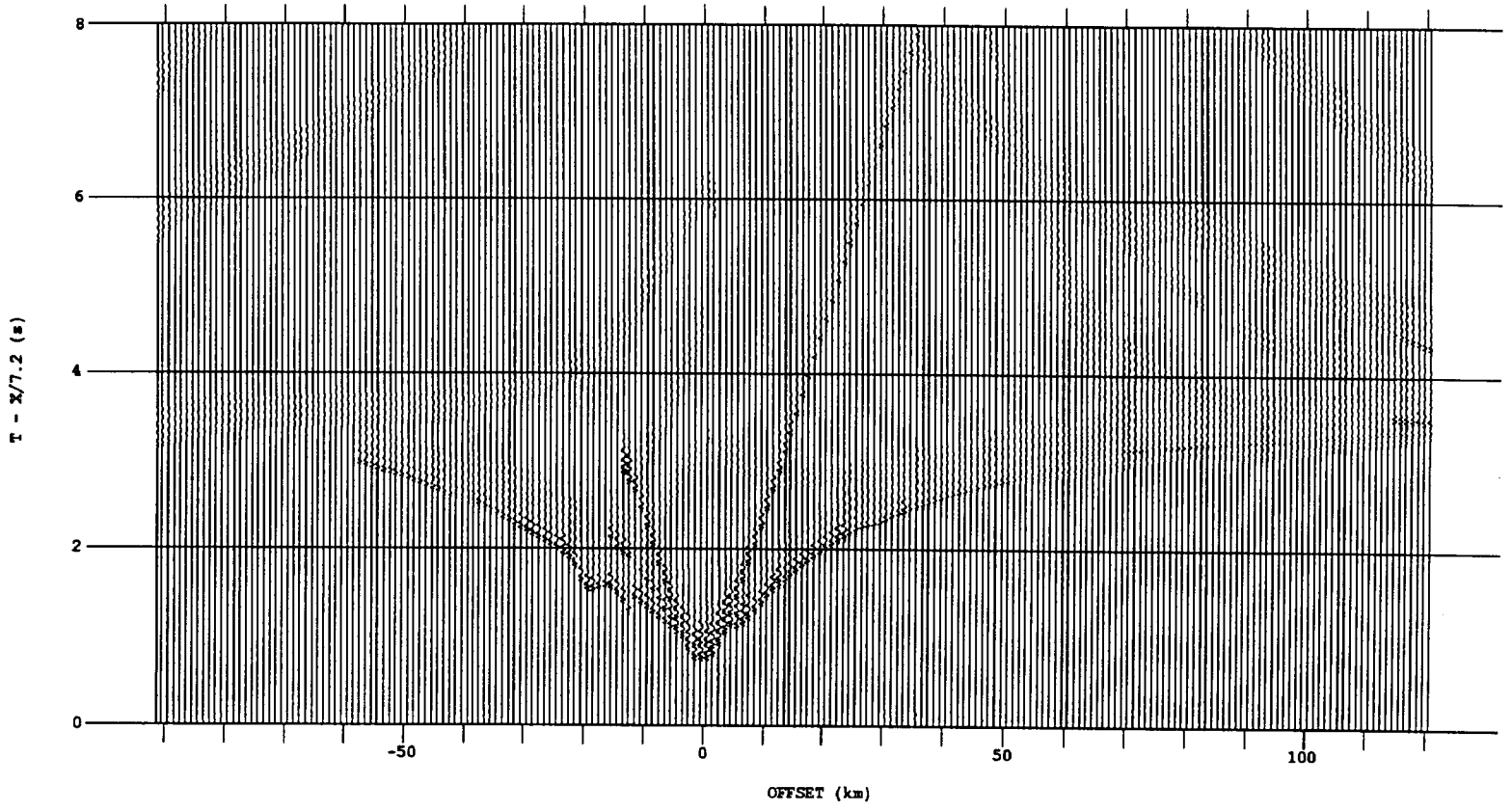

Figure 33. Synthetic section calculated for OBS-C4

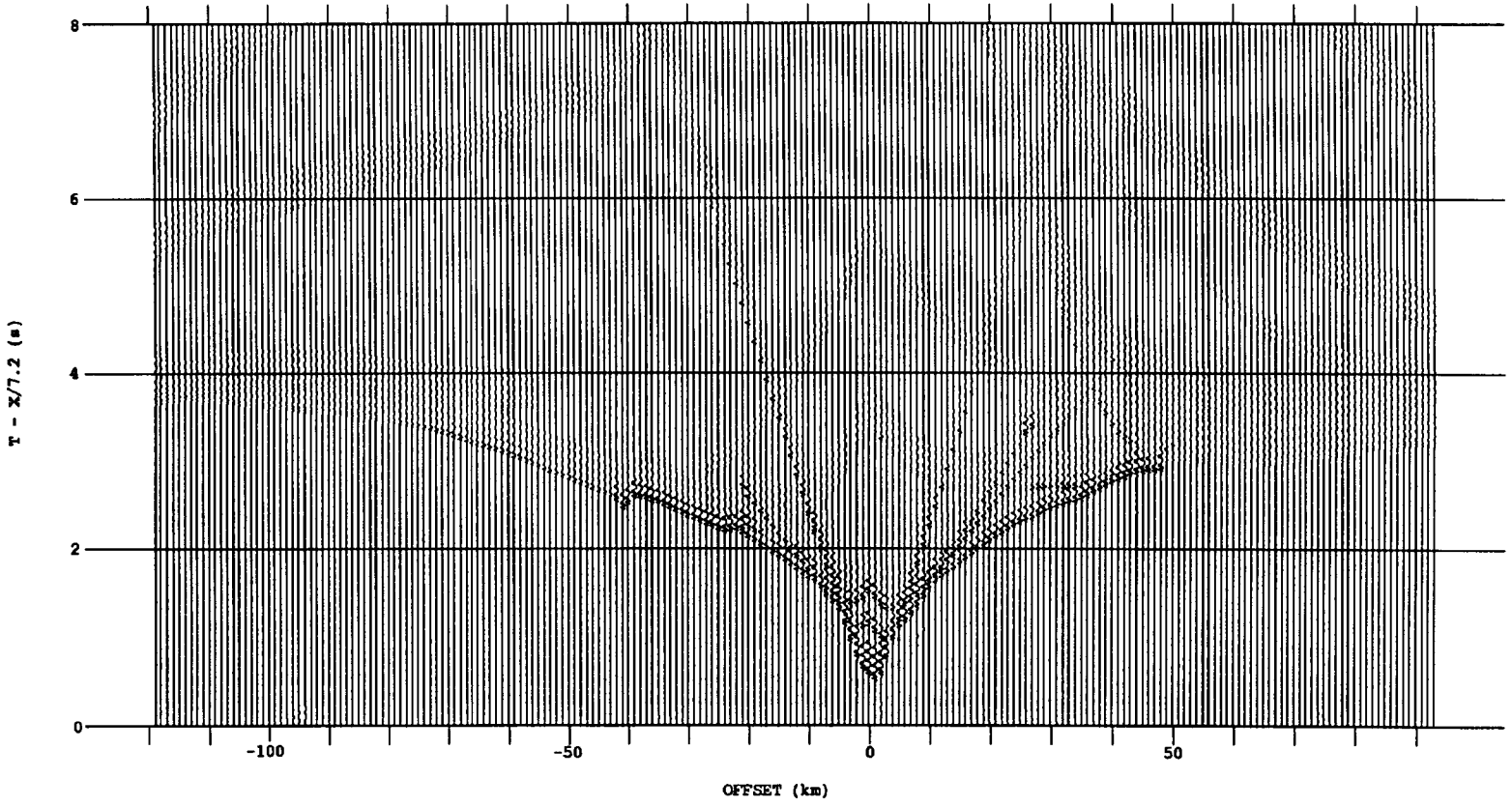

Figure 34. Synthetic section calculated for OBS-C9

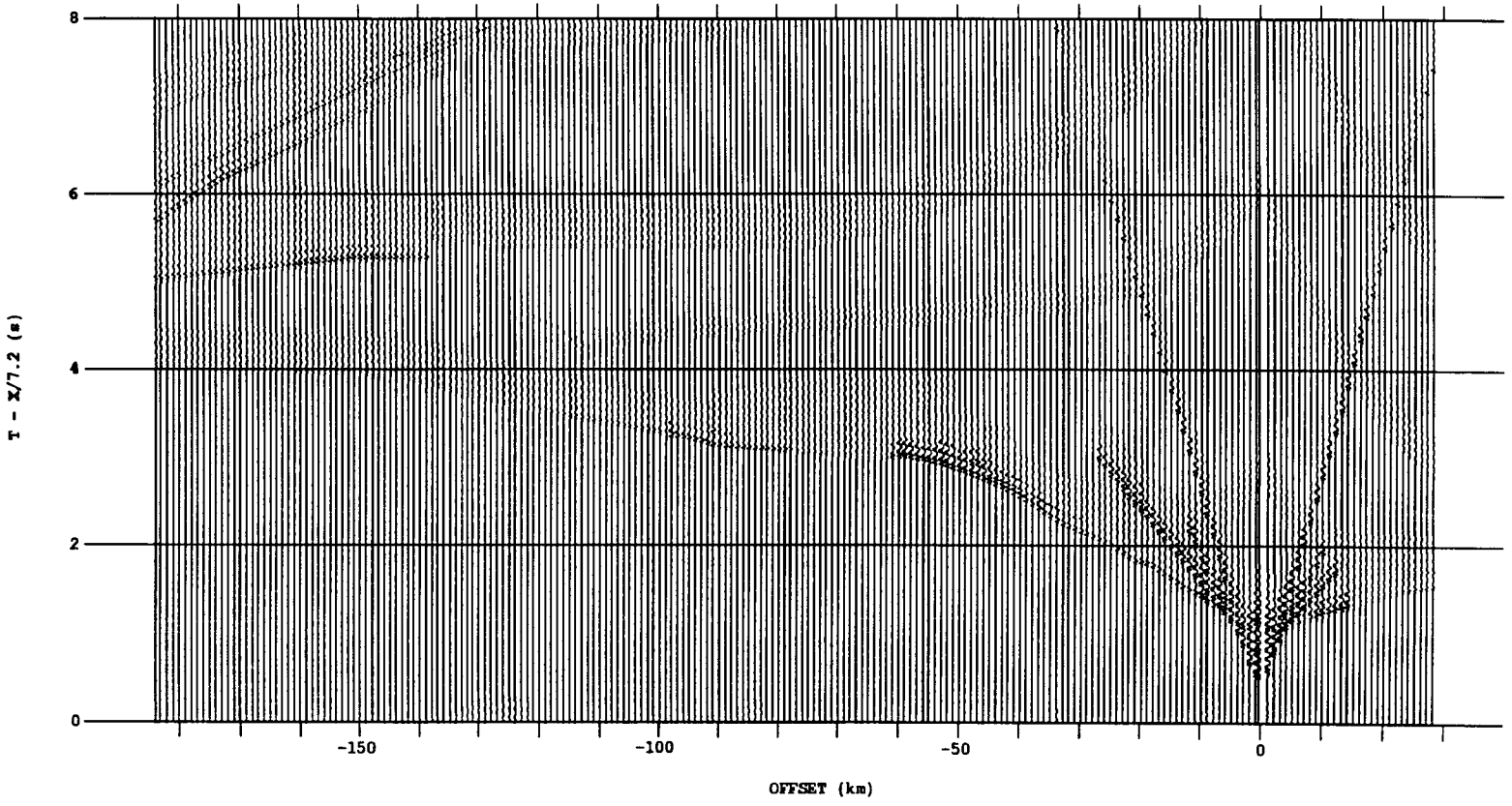

Figure 35. Synthetic section calculated for OBS-C3

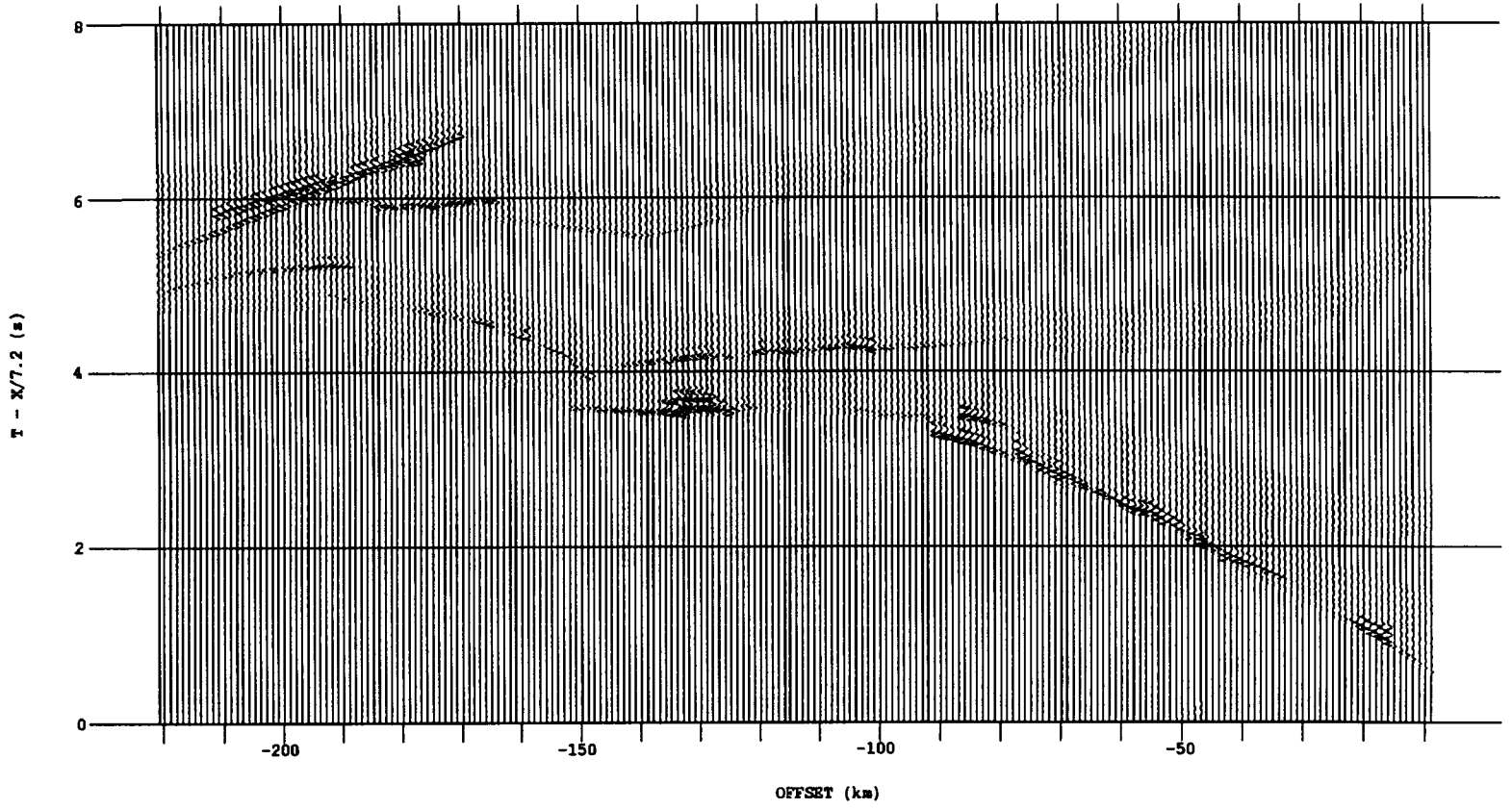

Figure 36. Synthetic section calculated for instrument C1

Appendix C: Instrument Location Plots

OBS location figures showing the original Coast Guard locations, the travel time circle results, and the least-squares inversion solutions. The prefered locations and the magnitude of the error ellipses resulting from the formal inversions are listed in Table 2 of the main text.

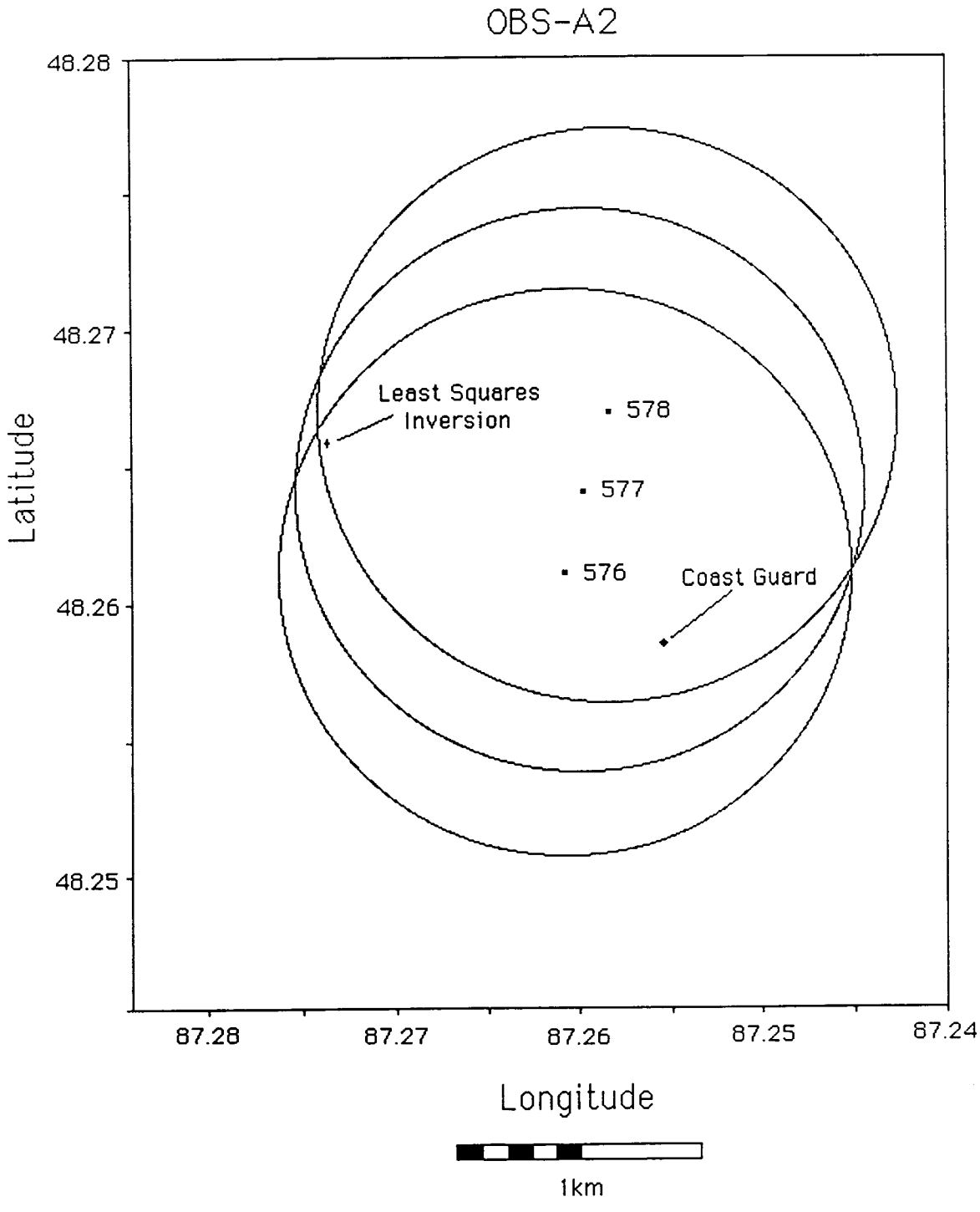

Figure 37. Instrument location plot for OBS-A2

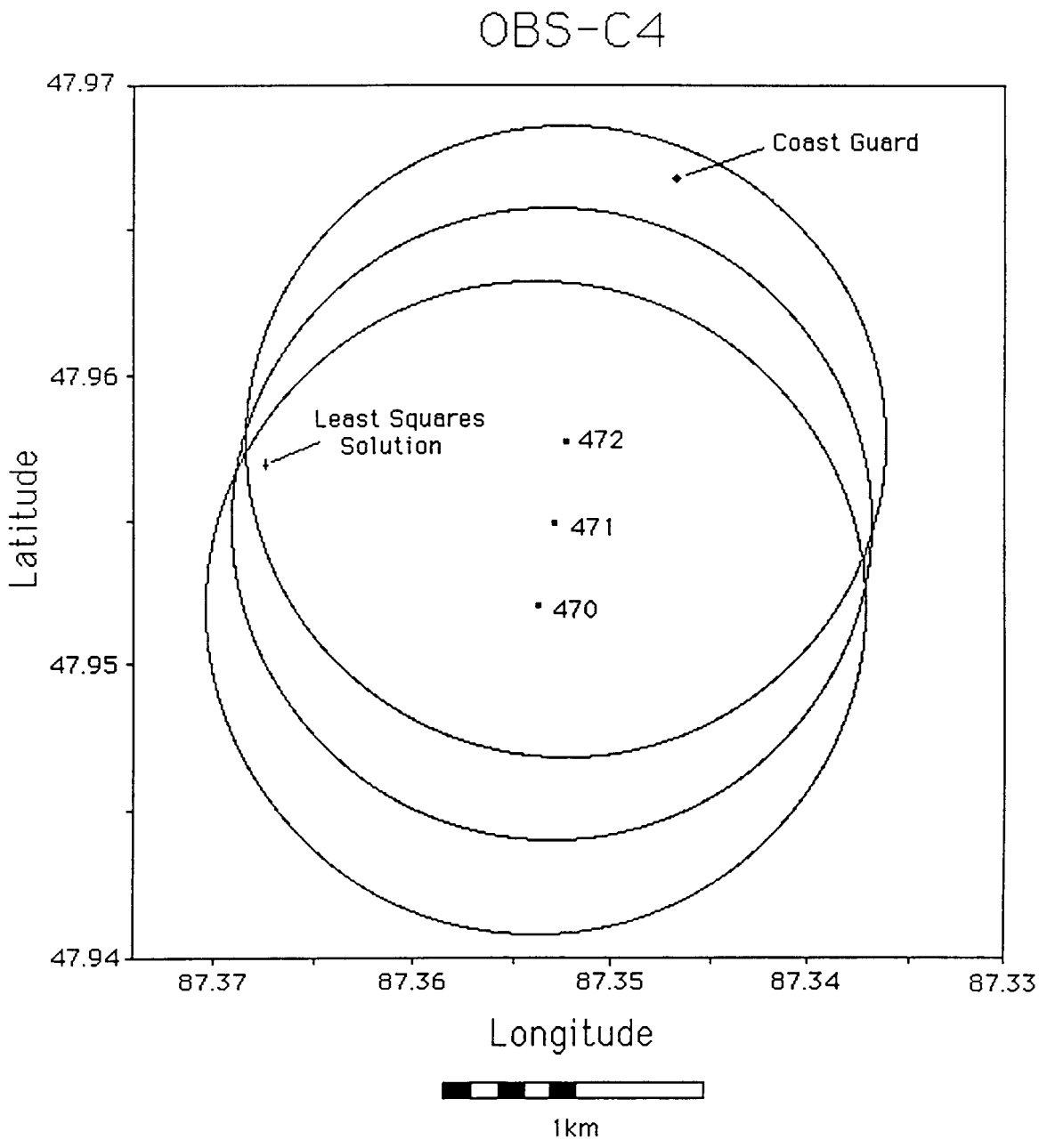

Figure 38. Instrument location plot for OBS-C4

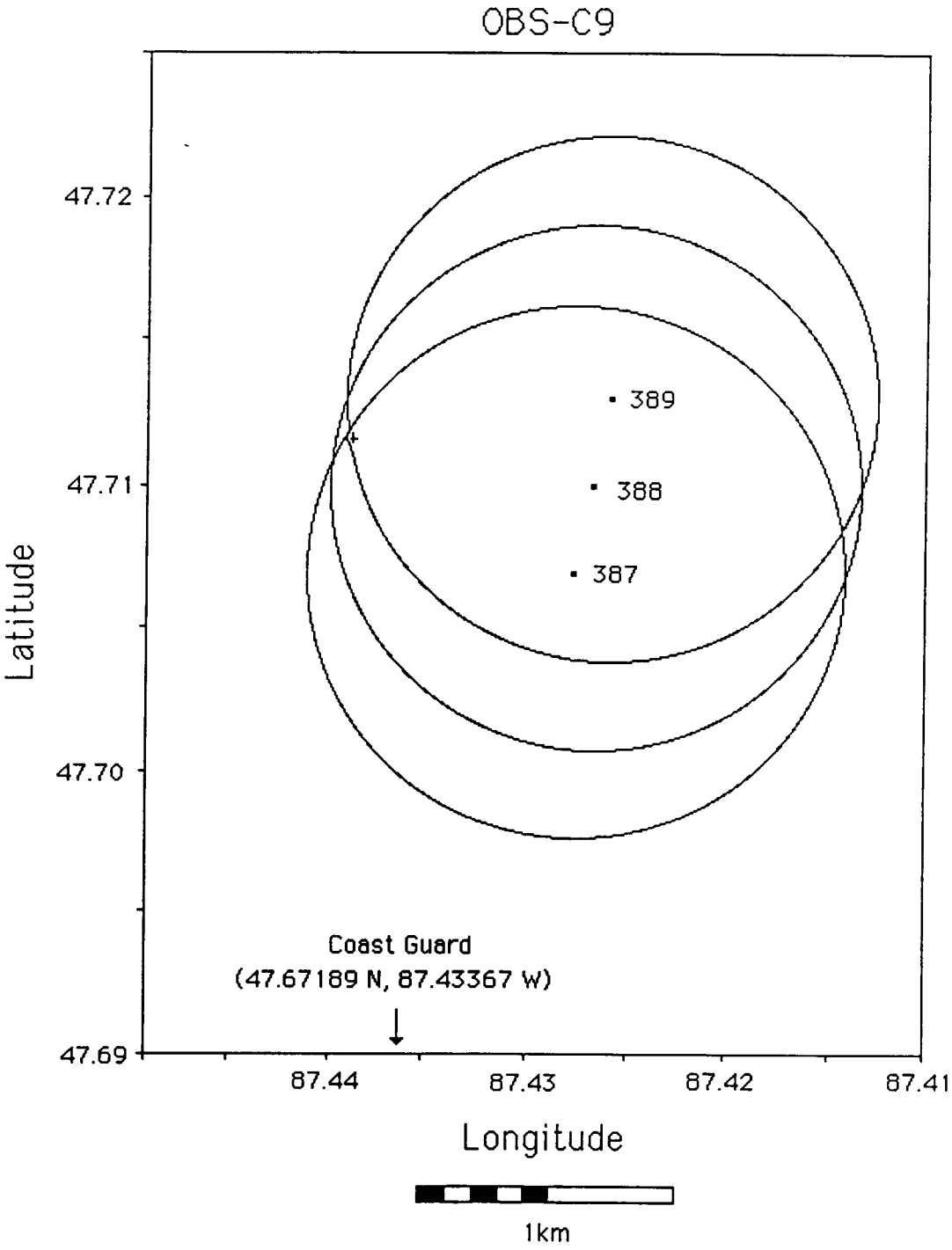

Figure 39. Instrument location plot for OBS-C9

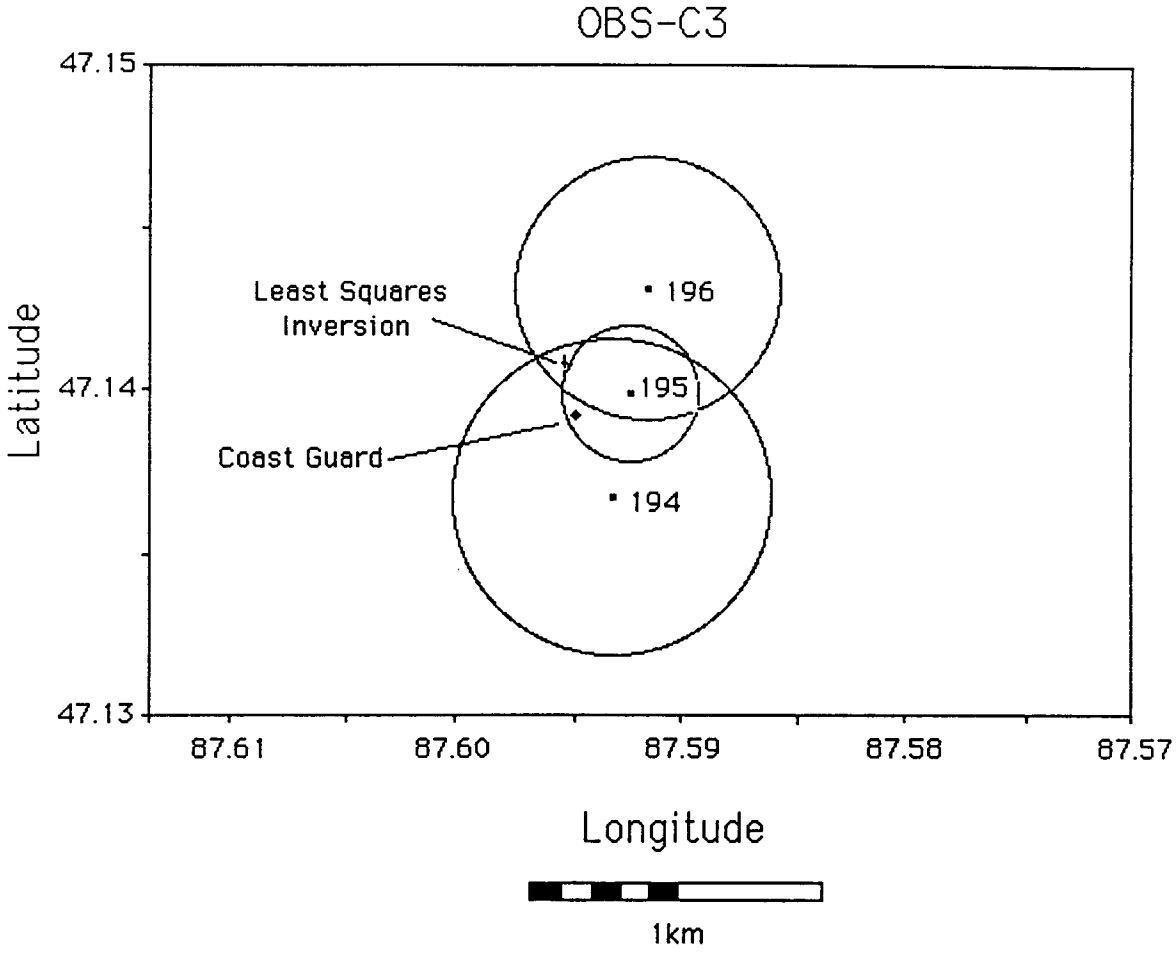

Figure 40. Instrument location plot for OBS-C3.